

**University of Alberta**

**Distribution System Condition Monitoring Using  
Active Disturbances**

by

**Xun Long**

A thesis submitted to the Faculty of Graduate Studies and Research in  
partial fulfillment of the requirements for the degree of

**Doctor of Philosophy**  
in  
**Power Engineering and Power Electronics**

Department of Electrical and Computer Engineering

©Xun Long  
Spring 2013  
Edmonton, Alberta

Permission is hereby granted to the University of Alberta Libraries to reproduce single copies of this thesis and to lend or sell such copies for private, scholarly or scientific research purposes only. Where the thesis is converted to, or otherwise made available in digital form, the University of Alberta will advise potential users of the thesis of these terms.

The author reserves all other publication and other rights in association with the copyright in the thesis and, except as herein before provided, neither the thesis nor any substantial portion thereof may be printed or otherwise reproduced in any material form whatsoever without the author's prior written permission.

## Abstract

Utility companies have benefited from the use of condition monitoring to optimize the performance of their assets and enhance power system reliability. This thesis starts with a review of different applications of condition monitoring in a distribution system, and one of the findings is that several challenges faced by condition monitoring cannot be fulfilled by passive methods or offline monitoring. It is also found that power electronics has been utilized as an effective manner to create active disturbance in a distribution system. Based on these findings, power electronics aided online monitoring methods are presented to address three challenging condition monitoring problems.

Proper grounding at a substation is a necessary practice for utilities to ensure substation safety and prevent equipment damage. The current practices of grounding grid evaluation are based on offline monitoring, which at best give one-shot measurement results. This thesis presents an active online method which can continuously monitor the condition of a grounding grid. The current is created by a thyristor-based signal generator and injected into the tested grounding grid. The measured touch voltage and step voltage are then evaluated to determine if hazardous spots are detected.

Fault detection in a de-energized feeder is another challenge for utilities, as all conventional passive detection methods cannot function in a de-energized system. This thesis describes an active method by using a three-phase thyris-

tor bridge to inject signals into de-energized downstream. The corresponding voltage and current are analyzed to determine if a fault still exists. A harmonic impedance based algorithm is also developed to detect a symmetrical fault, and distinguish a fault from a shunt capacitor or a stalled motor, which behaves like a fault when a voltage is applied.

Neutral-to-earth voltage has become an increased concern, as it not only has impact on livestock production, but also affects public safety. Utilities are actively seeking techniques that can effectively monitor neutral conditions. An active method to monitor neutral grounding integrity is presented. A small disturbance is injected into neutral by firing thyristors, and the neutral current flow is monitored to determine the neutral condition. The method can also be used to analyze the contributions of utility and customer to neutral-to-earth voltage.

## Acknowledgements

I would like to show my sincere gratitude to Dr. Wilsun Xu for his patient guidance, advice and encouragement throughout my research. I am fortunate for being able to work with a very considerate supervisor who cared so much about my work, and contributed a lot towards my understanding and thoughts. I deem it as my privilege to be his student. I ever remain grateful to him.

I am immensely pleased to place on record my heartfelt thanks to my co-supervisor Dr. Yun Wei Li who suggested the problem and provided inspiring guidance, without whose endless help and patience, the thesis would not have been successful.

I am pleased to thank every one working in the PDS-LAB who supported me in the last five years. I would never forget the help I got from Wencong Wang, Xiaoyu Wang, Enrique Nino, Janak Acharya, Yunfei Wang, Hooman Erfanian Mazin, Chris Lerohl, Joey Gallant, Hui Wang, Ming Dong, Chen Jiang, Pengfei Gao, Shenqiang Li, Qinxin Shi and Yu Tian. I am grateful to Dr. Jing Yong, provided helpful suggestions and constant support. I also would like to thank Ms. Patricia Barnes for helping me out of administrative challenges. I also extend my thanks to Albert Terheide for his help of laboratory experiments.

I do thank iCORE for their generous grants provided for my research.

I also record my appreciation to the committee members for the continued guideline from the beginning of the thesis to completion.

The completion of this thesis will mean a lot to my parents, Zhiyu Long and Ying Hua, who watched me from a distance while I worked towards my degree. Their selfless sacrificial life and great efforts with unceasing prayers has enabled me to reach the present position in life. This is also extensive to my sister Yi Long, family members, many friends who provided so much support and encouragement throughout this process.

Finally, and most importantly, I owe a lot to my wife, Liying Yan. It is difficult to find words to express my gratitude for her. Her support, encouragement and unwavering love were in the end what made this thesis possible.

# Table of Contents

<b>1</b>	<b>Introduction</b>	<b>1</b>
1.1	Condition Monitoring in Distribution System . . . . .	2
1.2	Overview of Condition Monitoring Methods . . . . .	6
1.2.1	Passive Methods Vs. Active Methods . . . . .	6
1.2.2	Offline Monitoring Vs. Online Monitoring . . . . .	6
1.2.3	Categorization of Condition Monitoring Methods . . . . .	8
1.2.4	Signal Generation in Active Methods . . . . .	10
1.3	Challenges Faced by Distribution System Condition Monitoring	13
1.3.1	Substation Grounding Grid Monitoring . . . . .	13
1.3.2	Fault Detection in De-energized Lines . . . . .	15
1.3.3	Monitoring of Neutral Grounding Integrity . . . . .	16
1.3.4	Detection of High Impedance Fault . . . . .	18
1.3.5	Transformers Condition Monitoring . . . . .	19
1.4	Research Objectives . . . . .	21
1.5	Thesis Outline . . . . .	22
<b>2</b>	<b>Online Monitoring of Substation Grounding Grid Conditions Using Touch and Step Voltage Sensors</b>	<b>24</b>
2.1	Introduction . . . . .	25
2.2	The Proposed Online Monitoring Scheme . . . . .	26
2.2.1	Testing Current Generation and Injection . . . . .	27
2.2.2	Touch/Step Voltage Based Sensor Network . . . . .	29
2.2.3	Intelligent Evaluation with Online Database . . . . .	34
2.3	Study of Current Distribution . . . . .	37
2.4	Computer Simulation of the Proposed Online Monitoring Scheme	41
2.5	Conclusion . . . . .	47
<b>3</b>	<b>Power Electronics Aided Fault Detection in De-Energized Feeders</b>	<b>49</b>
3.1	Introduction of Fault Detection Methods . . . . .	50

3.1.1	Self-Powered Signal Generation . . . . .	51
3.1.2	Powered From the Energized Side . . . . .	51
3.2	The Power Electronics Aided Fault Detection Method . . . . .	52
3.2.1	Three-Phase Thyristor Bridge Based Structure . . . . .	54
3.2.2	Phase-to-Ground Faults Detection . . . . .	55
3.2.3	Phase-to-Phase Faults Detection . . . . .	61
3.3	Computer Simulation Results . . . . .	64
3.3.1	Phase-to-Ground Fault . . . . .	66
3.3.2	Phase-to-Phase Fault . . . . .	68
3.4	Experiment Verifications . . . . .	70
3.5	Alternative Cascaded Structure . . . . .	74
3.6	Conclusion . . . . .	75
<b>4</b>	<b>Harmonic Impedance Based Symmetrical Fault Detection in De-Energized Feeders</b>	<b>78</b>
4.1	Characteristics of Symmetrical Fault in De-Energized Feeders	78
4.2	Harmonic Impedance of A De-Energized Feeder . . . . .	81
4.3	The Impact of Stalled Motor . . . . .	84
4.4	The Impact of Capacitor Bank . . . . .	87
4.5	Lab Experiment . . . . .	92
4.6	Conclusion . . . . .	99
<b>5</b>	<b>Monitoring of Neutral Grounding Integrity in Multi-Grounded Neutral System</b>	<b>100</b>
5.1	Introduction of Multi-Grounded Neutral System . . . . .	100
5.2	Review of Neutral Monitoring Methods . . . . .	102
5.2.1	Neutral Impedance Measurement (NIM) . . . . .	104
5.2.2	RF Signal Injection . . . . .	106
5.3	Challenges of Neutral Impedance Measurement . . . . .	107
5.4	Active Disturbance Based Neutral Monitoring . . . . .	110
5.5	Computer Simulation of the Proposed Scheme . . . . .	115
5.6	Conclusion . . . . .	120
<b>6</b>	<b>Identification of Neutral-to-Earth Voltage Contributors</b>	<b>122</b>
6.1	The Sources of NEV . . . . .	122
6.2	Active Disturbance Based NEV Monitoring Scheme . . . . .	126

6.3	Computer Simulation . . . . .	130
6.3.1	Verification of Utility Contribution Model . . . . .	130
6.3.2	Verification of The Proposed Active Method . . . . .	133
6.4	Field Test of the Proposed Active Method . . . . .	136
6.5	Secondary Neutral Condition Monitoring . . . . .	143
6.6	Conclusion . . . . .	144
<b>7</b>	<b>Conclusions and Future Work</b>	<b>146</b>
7.1	Conclusions and Contributions . . . . .	146
7.2	Recommendations for Future Work . . . . .	149
	<b>REFERENCES</b>	<b>151</b>
<b>A</b>	<b>Broken Neutral Detection On the Secondary Side</b>	<b>163</b>



## List of Tables

1.1	The applications of condition monitoring in a distribution system	4
1.2	Summary of the existing condition monitoring methods . . . . .	8
2.1	Parameters of computer simulation for current distribution study	37
2.2	Current distribution with a Delta-Yg connection . . . . .	40
2.3	Current distribution of Yg-Yg and Y-Yg connections . . . . .	40
2.4	Comparison of soil resistivity measurements data . . . . .	42
2.5	Comparison of the simulation results and IEEE values . . . . .	43
3.1	Overall control logic and detected fault types . . . . .	56
3.2	The system parameters of computer simulation . . . . .	65
3.3	The parameters of experiment verifications . . . . .	71
4.1	The parameters of a representative 25kV system . . . . .	80
4.2	The parameters of the lab experiment . . . . .	93
4.3	The parameters of an induction motor . . . . .	95
5.1	The existing neutral condition monitoring methods . . . . .	104
5.2	An example of loads switches in the proposed signal generator	115
5.3	The system parameters of computer simulation . . . . .	116
5.4	The verification of the neutral current flow model . . . . .	117
5.5	The arrangement of the varied loads . . . . .	117
5.6	The calculated neutral impedance in different situations . . . . .	120
6.1	The system parameters of computer simulation . . . . .	131
6.2	The parameters at the customer side in computer simulation .	132
6.3	The verification of the utility contribution model . . . . .	133
6.4	The verification of the utility contribution model when simplified	134
6.5	The simulation results for the calculation of k. . . . .	134
6.6	The phase-to-phase load Zab in different cases. . . . .	135
6.7	The arrangement of the varied loads . . . . .	138
6.8	The measured current in different scenarios . . . . .	141

## List of Figures

1.1	The structure of a typical radial distribution system. . . . .	3
1.2	The monitoring and detection process of passive and active methods. . . . .	6
1.3	Current coupling is used in power line communication. . . . .	11
1.4	The capacitor voltage versus time during energy discharge. . .	12
1.5	The performance of a grounding grid during a single phase-to-ground fault. . . . .	14
1.6	Fault detection in de-energized lines is another challenge. . . .	15
1.7	Condition monitoring of neutral network is also a big concern of utility and livestock farmers. . . . .	17
2.1	The process of the proposed online monitoring scheme. . . . .	27
2.2	The remote current injection scheme . . . . .	28
2.3	The local current injection scheme. . . . .	29
2.4	A network of touch/step voltages sensors. . . . .	30
2.5	(a) The voltage measurement (1-step voltage, 2-touch voltage), (b) the structure of a sensor. . . . .	31
2.6	The Thevenin equivalent circuits of (a) touch voltage measurement, (b) step voltage measurement . . . . .	32
2.7	The evaluation process with database . . . . .	36
2.8	Computer simulation for current distribution study. . . . .	37
2.9	The structures of a tower and a pole. . . . .	38
2.10	Current distribution of the remote scheme with respect to distance from a substation. . . . .	39
2.11	Current waveforms of current distribution study. . . . .	40
2.12	Current distribution study of a Yg-Yg connection substation. .	41
2.13	The designed grounding grid in the computer simulation. . . .	42
2.14	The potential profile of a grounding grid diagonal line. . . . .	43
2.15	The potential profile with 60A grounding grid current. . . . .	44
2.16	The conductors on the left edge are stolen. . . . .	45
2.17	The potential profile after theft. . . . .	45

2.18	The soil resistivity in different seasons. . . . .	46
2.19	Three suspect spots are picked up from the diagonal line. . . .	46
2.20	Touch voltages of three suspect spots in different seasons. . . .	47
3.1	The review of the existing detection methods. . . . .	50
3.2	Single-line representation of the proposed fault detection method.	53
3.3	Waveforms of: (a) thyristor voltage and current, (b) measured voltage and current at the point X. . . . .	54
3.4	Three-phase thyristor bridge based fault detection scheme. . .	55
3.5	The gating control logic in two fault detection modes: (a) phase-to-ground fault, and (b) phase-to-phase fault. . . . .	56
3.6	Single-line equivalent circuit with zero sequence current injection.	57
3.7	The current waveforms under (a) no fault with balanced three- phase currents, and (b) a single line-to-ground fault with un- balanced three-phase currents. . . . .	58
3.8	The equivalent impedance under a single phase-to-ground fault.	59
3.9	Voltage and current pulses generated with different thyristor firing angles. . . . .	60
3.10	Signal injection for phase-to-phase fault detection. . . . .	62
3.11	Voltage and current pulses when a phase A-to-phase B fault exists. . . . .	62
3.12	Details of the three-step fault detection algorithm. . . . .	64
3.13	Configuration of the computer simulation system . . . . .	65
3.14	Three-phase currents in three steps without fault. . . . .	66
3.15	Three-phase currents in three steps under a phase C-to-ground fault. . . . .	67
3.16	Current waveforms of phase C with different fault resistances.	67
3.17	Current difference between phases under a phase C-to-ground fault. . . . .	68
3.18	Three-phase currents in three steps under a phase A-to-phase B fault. . . . .	69
3.19	The sensitivity study of a phase-to-phase fault. . . . .	70
3.20	Three-phase currents in three steps under multiple faults. . . .	71
3.21	The equivalent circuit of the experimental testing system. . . .	72
3.22	Measured voltage waveforms in the lab experiment. . . . .	72

3.23	Measured current waveforms in the lab experiment. . . . .	73
3.24	Measured current waveforms with different fault resistances. . .	74
3.25	Measured current waveforms with different firing angles. . . .	74
3.26	An alternative cascaded structure. . . . .	75
3.27	The control logic of the cascaded structure. . . . .	76
4.1	The proposed scheme for symmetrical faults detection. . . . .	79
4.2	The equivalent circuit with a symmetrical fault. . . . .	79
4.3	The voltage and current in different conditions. . . . .	80
4.4	A de-energized downstream is considered as a linear network. .	81
4.5	The harmonic resistance $R(f)$ in unfaulted and faulted cases. .	83
4.6	The harmonic reactance $X(f)$ in unfaulted and faulted cases. .	83
4.7	The equivalent circuit of a stalled motor. . . . .	85
4.8	(Note: the stalled motor: 5000hp, starting p.f.=0.2, inrush current 700%, fed with a three-phase 5MVA transformer, 25kV/4.16kV, $z=0.05$ ) . . . . .	85
4.9	The effect of a motor on the current pulse. . . . .	86
4.10	The harmonic reactance $X_f$ with a stalled motor. . . . .	87
4.11	A three-phase shunt capacitor bank is connected to a distribu- tion system. . . . .	88
4.12	The effect of a capacitor on the current pulse. . . . .	88
4.13	Harmonic resistance with a capacitor. . . . .	89
4.14	The harmonic impedance when both a 2.5MVA capacitor and a 5000hp motor connected. . . . .	90
4.15	The harmonic impedance when both a 0.25MVA capacitor and a 5000hp motor are connected. . . . .	91
4.16	The overall logic for symmetrical fault detection. . . . .	92
4.17	The diagram of the low voltage lab test setup. . . . .	93
4.18	Comparison of harmonic resistance $R(f)$ . . . . .	94
4.19	Comparison of harmonic reactance $X(f)$ . . . . .	94
4.20	Current waveforms of the induction motor test. . . . .	95
4.21	Harmonic reactance $X(f)$ of the induction motor test. . . . .	96
4.22	High impedance fault test with a tree branch. . . . .	96
4.23	Current waveforms in a tree branch test. . . . .	97
4.24	High impedance fault test with a box of mud and dirt. . . . .	98

4.25	Current waveforms in a mud and dirt test. . . . .	98
4.26	Harmonic reactance in the high impedance fault tests. . . . .	99
5.1	The typical structure of a MGN system. . . . .	101
5.2	A broken neutral largely increases neutral-to-earth voltage. . .	102
5.3	A typical Fall-of-Potential based method. . . . .	105
5.4	A typical staged single-phase fault based method. . . . .	106
5.5	An open conductor detector system based on communication.	107
5.6	The magnitude and angle of the NTE impedance with different length. . . . .	108
5.7	The neutral is broken at certain section. . . . .	109
5.8	The neutral impedance when a section of the neutral is broken.	109
5.9	The new approach for monitoring primary neutral condition. .	111
5.10	The equivalent circuit of unbalanced current caused by cus- tomer's loads. . . . .	112
5.11	Redrawing the equivalent circuit by using virtual voltage source and impedance. . . . .	113
5.12	The customer side of the fully-simulated model. . . . .	116
5.13	Test results for the factor g calculation. . . . .	118
5.14	The primary neutral is broken at both sides of the transformer connection point. . . . .	119
5.15	The primary neutral is broken far from the transformer con- nection point. . . . .	120
6.1	The current flow when only utility contributes unbalanced cur- rent. . . . .	123
6.2	The current flow when only customer contributes unbalanced current. . . . .	124
6.3	Neutral current in one day from a house test. . . . .	125
6.4	An equivalent circuit of Figure 6.1. . . . .	126
6.5	Another equivalent circuit of Figure 6.1 with a virtual voltage source. . . . .	127
6.6	The proposed active method to calculate the factor k. . . . .	128
6.7	A complete signal generator for NEV source identification. . .	129
6.8	A fully-simulated model of the utility side. . . . .	131
6.9	A five-port load model used in the simulation. . . . .	132

6.10	A ladder network compared to paralleled groundings. . . . .	133
6.11	Simulation results for the calculation of $k$ . . . . .	135
6.12	The house test arrangement. . . . .	136
6.13	Two sets of light bulbs are used as an unbalanced current generator. . . . .	137
6.14	The illustration of the measured currents when only utility contributes unbalanced current. . . . .	138
6.15	The illustration of the measured currents when only customer contributes unbalanced current. . . . .	138
6.16	Seven scenarios for creating neutral current disturbance. . . .	140
6.17	Background currents of phase A, phase B and neutral. . . . .	141
6.18	The phase currents when the loads switched from Scenario 1 to Scenario 7. . . . .	141
6.19	LMS method used for the calculation of $s$ . . . . .	142
6.20	The currents of phase A, phase B and neutral when loads changed. . . . .	142
6.21	LMS method used for the calculation of $s$ when loads change. . . . .	143
6.22	The secondary neutral is broken. . . . .	144
A.1	Unequal loads are connected with an open neutral. . . . .	163
A.2	Reviews of the existing open neutral detection methods. . . .	164
A.3	A loss of neutral detector using capacitor discharge. . . . .	165
A.4	A GFCI with open neutral protection using leakage current. . .	165
A.5	A comparator with measuring the voltage between an artificial neutral and the neutral. . . . .	166
A.6	A GFCI with a voltage sensitive device. . . . .	167
A.7	The transmitter and receiver of the RF signal based scheme. . .	168
A.8	A continuous grounding-neutral conductor monitoring system. . .	169

## **List of Abbreviations**

AC	Alternating Current
ADC	Analog-to-Digital Conversion
CT	Current Transformer
DA	Distribution Automation
DC	Direct Current
DG	Distributed Generation
DGA	Dissolved Gas Analysis
FFT	Fast Fourier Transform
FOP	Fall-of-Potential
GPR	Ground Potential Rise
GTO	Gate Turn-Off
LSM	Least Squares Method
MCU	Micro Control Unit
MGN	Multi-Grounded Neutral
NEV	Neutral-to-Earth Voltage

NIM Neutral Impedance Measurement

PD Partial Discharge

PT Potential Transformer

SFRA Sweep Frequency Response Analysis



# Chapter 1

## Introduction

In power industry, a distribution system is the last stage of power delivery to end users. Beginning from substations, a distribution system consists of transformers, distribution feeders, circuit breakers and other units. Failure of any component along the path of energy delivery may result in outage, public hazard and economic loss. Utilities are therefore very interested in monitoring these critical assets to manage distribution systems safely and efficiently.

Relays are widely used in distribution systems to detect a failure and control a breaker to switch off a faulty line or transformer. However, this type of monitoring cannot prevent a fault or detect an incipient fault. Moreover, lock-out of a circuit results in outage affecting customers negatively. Another monitoring scheme is based on measurements in a regular time interval. It may detect potential faults but it probably misses hazards developed between measurements.

Power industry has more interests in condition monitoring in the last decade, which continuously measures voltage, current, or other parameters. The measured values are compared with the preset thresholds to determine if the monitored device is healthy or not. Condition monitoring provides real-time

information, and any change in condition can be measured and compared in a timely manner. These strategies (relays, time monitoring or condition monitoring) are all based on passive measurements, which focus on detection of existing signals in a power system.

Recently, another type of monitoring has emerged, in which signals are created and injected into a distribution system and then the corresponding voltage and current are analyzed to reveal the performance of the monitored device. In contrast to passive monitoring, which is limited to monitor the existent signals, active monitoring transmits and detects unique signals created by signal generators. These signals are specially designed according to different applications.

In this introductory chapter, an overview of condition monitoring and its applications are presented. The existing passive and active methods are reviewed. The challenges faced by distribution system are discussed. The scope and outline of this thesis are presented at the end of this chapter.

## **1.1 Condition Monitoring in Distribution System**

As shown in Figure 1.1, a distribution system typically has a radial structure and it starts from a substation where power is converted from high voltage (e.g. 138kV) to medium voltage (e.g. 25kV). Then, power radiates out into distribution lines until reaching industrial and residential customers. Service transformers are used to step down the system voltage to a level suitable for industrial devices or residential appliances.

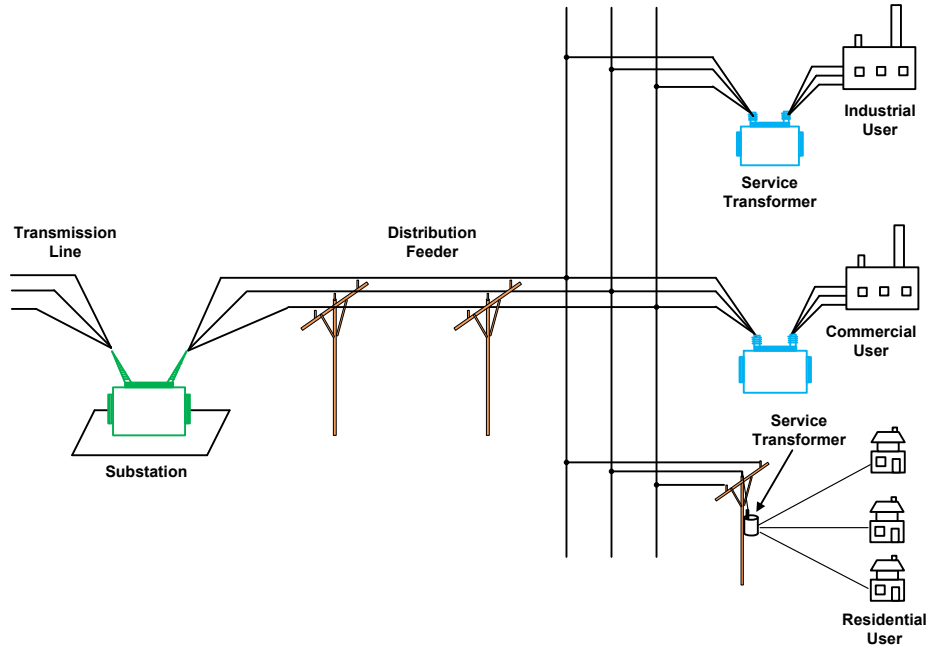


Figure 1.1: The structure of a typical radial distribution system.

Condition monitoring of these assets is important for utilities, which helps prevent equipment failure and enhance system reliability. The use of condition monitoring allows predictive maintenance, and operators are able to remove the faulty component before it causes outage or damage to other devices. Moreover, condition monitoring also help detect unperceived hazards to ensure the safety of workers and the public. Table 1.1 summarizes its applications in a distribution system.

To provide reliable energy supply, primary components in a substation such as transformers, buses and switchgears are monitored, and data are collected periodically to optimize operation and maintenance. For example, sensitive buses are selected based on data mining technologies [1] to assist system operators to apply voltage adjustment to minimize load reduction. Additionally, the condition of a grounding grid is highly related to substation safety. The

Table 1.1: The applications of condition monitoring in a distribution system

Substation	*Sensitive Buses Detection *Grounding Grid Impedance Measurement *Grid Integrity Monitoring
Feeder	*Cable Diagnostics *Overheating Monitoring *High Impedance Fault Detection
Switchgear	*Insulation Resistance Test *Thermography Monitoring *Discharge/Arcing Detection
Transformer	*Frequency Response Analysis *Winding Resistance Test *Vibration Monitoring
Distributed Generation	*Frequency Shift Detection *Anti-Islanding Disturbance Analysis *Voltage Monitoring
System	*Power Quality Monitoring *SCADA and DA *Frequency Disturbance Monitoring

impedance of a grounding grid is periodically measured [2] and its integrity is also routinely checked [3].

A distribution feeder typically has a length of several kilometers or even longer. The health of a cable is easily affected by weather, mechanical stresses and normal aging. Cable diagnostics is a necessary practice for utilities to detect precursor events so as to prevent a large failure later [4][5]. For example, an open cable is identified [6], and the faulty component can be removed prior to an outage. Overheating is another common reason to lead to premature cable aging [7]. Thermography monitoring is helpful to identify overheated sections from either overhead lines [8] or underground cables [9].

Similarly, easy-aging is a challenge of switchgear as well. Diagnostic of insulation resistance on a regular basis is very important for system reliability

and safety [10]. Vibrational signal [11] and Acoustic signature [12] can also be utilized to detect mechanical malfunction and other abnormal behaviors in a switchgear. In addition, partial discharge (PD) and small arcing are monitored to prevent equipment failure or outage [13].

Transformers are monitored in various ways [14][15]. Potential transformer (PT) and current transformer (CT) are used for voltage and current monitoring [16][17]. In addition, temperature, moisture and vibration are monitored to indicate the health of a transformer [18][19]. On top of that, transformer winding resistance are routinely tested in a de-energized mode [20].

A modern distribution system has integrated distributed generation (DG) from a variety of sources, such as photovoltaic, wind turbine and fuel cells [21]. With increased proliferation of distributed generation, islanding detection has become one major technical concern. The changes of frequency, power and voltage are monitored to determine if an islanding exists [22]. Active methods are also used by creating small disturbance into distribution system and measuring the change of impedance or system response [23].

One trend in condition monitoring is that individual monitors and sensors have been connected to form a large monitoring network. For example, a real-time power quality monitoring network is built in [24]. Supervisory Control And Data Acquisition (SCADA) and Distribution Automation (DA) are also widely used to monitor the entire distribution system [25]. Moreover, with the help of GPS and advanced telecommunication technologies, a frequency distribution monitoring network in [26] can simultaneously monitor frequency disturbance in a wide area.

## 1.2 Overview of Condition Monitoring Methods

### 1.2.1 Passive Methods Vs. Active Methods

The applications of condition monitoring are typically achieved by two different methods: passive methods and active methods. In a passive method, a signal is measured to monitor the change of a status, and this signal is from a distribution system's normal operation. In an active method, controllable signals are injected into a distribution system and system responses are monitored. Figure 1.2 shows the monitoring processes of passive and active methods. Passive methods typically only have two steps: signal detection and processing. In contrast, active methods consist of the following steps: 1) signal generation and injection; 2) signal detection and extraction; and 3) signal processing, which might have a feedback loop to adjust signals if necessary.

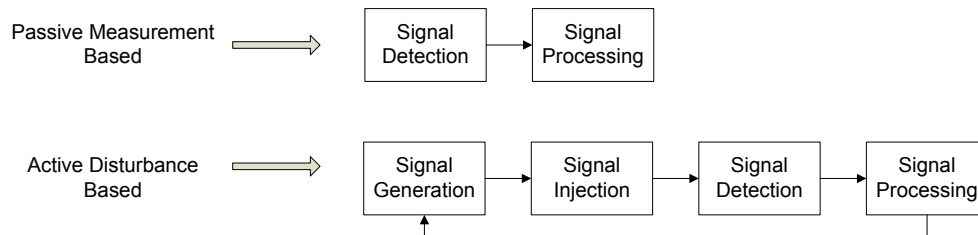


Figure 1.2: The monitoring and detection process of passive and active methods.

### 1.2.2 Offline Monitoring Vs. Online Monitoring

From the perspective of continuity, monitoring can be categorized into offline monitoring and online monitoring [27]. An offline monitoring uses diagnostic

tests discontinuously and manually. It usually requires isolation of the monitored devices, and sometimes an operating device has to be de-energized for a diagnostic test, which largely affects power system normal operation. With the help of advanced sensory electronics, communication and web-based technology, online monitoring has become available in recent years, which enable continuous and in-service monitoring of the key parameters. Compared to offline monitoring, online monitoring has several benefits.

1. Online monitoring is capable of monitoring a device or system without interrupting its normal operation. This in-service monitoring largely increases efficiency and reduces the cost of labor.
2. Online monitoring makes it possible to have real-time response, which is very useful to prevent equipment failure or rapidly restore power from breakdown.
3. Offline test needs to rebuild test environment each time. For example, cables and electrodes have to be reinstalled for substation grounding impedance measurement every time, which is time-consuming and ineffective. In contrast, after the sensors and other required devices are placed, there is no need to re-deploy these test instruments in online monitoring.

However, offline tests cannot be fully replaced by online tests. Some parameters have to be tested in a de-energized mode, such as switchgear insulation resistance test [10] and transformer winding resistance test [20].

### 1.2.3 Categorization of Condition Monitoring Methods

Table 1.2 summarizes the existing condition monitoring methods in accordance with signal sources and test continuity.

Table 1.2: Summary of the existing condition monitoring methods

	<b>Passive</b>	<b>Active</b>
Offline	*Cable Partial Discharge Mapping *Insulation Resistance Test *Transformer Winding Resistance	*Grounding Impedance
Online	*Switchgear Partial Discharge *Transformer Vibration *High Impedance Fault *Power Quality Monitoring *Frequency Monitoring Network *SCADA and DA	*Open Cable Detection *Substation Grid Integrity *DG Anti-Islanding

1. Passive Methods. Conventional monitoring approaches are based on passive methods. Without signal generation and injection, passive methods are normally simple to use, and they have been widely used in a single unit diagnostic or an entire system monitoring.

- Offline monitoring. Switchgear insulation resistance test [10] and transformer winding resistance test [20] are needed to be conducted in a de-energized mode. A cable PD mapping test [28] is also performed in an offline condition.
- Online monitoring. Passive online monitoring is the mainstream of condition monitoring. Online thermal monitoring can help detect overheated cable in a timely manner [7]. The real-time monitoring of transformer parameters including frequency, temperature and



vibration is also important for transformer protection [14]. Moreover, distribution network monitoring including power quality [24], SCADA system [25] and frequency disturbance [26] are all based on passive online monitoring.

2. Active Methods. Signal generation and injection, required by active methods, have been a big challenge of power system for a long time. The requirement of signal generation also increases the cost of an active solution. Therefore, the applications of active monitoring are limited to certain areas.

- Offline monitoring. A typical example of an active offline method is substation grounding grid impedance measurement [2]. To avoid the interference from power system, a substation is required to be isolated from power grid for the test. A current is injected and the corresponding voltage is measured to calculate the grounding impedance.
- Online monitoring. Active online monitoring recently has become a popular technical topic, which can be considered as an integration of power line signaling and condition monitoring. In [29], after an open conductor is detected, a tripping signal is injected into neutral line to activate a circuit breaker so as to isolate the faulty conductor. In [30], a unique signal is created in a substation and a detector located at a downstream DG site continuously monitor this signal. Absence of the signal is utilized as a sign of islanding, which will trigger DG protection. There are some other types of

active methods available for DG anti-islanding, such as harmonic content detection [31], impedance estimation [32] and active frequency drift [33].

3. Hybrid Methods. A hybrid method takes advantages from both passive methods and active methods. In [34], the real power shift (active technique) is initiated only when the islanding is suspected by passive techniques. As passive techniques don't disturb power system, this hybrid method can minimize the negative impact of active disturbances.

#### 1.2.4 Signal Generation in Active Methods

Signal generation was a technical barrier for expanding applications of active methods in a distribution system. It is well known that the series inductances and shunt capacitances are inherent in distribution lines, and signal attenuation become significant with the increase of frequency. In addition, High energy is required for a low frequency signal to transmit in power lines. Current technologies of signal generation are summarized as following:

- Current coupling. Current coupling is a practical way to induce a signal into distribution feeders, and it has been widely used in power line communication. As shown in Figure 1.3, a magnetic coupling circuit in [35] consists of a core, a phase conductor and a winding.

The signal generated from the winding is coupled to the phase conductor via the core. The core is made of ferrite or other soft magnetic material with substantial permeability and relatively low loss over the signal fre-

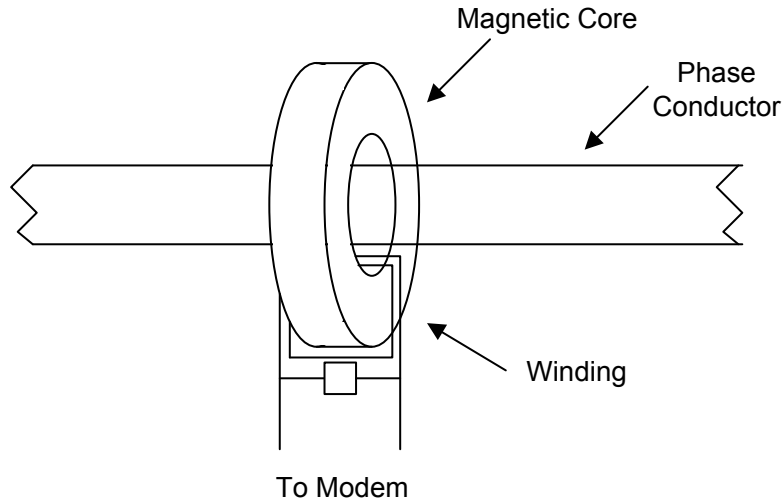


Figure 1.3: Current coupling is used in power line communication.

quencies. Current coupling can also be used in current cancellation. A stray voltage mitigator is described in [36], which couples a compensating current to a ground electrode in order to substantially cancel ground current. Similarly, a neutral current compensating device is described in [37] by means of current coupling. However, a common drawback of current coupling is that the coupled energy is usually very small. Additionally, the size and weight of a core increase at low frequencies.

- Capacitor discharge. Capacitor discharge is a valid solution to inject high voltage signal. In [38], it presents a compact signal generator by using capacitor discharge. The capacitor is pre-charged by a battery to  $10kV$ , then it is controlled to discharge the energy into a feeder. The responses of voltage and current are analyzed to estimate line impedance for fault detection. Figure 1.4 from [38] shows a capacitor voltage profile during discharge. It is seen that the energy of a capacitor is limited by its size, and the voltage in a discharge process is uncontrollable.

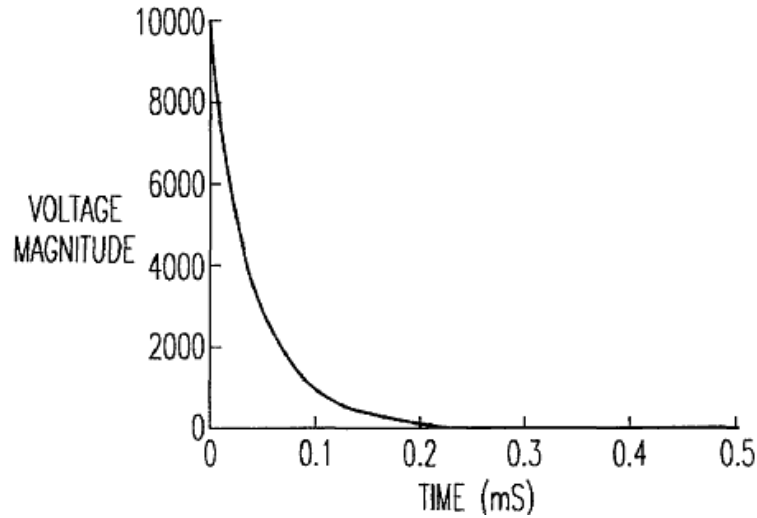


Figure 1.4: The capacitor voltage versus time during energy discharge.

- Power electronics. Power electronics is originally designed for the control and conversion of electric power. Recently, it has been used for creating small disturbance into power system. Its operating current and voltage are fairly high, which are suitable for signal injection in a distribution system. Another significant advantage is that signal strength are controllable by adjusting the firing angle of power converters. Since power electronics has become a safe, reliable and highly efficient solution, the applications of active methods have been largely increased. In [30], an active anti-islanding scheme is described, which controls a thyristor to create a discernible shift on the selected zero-crossing points. The presence of the shift represents “1”. Otherwise, it is “0”. In [39] a fault detector is presented wherein a gate turn-off (GTO) thyristor is controlled to fire at the peak of the AC voltage to create a high voltage square-wave pulse to stimulate the downstream responses. With the reduced cost of semi-conductor, power electronics based solutions will become more cost-effective.

Based on the above discussion, both passive methods and active methods are indispensable in condition monitoring. Passive methods are simple to use, and usually more economical than active methods. However, some condition monitoring cannot be performed by passive measurements due to the fact that the signals existing in power systems are limited. Instead, active methods are able to create the desired signals to fulfill the challenging monitoring tasks. A good example is when a distribution system is de-energized, all passive methods cannot function with the disappearance of electrical signals. In contrast, active methods can create and inject appropriate signals into the de-energized system and then monitor the system responses.

### **1.3 Challenges Faced by Distribution System Condition Monitoring**

Although condition monitoring has been researched for decades and a lot of applications have been developed, several challenges still exist. Five main challenges are introduced in this work. Three of them are selected to be further addressed in this thesis and will be discussed in the following chapters.

#### **1.3.1 Substation Grounding Grid Monitoring**

A grounding grid is designed to reduce the ground potential rise inside and outside of a substation during a fault. As shown in Figure 1.5, when lightning or other system contingency happens, a grounding grid creates a low

impedance path to lead fault current down to remote earth point and restrict the voltages at connecting points of electrical devices into an acceptable range. Additionally, a grounding grid can change the distribution of surface potentials and lower touch voltage and step voltage which are important for human or device safety in substations.

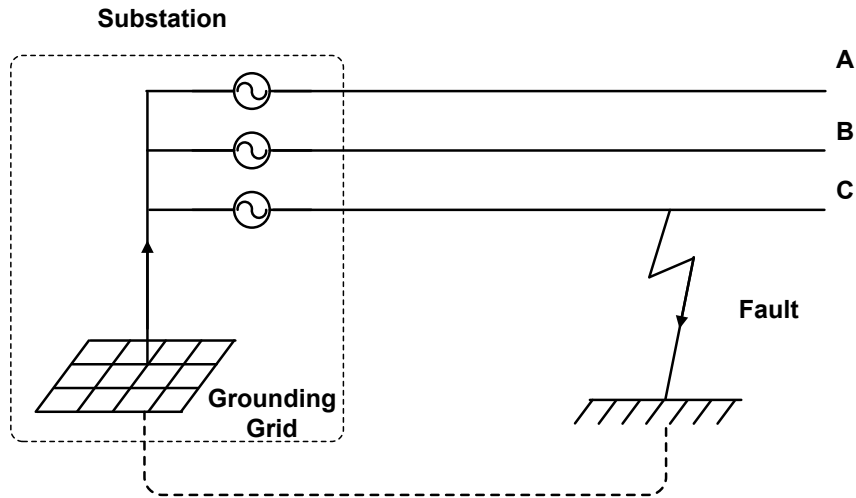


Figure 1.5: The performance of a grounding grid during a single phase-to-ground fault.

However, the performance of a grounding grid is affected by various factors such as unqualified jointing, soil erosion and theft of grounding rods [40]. To ensure a grounding grid is working under a good condition, techniques for monitoring and diagnosing the integrity of a grounding grid have been developed for many years [41][42]. Most existing methods are based on off-line measurements [43][44][45] with several defects. For example, the test system has to be redeployed when a new test is needed, and test results are largely dependent on the soil conditions during measurements [46]. To achieve accurate measurements, some tests even require to shut down the whole substation [47]. Moreover, sudden changes of a grounding grid such as those caused by theft cannot be identified in time with a long interval between

two measurements. Therefore, an active online method is highly desired for substation grounding grid monitoring.

### 1.3.2 Fault Detection in De-energized Lines

Another challenge is how to identify a fault in a de-energized system. When a part of a distribution system is locked out due to storm, faults or maintenance, it is possible that human or animals are in contact with downed conductors as shown in Figure 1.6. Restoring the energy in this situation could be very hazardous. Additionally, if a fault still exists, re-energizing the feeder can generate inrush current and damage the downstream devices. As the required electrical inputs, such as voltage and current, are zero in a de-energized system, all passive techniques are not applicable here.

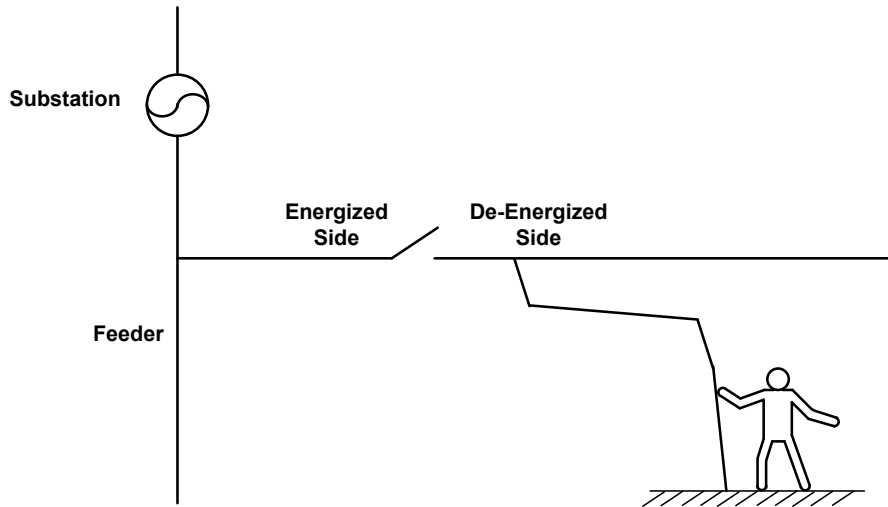


Figure 1.6: Fault detection in de-energized lines is another challenge.

The existing active schemes can be classified into two types according to the sources of the injected signal: self-powered and powered from the energized side. Self-powered methods [48] use battery or capacitor to inject detection

signals into power system. However, the signal strength is usually fixed and limited. Borrowing energy from the energized side can eliminate the use of extra power supply [49][50], but the existing methods cannot identify different types of faults in a single device.

To activate responses of a de-energized line, the key point is injection of an appropriate signal. This signal must have strong adaptivity. A low signal is required at the beginning which can be considered as an alarm to whom is touching conductors. Then, the signal is adjusted to reach a high level to mimic the medium voltage stress experienced by feeders. In addition, a stalled motor or a capacitor may mislead fault detection as they have similar performances to a fault. When energy is restored, either a stalled motor or a capacitor can raise a large inrush current which may cause nuisance trips of circuit breakers.

### **1.3.3 Monitoring of Neutral Grounding Integrity**

The third challenge is condition monitoring of a neutral network. In a three-phase four-wire distribution system, a neutral line is grounded at several points along its route [51]. With this arrangement, a high fault current will be created to trigger over-current protection devices in the case of a short-circuit [52]. When a system is not perfectly balanced, however, unbalanced currents flow into neutral systems and a portion of them circulates through groundings, which in turn produce neutral-to-earth voltage (NEV) as illustrated in Figure 1.7.



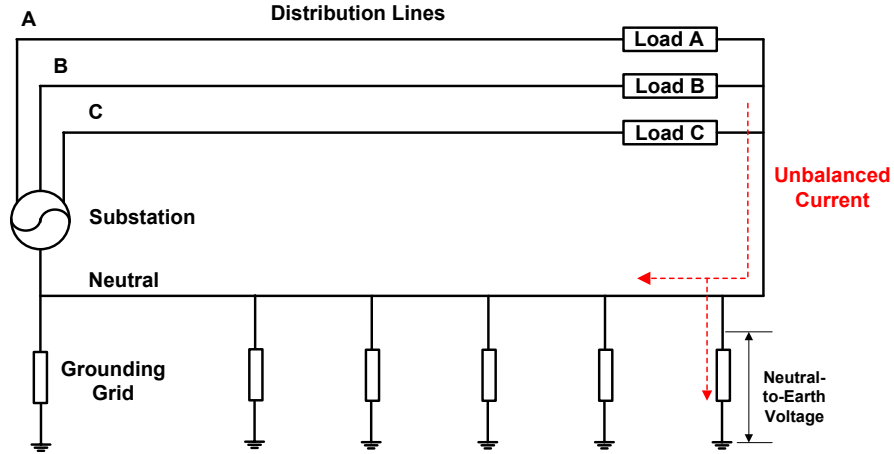


Figure 1.7: Condition monitoring of neutral network is also a big concern of utility and livestock farmers.

Broken neutral is a common reason to cause significant NEV, as it forces more current into grounds. Customers may also experience poor power quality with a poorly-connected neutral. For these reasons, routine checking of the neutral condition and monitoring NEV are good practices to prevent potential problems.

Unfortunately, there is no simple way to detect a broken or loose-connected neutral. Current practice is a trial-and-error process which combines visual inspection and selective disconnection of certain customer sites. Such a method is not only time consuming but also impact customers negatively due to temporary shutdown of power supply. Utilities have high interests in developing a precise and fast method to monitor the integrity of neutral system more efficiently.

On the other hand, it is highly desirable to develop a method to identify contributors to neutral-to-earth voltage. Since the measured neutral current consists of unbalanced currents from both utility and customer sides, it is

difficult to separate one from the other by using passive measurement. Active methods are attractive to solve this problem, as they are capable of creating disturbance from each side and monitoring neutral current contribution respectively.

#### **1.3.4 Detection of High Impedance Fault**

High Impedance Faults (HIF) usually occur at primary network level in electrical distribution systems [53]. When a downed or otherwise faulted conductor comes in contact with an object such as a tree or a surface of poor conductivity, or when a dirty insulator causes flashover between a conductor and ground, a fault is created but it does not draw sufficient current to be recognized and cleared by the conventional over-current relays or fuses [54].

Unlike overcurrent faults, which could damage the normal operation of power system, HIF is typically a safety issue for distribution systems. There are two basic types of high impedance faults: passive faults and active faults [55]. A passive fault does not generate an electric arc, which is more dangerous because the conductor does not give any visual indication of a hazard condition. An active fault produces an electric arc at the end of broken lines or cables. Most of HIFs are active faults associated with arcing which results in a risk of fires. Therefore, protection against HIF is essential.

Research on high impedance fault detection has been conducted for decades. While some progress has been made, a complete solution has not been found

because the fault current is too small for detection. The early work focused on the development of sensitive relays to detect such faults. Compared to phase relays, ground relays are helpful for clearing HIFs as they are more sensitive than phase relays. However, these relays still cannot detect most of high impedance faults with very low currents in practice. With the development of signal processing, fast computation and advanced communication, a lot of detection methods have been developed after studying the characteristics of HIF current, such as random and asymmetry based methods [56], harmonic and interharmonic based methods [57]. Composite systems which consist of several individual algorithms from time domain and frequency domain are also developed in [58][59].

However, various normal operations, like capacitor bank operations, transformer tap changing and switch operations, unfortunately create the similar transient as HIF that causes distinguishing HIF from normal operations very complicated. As fault implementation of HIF detector for feeder tripping may increase outages and create new hazards, the reliability of discrimination becomes the major concern for the detection.

### **1.3.5 Transformers Condition Monitoring**

Transformers are the most costly capital equipment in power system and they are designed for a long lifetime. To optimize their operations and maximize their lifetime, utilities are highly interested in evaluating the condition of transformers. Insulation behavior is a main indicator [60] to assess the performance of a transformer. Active parts including core, windings, insulation oil,

bushing and on-load tap changer are important to determine the degradation of an insulation system. The monitoring and assessment of such components are critical to identify malfunction and prevent incipient failures.

Although several tests have been improved from offline measurement to online measurement, some tests are still required to be carried out in an offline mode, such as transformer winding resistance measurement, turns ratio test and sweep frequency response analysis (SFRA). For example, SFRA is implemented to investigate the mechanical integrity of a transformer [61]. A given frequency is injected from a winding, and the resulting signal is measured at the other end. The comparison of results from the current test with previous tests indicates the movement of the windings within the testing transformer. However, all these offline based methods need to de-energize a testing transformer and take it off from service before tests, which largely affects system reliability.

By using the advanced sensory and communication technologies, a lot of tests can be conducted in an online mode, such as monitoring of tap changer vibration, oil moisture and temperature, dissolved gas analysis (DGA), and partial discharge detection. For example, a scheme based on vibration signatures is introduced in [62] for monitoring of transformer on-load tap-changers. A sensor is attached to a testing transformer to detect signal produced by contact movements. The collected data is then analyzed to compare with a number of signatures of normal conditions. An alarm is raised in a timely manner when a monitored parameter exceeds the preset limit. On the other hand, the test results can also help optimize the maintenance if the monitored value is within the limit, which indicates the testing transformer is still in the healthy state.

However, there are several challenges associated with these online monitoring methods. Selection of thresholds is very critical. False alarm can be triggered if thresholds are not selected appropriately. Another challenge is that the signatures of vibration, moisture and temperatures are not the same in different transformers. A learning process has to be considered before implementing the online monitoring. For a large power system, the efficiency is affected due to the investment of time for this learning process.

## 1.4 Research Objectives

The scope of this thesis focuses on improving the effectiveness of condition monitoring in distribution systems by using active disturbance based techniques. With the help of power electronics, modern computer and communication technologies, this thesis aims to address challenges faced by condition monitoring in three different subjects, including: substation grounding grids monitoring, fault detection in de-energized lines and neutral grounding monitoring. The research objectives are summarized as following:

1. Present the problems of substation grounding grid monitoring, and propose a current injection based scheme which is able to address safety concerns of a substation. In addition, develop an online monitoring scheme to continuously monitor a grounding grid.
2. Investigate fault detection in de-energized feeders, and design a device to detect different types of faults in a three-phase power system. Develop an algorithm to distinguish a fault from a stalled motor or a capacitor

bank, which behaves like a short-circuit when voltage is applied.

3. Study the impact of broken or loose-connected neutral on neutral-to-ground voltage, and investigate the challenges of neutral monitoring. Develop an active method based on this study to monitor neutral condition. Furthermore, propose an algorithm to quantify the contributions of the utility and customer to neutral-to-ground voltage.

## 1.5 Thesis Outline

Real-time evaluation of a substation grounding grid is an effective approach to ensure substation safety. Chapter 2 describes a power electronics based online monitoring scheme to assess the performance of a grounding grid. Unlike conventional approaches which measure substation grounding impedance, this scheme uses step voltage and touch voltage as safety indicators. By taking advantage of online database, the voltages are continuously measured and compared to the present thresholds and historical data. The proposed online monitoring scheme can effectively reveal the up-to-date condition of a grounding grid from safety perspective. This work is published in [63].

The key challenge of fault detection in a de-energized system is how to inject an appropriate signal into downstream. Chapter 3 presents the characteristics of a de-energized system, and describes a thyristor-aided fault detection scheme to address the challenge. Various combinations of signals are created in a signal generator for detecting different types of faults. The algorithms for asymmetrical faults identification are also introduced. The effectiveness of

the proposed active scheme is verified through simulation and lab tests. This work is published in [64].

Chapter 4 presents a harmonic impedance based algorithm for symmetrical fault detection, which analyzes the features of harmonic impedance in different conditions to determine if a symmetrical fault exists. In addition, it can distinguish a fault from a stalled motor or a shunt capacitor, which behaves like a short-circuit when a voltage is applied. This algorithm is tested through simulation and lab experiments. This work is published in [65].

By forcing more current flowing into ground, a poorly-connected neutral can largely increase neutral-to-earth voltage, which is hazardous to livestock and public safety. Chapter 5 describes an active disturbance based method which analyzes the sources of unbalanced currents to indicate the integrity of neutral grounding. As the neutral impedance measurement is not required, the effort of finding a zero potential earth point is avoided.

Chapter 6 describes an active method to determine the contributors of neutral-to-earth voltage. Current disturbance is created from the utility and customer sides, respectively. The sources of unbalanced current are analyzed to determine the contributions of utility and customer. The proposed neutral current flow models are verified in computer simulation and the active method is experimentally proved through a test in a residential house.

Chapter 7 presents the thesis' conclusions and contributions, followed by recommendations for future research.

## Chapter 2

### Online Monitoring of Substation Grounding Grid Conditions Using Touch and Step Voltage Sensors

Proper grounding is the first line of defense against lightning or other system contingency to ensure the safety of operators and power apparatus. A poor grounding system not only results in unnecessary transient damages, but also causes data and equipment loss, plant shutdown, as well as increases fire and personnel risk. This chapter describes an online monitoring scheme which continuously injects current into a grounding grid and measures the corresponding touch voltage and step voltage to assess substation safety. The testing current is created by a thyristor-based signal generator which is connected between a phase conductor and ground to stage a temporary and controllable fault. There is no extra cable needed for current flow as power line is utilized as a path for current injection. With the help of an online database, the assessment can be performed in real-time. This scheme is very suitable for long-term online monitoring.



## 2.1 Introduction

The performance of a grounding grid is affected by various factors such as unqualified jointing while building, electromotive force of grounding current, soil erosion and theft of grounding rods. Thus, monitoring and diagnosing the condition of a grounding grid has been an active research field for many years. However, almost all techniques implemented or proposed for grounding monitoring are offline types where special instruments are installed for grounding condition check on a regular or as-needed basis. These existing methods can generally be categorized into two types: measurement of grounding impedance and detection of grounding integrity.

The Fall-of-Potential (FOP) method is the basic scheme for grounding impedance measurement and it has been implemented for many years. Its key point is to correctly locate the potential probe, which is quite time-consuming. A lot of variations have been proposed to improve this scheme, such as by using variable frequency source [41] or implementing multiple electrodes [42]. A method taking account of current split in transmission and distribution grounding system is further developed in [43] for accurately measuring the impedance of in-service substations. However, the potential probes are still indispensable in these FOP-based schemes. Several enhanced grounding grid computer models are developed recently with considering soil layers' depth in [44][45] or based on electromagnetic field methods [66][67]. But, the accuracy of these models relies on the soil resistivity measurement. Once the soil condition is changed, potential electrode needs to be re-located and it obviously increases labors.

Monitoring the integrity of a grounding grid is another way to evaluate the performance of grounding grid [68]. However, the computation of this method depends on many uncertain factors such as soil conductivity, humidity and climate [69]. A device based on measuring magnetic induction intensity is designed to diagnose the grounding grid corrosion in [70]. It requires the current injection between all possible grounding leads on the ground surface to increase accuracy, which is not practical in a large scale substation.

All of the aforementioned methods are offline-based, which at best give one-shot measurement results. If another set of results is needed, the measurement system must be redeployed. The offline-based methods have significant disadvantages. Firstly, the results are largely dependent on the soil condition at the time of measurement. Secondly, sudden changes of a grounding grid such as those caused by theft cannot be identified timely. To solve these problems, the methods that can monitor the grounding condition on a continuous, i.e. online, basis is highly desired.

## **2.2 The Proposed Online Monitoring Scheme**

As shown in Figure 2.1, the process of the proposed online monitoring scheme includes a) current generation and injection, b) touch voltage and step voltage measurement and c) safety assessment. If the variation between the newly measured data and historical data is below the preset threshold plus the measured data does not exceed the limits defined in the IEEE standard [40], the grounding grid under test is considered to be in a good condition. Otherwise, a warning event will be created and then mandatory inspections in the sus-

pected spots with high touch voltage or step voltage will be carried out.

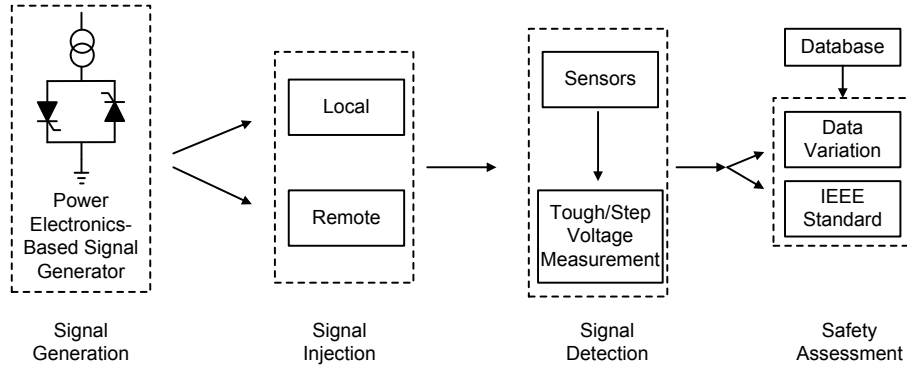


Figure 2.1: The process of the proposed online monitoring scheme.

### 2.2.1 Testing Current Generation and Injection

The signal generator for testing current generation consists of a pair of thyristors connected to the supply via a single-phase step-down transformer, which convert high voltage or medium voltage to low voltage ( $< 1kV$ ) for the normal operation of thyristors. When the thyristors are fired with a preset firing angle, a testing current will be injected into the system from the primary side of the transformer [30]. The two thyristors are operated alternately to create a sinusoidal waveform. To reliably measure the resulting touch and step voltages, the duration of injected current cannot be too short to establish stable potential profiles [71]. The minimum time for tolerable touch or step voltage calculation is  $30ms$  according to [40]. On the other hand, the injected current is required not to interrupt the normal operation of grounding fault protection relay, in which the minimum trip time is about  $100ms$  [72]. In this work, the duration of current injection is therefore set to  $50ms$ , which is within the range between  $30ms$  to  $100ms$ . Unlike grounding impedance measurement, which needs a square waveform to obtain various frequency

components to avoid the fundamental frequency interference from power system, this work focuses on safety evaluation at substations and the sinusoidal waveform is used to mimic a shot-circuit.

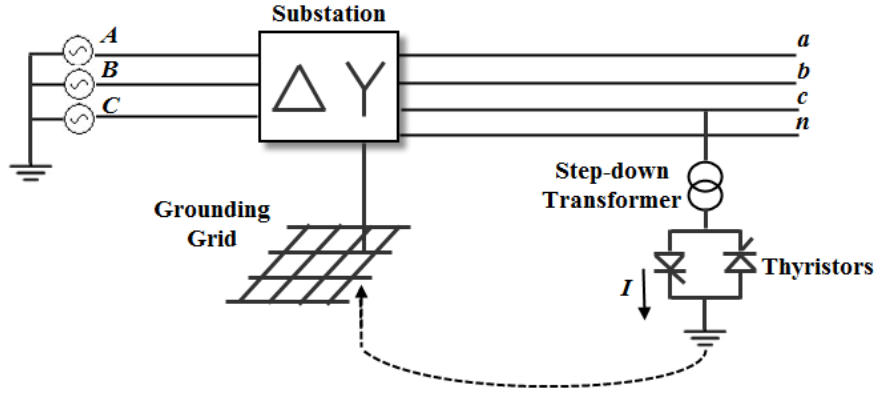


Figure 2.2: The remote current injection scheme

This signal generator can be installed either remotely or locally. In the remote source scheme (See Figure 2.2), the signal generator is installed at a downstream site far from the substation to minimize the impact of the current injection to the ground potential profile. As ground is utilized as a current path from the injected site to the substation grounding grid, the extra current cable is not needed [73].

In the local source scheme, the signal generator including a step-down transformer can be installed in the substation as shown in Figure 2.3. The current is directly injected in a substation and it returns from the power source. Since the device is located in a substation, maintenance can be conveniently achieved, which is important for long-term monitoring. However, a large transformer is needed as the signal generator has to be installed at the high voltage side in a substation. This signal generator cannot be installed at the grounded secondary side, since a current loop is established via the grounded

neutral and the test current will not flow through the tested grid to the remote earth [74].

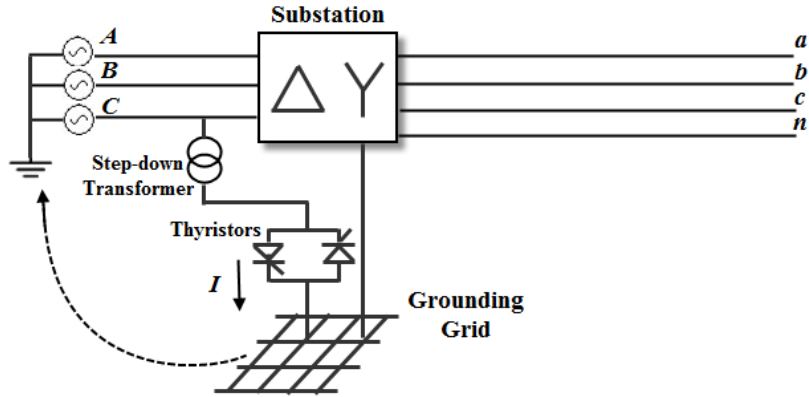


Figure 2.3: The local current injection scheme.

### 2.2.2 Touch/Step Voltage Based Sensor Network

The current injected into a grounding grid results in the rise of touch voltage and step voltage, which are directly related to personal safety in and around a substation. Touch voltage is defined as the potential difference between an exposed metallic structure within reach of a person and a point where that person is standing on the earth, while step voltage is defined as the difference in potential between two points in the earth spaced one meter (a step) apart [75]. The measurement of touch and step voltages can be easily conducted at many points of interest in the substation, which is very suitable for long-term online monitoring.

A wireless sensor network for touch and step voltages monitoring is shown in Figure 2.4. Typically, a grounding grid is buried 0.5 ~ 1 meter under ground. The touch/step voltage sensors are distributed at corners of a grounding grid

and some other frequently visited spots with special concern of human safety. All of these sensors can transmit signals wirelessly to a central computer. The computer is responsible to collect, classify and update the data recorded from sensors.

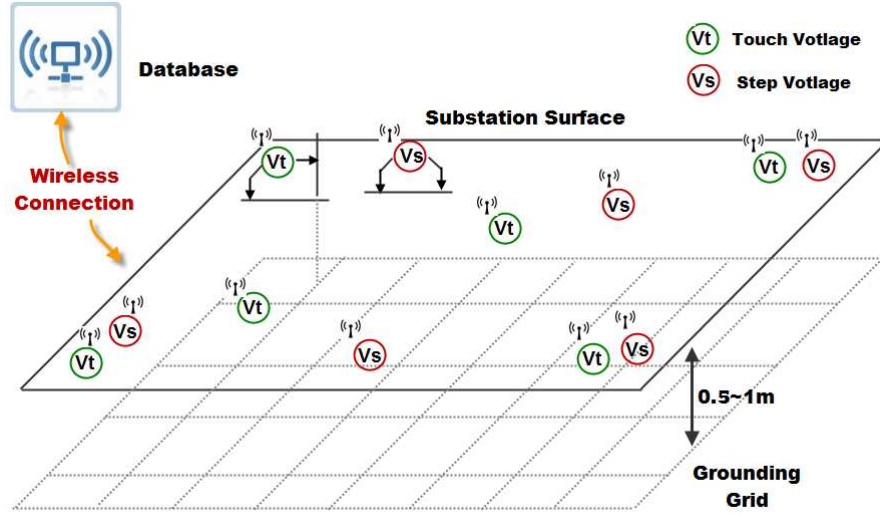


Figure 2.4: A network of touch/step voltages sensors.

According to the IEEE Standard 81.2 [75], the simulated-personnel method is recommended for touch and step voltages measurement. This method utilizes a resistor with  $1000\Omega$  resistance represents human body resistance and is connected between two “feet”. Each foot is made by a metallic plate with  $200\text{cm}^2$  surface area and  $20\text{kg}$  weight. A voltmeter is installed across the resistor with high internal impedance so as not to influence measurements. A device is designed to measure either touch voltage or step voltage as seen in Figure 2.5. The distance  $D$  between two feet is adjustable, which is  $0.5\text{m}$  for  $V_{touch}$  measurement and  $1\text{m}$  for  $V_{step}$  measurement, respectively. Moreover, an extra probe is used to contact the exposed conductive surface for touch voltage measurement.

A voltage transducer is used to measure the voltage across  $R_b$ . The measured value is converted to the digital format by using an analog-digital-conversion (ADC) module. A micro control unit (MCU) processes the data, and the results are finally transmitted to a central computer through a wireless communication module. In this research, 2.4GHz Zigbee signal is used for wireless transmission [76], as its range can be reach up to 100 meters, which is adequate for a small or medium size distribution substation. Moreover, it can be easily configured to handle a wireless sensor networking application at a low cost.

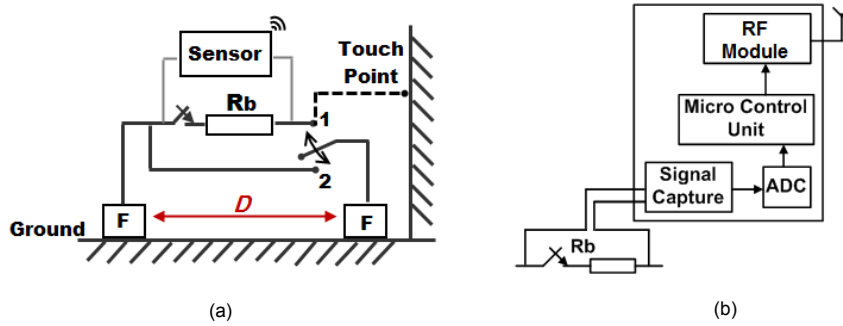


Figure 2.5: (a) The voltage measurement (1-step voltage, 2-touch voltage), (b) the structure of a sensor.

The Thevenin equivalent circuits of touch/step voltage measurements are shown in Figure 2.6.  $V_{dt}$  is the potential difference between the feet and the touch point,  $V_t$  is the touch voltage,  $R_{fp}$  is the foot resistance when two feet are in parallel,  $R_b = 1k\Omega$  is the human body resistance, and  $V_{ds}$  is the potential difference between two feet,  $V_s$  is the step voltage,  $R_{fs}$  is the foot resistance when two feet are in series. The touch voltage and step voltage can be expressed as

$$V_t = \frac{V_{dt}}{R_b + R_{fp}} \times R_b \quad (2.1)$$

$$V_s = \frac{V_{ds}}{R_b + R_{fs}} \times R_b \quad (2.2)$$

However, the metallic plates installed on the surface of the ground are likely to be corroded due to humidity or other factors, which results in the increase of their resistance accordingly. Equations (2.1) and (2.2) indicate that the measured voltage ( $V_t$  or  $V_s$ ) decreases with the increase of the “feet” resistance ( $R_{fp}$  or  $R_{fs}$ ) with the same potential difference ( $V_{dt}$  or  $V_{ds}$ ). In this case, the measured touch/step voltage will be lower than the normal value and it may mislead the assessment.

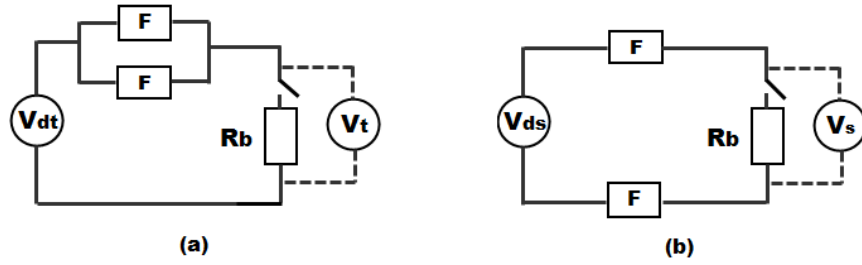


Figure 2.6: The Thevenin equivalent circuits of (a) touch voltage measurement, (b) step voltage measurement

To eliminate the effects of the “feet” resistance variation, the voltages are measured twice, one in a close circuit during one signaling period and the other in an open circuit during the next signaling period. As the switching is operated after current injection, it would not cause arcing and it also has no requirement on the switching speed. As shown in Figure 2.6, an electrical contactor is utilized for the switching purpose. In an open circuit, touch voltage  $V_{t.oc} = V_{dt}$  and  $V_{s.oc} = V_{ds}$ . Resolve (2.1) and (2.2), the resistance of  $R_{fp}$  or  $R_{fs}$  can be obtained.

$$R_{fp} = \left( \frac{V_{t.oc}}{V_t} - 1 \right) \times R_b \quad (2.3)$$

$$R_{fs} = \left( \frac{V_{s.oc}}{V_s} - 1 \right) \times R_b \quad (2.4)$$



If the variation between the estimated  $R_{fp}$  (or  $R_{fs}$ ) and its nominal value is larger than a predetermined value, the measured  $V_t$  (or  $V_s$ ) cannot be directly used. In this case, the metallic feet need to be replaced by a new pair of plates. Alternatively, these voltages ( $V_t$  and  $V_s$ ) can be adjusted according to the following equations

$$V_t = \frac{V_{t.oc}}{R_b + R_{f_{pn}}} \times R_b \quad (2.5)$$

$$V_s = \frac{V_{s.oc}}{R_b + R_{f_{sn}}} \times R_b, \quad (2.6)$$

where  $R_{f_{pn}}$  is the nominal value of  $R_{fp}$ ,  $R_{f_{sn}}$  is the nominal value of  $R_{fs}$ . According to [40], the limit of touch/step voltage is a function of a) shock duration or fault clearing time  $t_s$ , b) system characteristics, c) body weight and d) foot contact resistance as shown in (2.7) and (2.8). The constant  $k$  is 0.116 for a person with 50kg body weight, while it is 0.157 for a person with 70kg body weight.  $C_s$  is the surface layer derating factor, and  $\rho_s$  is the surface material resistivity in  $\Omega \cdot m$ .

$$V_{t.limit} = (1000 + 1.5C_s \cdot \rho_s) \frac{k}{\sqrt{t_s}} \quad (2.7)$$

$$V_{s.limit} = (1000 + 6C_s \cdot \rho_s) \frac{k}{\sqrt{t_s}} \quad (2.8)$$

Since the injected current is much smaller than the maximum fault current, the measured touch/step voltage is therefore much lower than the limits defined in (2.7) and (2.8). Thus, the original measured data is intentionally scaled up to the maximum value by using (2.9) and (2.10) when the data transfer to the database. The decision is then made by the comparison of the measured data with historical data or with the limits provided by (2.7) and

(2.8).

$$V_{tmax} = V_t \times \frac{I_{fault}}{I_{injection}} \quad (2.9)$$

$$V_{smax} = V_s \times \frac{I_{fault}}{I_{injection}} \quad (2.10)$$

For personal safety consideration, touch voltage is more severe than step voltage [77]. The current caused by touching an exposed conductor flows through the heart, whereas the one caused by step voltage bypass the heart. Therefore, a tolerate touch voltage is much lower than a tolerate step voltage. Generally, satisfying the touch voltage safety criteria in a substation automatically ensures the satisfaction of the step voltages safety criteria. In this work, most areas in the substation are examined for touch voltage, and only the edges of the grid are examined for step voltage.

### 2.2.3 Intelligent Evaluation with Online Database

Another novel feature of the proposed scheme is the implementation of online database. It is known that the resistivity of the surface soil layer would be changed in different seasons, which may cause touch/step voltages moving to the hazard side [69]. For example, if the thickness of a low-resistivity soil layer in raining season is smaller than the buried depth of a grounding grid, the touch voltage increases. For another example, the high resistivity soil layer formed in a freezing season would cause the increase of the touch/step voltage as well. One major defect of the existing offline monitoring method is the inability of tracking seasonal influences on substation safety. With the support of an online database, the changes of touch/step voltage can be continuously monitored and recorded. Particularly, during the severe conditions,

like continuous raining or freezing seasons, the frequency of online monitoring can be increased in order to find the potential hazards in time.

Corrosion, which can cause damages of effective connections among conductors, is another factor affecting a substation grounding system. The grounding grid corrosion is caused by acid or alkali in soil and the corrosion rate can reach up to 8.0mm per year according to statistic results [78]. This situation becomes worse as a steel-grounding or galvanized steel-grounding system is widely used, which is more easily corroded than copper so that it requires more accurate and more frequent assessment of a grounding grid.

Theft of grounding rods can suddenly change the integrity of a grounding grid. Failing to detect this change in a timely manner will cause serious consequences. Therefore, the changes of touch and step voltages at the same point are recorded, so that synthesized and reliable estimation can be made not only depending on the IEEE standard but also on the variation due to seasonal influence, corrosion or theft.

Based on the above analysis, an intelligent evaluation (See Figure 2.7) can be made as following:

1. Generate and inject a testing current into a grounding grid periodically. Measure the resulting touch/step voltages with a sensor network.
2. Transfer the data to a central database. Scale the measured touch/step voltages to the maximum touch/step voltage.
3. Compare the maximum touch/step voltage with IEEE standard under

the same parameters, like fault clearing time and the body weight, etc. If it exceeds the safe value, a warning event is created and the suspected location is reported to substation operators for further analysis.

4. Compare the measured touch/step voltages with the historical data at the same location. If the variation is larger than the preset threshold, a warning event is created even though the actual value does not exceed the standard. A mandatory examination will be taken around the suspected point to check if the conductors are stolen or broken due to corrosion.
5. If no suspected spot is found, the database is updated with the new measured data and meteorological parameters, such as temperature and humidity. Then, after a preset period, go back to the first step.

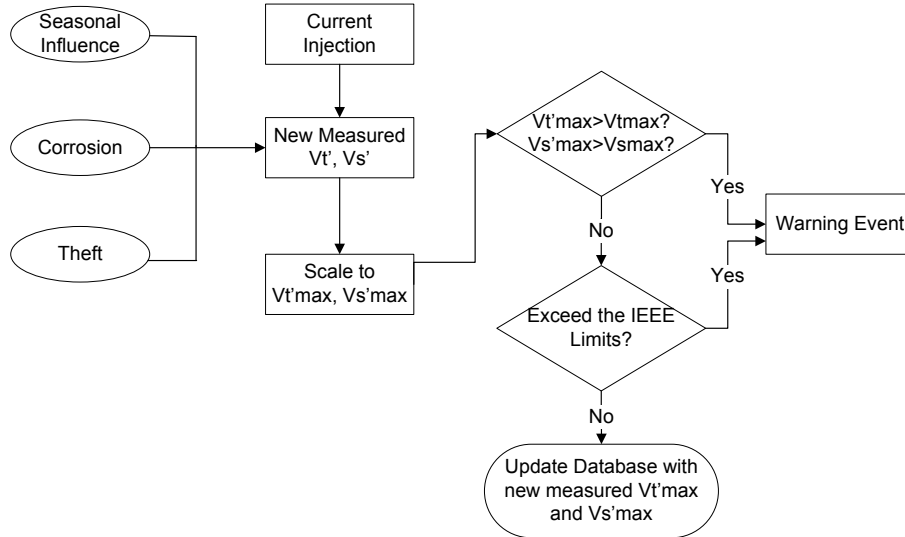


Figure 2.7: The evaluation process with database

## 2.3 Study of Current Distribution

A simulation model is built to study current distribution of both remote and local injection schemes as shown in Figure 2.8. The testing substation converts power from 125kV to 25kV via a Delta-Yg connection transformer. An overhead ground wire, so called skywire, accompanies with transmission lines. The ground resistance of a tower is  $32\Omega$ . At the secondary side, the neutral line of a distribution system is multiple-grounded with  $15\Omega$  at each grounded connection. The structure details of a tower and a pole are illustrated in Figure 2.9. Other parameters are listed in Table 2.1.

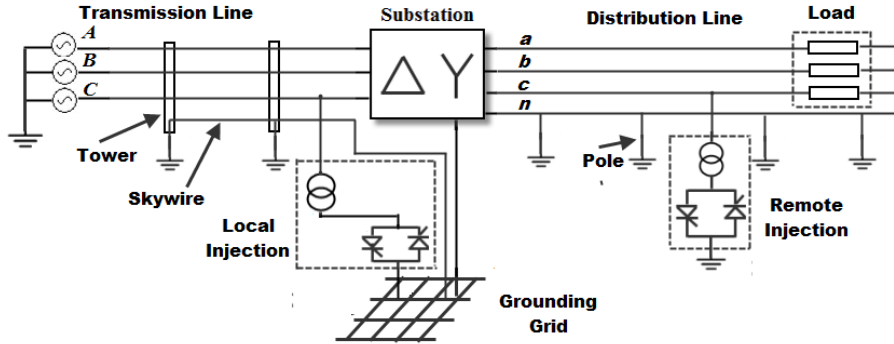


Figure 2.8: Computer simulation for current distribution study.

Table 2.1: Parameters of computer simulation for current distribution study

Power Supply	3phs, 60Hz, $V_{LL}=115\text{kV}$ , $X=3.0\Omega$
Substation Transformer	50MVA, 115kV/25kV, Delta-Yg.
Transmission Line Tower	$R_{g-tower} = 32\Omega$ .
Distribution Line Pole	$R_{g-pole} = 15\Omega$ .
Grounding Grid Impedance	$R=0.2\Omega$ , $L=10\text{mH}$ .
Load	R-L load, 4MVA, p.f.=0.9

In the remote injection scheme, a temporary fault is staged at downstream of a substation to create a fault current between a phase and ground. However,

with the presence of the multiple grounded points on the neutral, such as pole grounds and transformer grounds, the current is divided before reaching the substation grounding grid. As shown in Figure 2.10, the current division of the remote injection scheme depends on the distance between the location of the staged fault and a substation. The injected current is  $I_f$  and the grounding grid current is  $I_g$ . When the staged fault is located 5km away from the testing substation, only 37% of the injected current flows back through the substation grounding grid.

The local injection scheme requires a pair of thyristors connected between a single phase of transmission line and the grounding grid by a step-down transformer. Due to the existence of overhead ground wires and neutral lines, not all fault current flow through a grounding grid to the remote earth [74]. The simulation results (see Table 2.2) show that 73.58% current ( $I_g$ ) across the grounding grid, 26.70% current ( $I_s$ ) in skywires and 10.59% current ( $I_n$ ) in neutral lines. Disconnecting skywires and neutral lines can largely increase

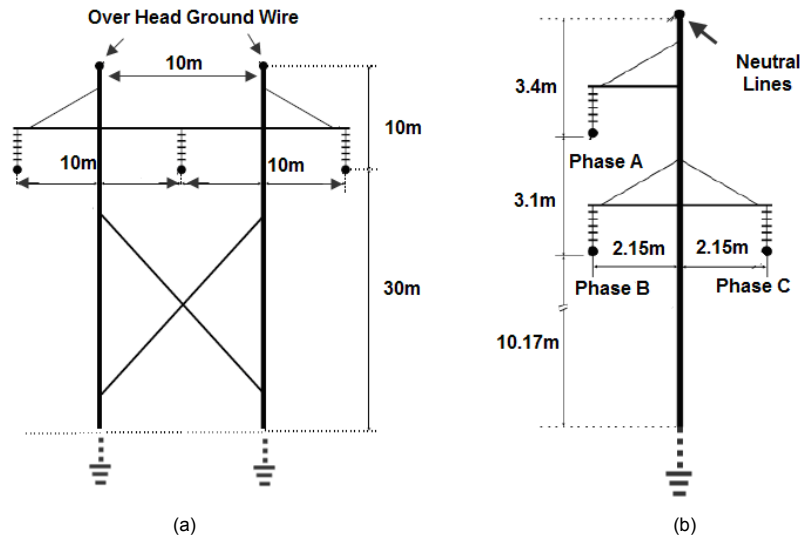


Figure 2.9: The structures of a tower and a pole.

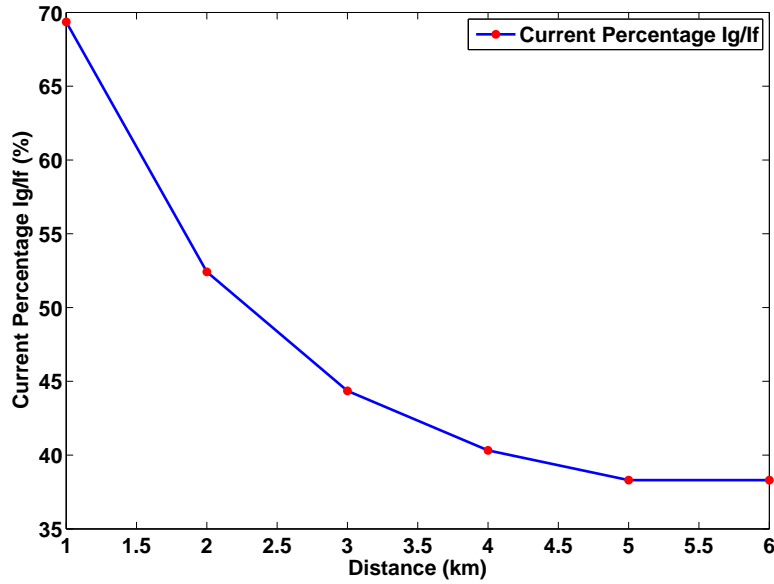


Figure 2.10: Current distribution of the remote scheme with respect to distance from a substation.

the grounding grid current. However, it is impossible to disconnect these grounded wires for long time monitoring in reality. From touch voltage simulation which will be discussed later, 60A current flowing into a grounding grid can result in about 3 ~ 13V touch voltage, which is large enough for effective detection. The current waveforms for the local injection scheme are shown in Figure 2.11. Typically, there are relays implemented in the substation for ground fault protection. These protective relays have an inverse current/time characteristic, which suggests they can tolerate high current with a short duration. As the duration of the injected 60A current is about 50ms, shorter than 0.1s, it does not interrupt the normal operation of the protective relays [72].

Figure 2.12 shows a substation transformer with a Yg-Yg connection. A staged fault is created at the primary side when the thyristors are turned on

Table 2.2: Current distribution with a Delta-Yg connection

	$I_f$	$I_g$	$I_s$	$I_n$	$I_g/I_f\%$
All Connected	85.87	63.18	22.93	9.10	73.58%
Neutral Disconnected	85.70	69.72	23.13	0	80.77%
Skywire Disconnected	84.31	75.73	0	12.02	89.82%
All Grounded Lines Disconnected	85.43	81.42	0	0	95.31%

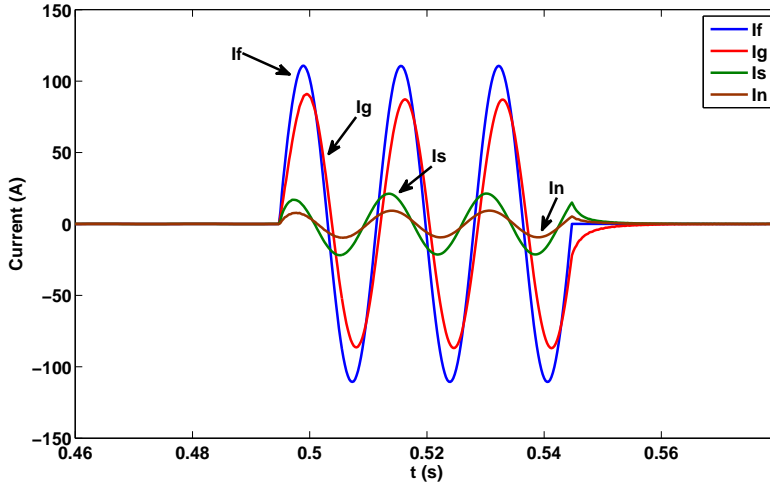


Figure 2.11: Current waveforms of current distribution study.

for 50ms. The computer simulation results are listed in Table.2.3. If all the grounded wires are connected, the current ratio of  $I_g/I_f$  is 81.9% for Yg-Yg connection and it is 76.8% for Y-Yg connection.

Table 2.3: Current distribution of Yg-Yg and Y-Yg connections

<b>Transformer Type</b>	$I_f$	$I_g$	$I_s$	$I_n$	$I_g/I_f\%$
Yg-Yg	82.02	67.17	16.26	7.78	81.9%
Y-Yg	84.87	65.18	21.93	10.10	76.8%



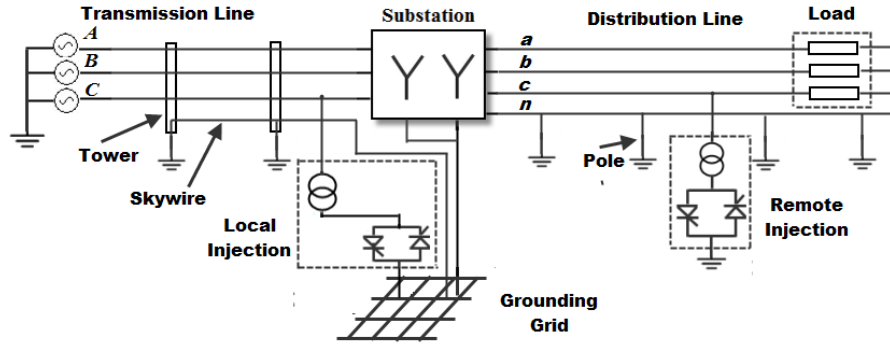


Figure 2.12: Current distribution study of a Yg-Yg connection substation.

## 2.4 Computer Simulation of the Proposed Online Monitoring Scheme

Computer simulations have also been conducted in CYMGRD [79] to measure touch/step voltages and analyze the influence of seasonal changes, corrosion and theft. The designed grounding grid as shown in Figure 2.13 is 150 meters long and 100 meters wide. All conductors are buried at a depth of 0.5 meters. X-axis has 8 conductors and Y-axis has 10 conductors. The diameter of all conductors is 19.1 mm. Plus, 30 grounding rods are vertically connected to the grounding grid. Each rod is 5 meters long with diameter 2.858 cm. Moreover, the station surface is with crushed rock of 2500 Ohm-meter resistivity at a thickness of 0.3 meters and the exposure duration is 0.36s with 4000A fault current.

A two-layer soil model is implemented for the soil resistivity simulation. From the data provided by IEEE standard (See Table 2.4), both the upper and lower layers resistivity can be calculated and the depth of the upper layer can be estimated as well. The results from this soil model calculation are consistent

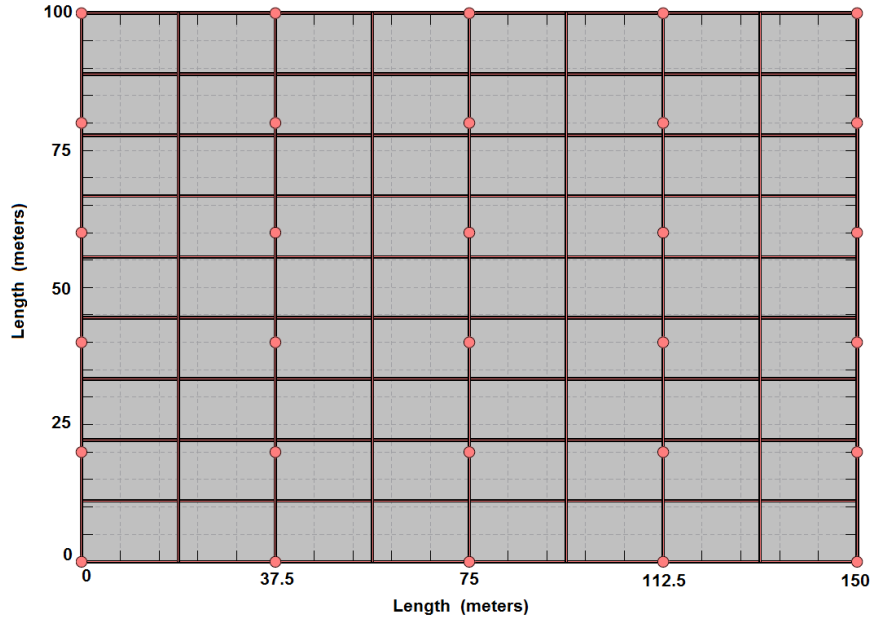


Figure 2.13: The designed grounding grid in the computer simulation.

with the calculated values from the IEEE standard as shown in Table 2.5. The maximum permissible touch and step voltages calculated by (2.7) and (2.8) are 1084.2V and 3551.8V respectively.

Table 2.4: Comparison of soil resistivity measurements data

Distance(m)	1.524	4.573	6.098	9.146	15.244
R ( $\Omega$ )	29.55	9.39	6.46	3.52	1.50
$\rho$ ( $\Omega \cdot m$ )	283.06	269.67	247.57	202.12	144.05
Distance(m)	21.341	27.439	33.537	39.634	45.731
R ( $\Omega$ )	0.90	0.64	0.51	0.42	0.36
$\rho$ ( $\Omega \cdot m$ )	120.28	110.68	106.41	104.34	103.16

The potential profile of a grounding grid diagonal line is shown in Figure 2.14. Apparently, touch voltages at corners are much larger than those in the center due to the fact that fewer conductors are buried around corners than the center. This profile also confirms that the value of maximum permitted touch potential has a dominant role in determining the design of a grounding grid.

Table 2.5: Comparison of the simulation results and IEEE values

	Upper Layer Resistivity ( $\Omega \cdot m$ )	Lower Layer Resistivity ( $\Omega \cdot m$ )	Upper Layer Thickness (m)
IEEE Std.	300	100	6.1
Simulation	298.26	99.98	6.11

If a grid satisfies the requirements for safe touch potentials, it is very unlikely that the maximum permitted step potential will be exceeded. In Figure 2.14, the margin between the calculated touch voltage and the permissible touch voltage is about 200 ~ 800V, while this margin for step voltage is as large as 3500V.

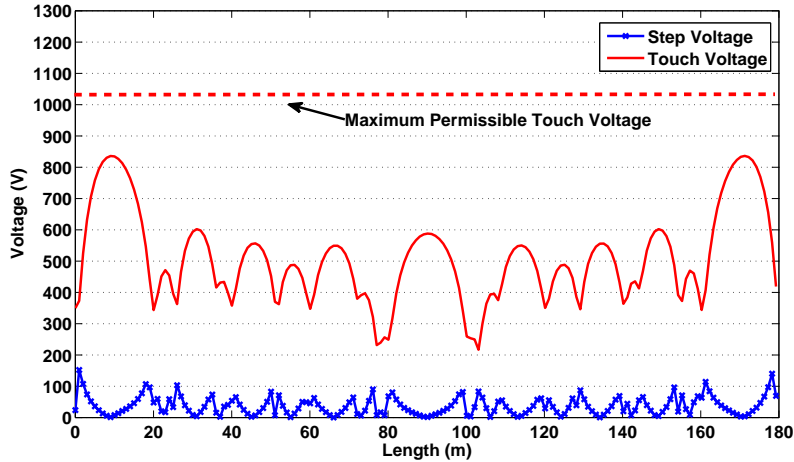


Figure 2.14: The potential profile of a grounding grid diagonal line.

The profile in Figure 2.15 is obtained with 60A grounding grid current, which causes the touch voltage between 3 ~ 13V. The voltages within this range can be detected by the voltage sensors. For safety evaluation, the actual voltages are scaled up to the maximum values in the database according to (2.9) and (2.10).

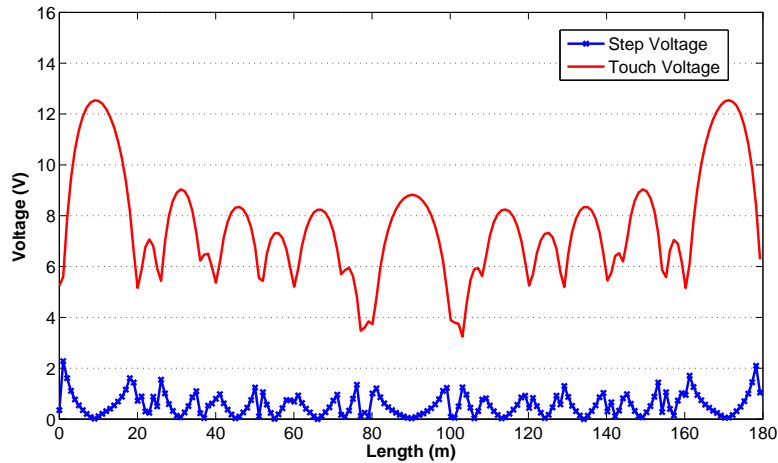


Figure 2.15: The potential profile with 60A grounding grid current.

With the support of an online database, synthesized and reliable estimation can be made depending on IEEE standard constraint and recorded data variation. To better clarify the concept of the safety evaluation process, two scenarios are discussed. One is theft and the other is the change of soil resistivity due to seasonal influence. As shown in Figure 2.16, the conductors on the left edge of a grounding grid are stolen so that touch voltage around that area is largely increased as illustrated in Figure 2.17.

When comparing the profiles of Figure 2.14 and Figure 2.17, it is easy to detect the difference in the corner area. An alarm is created immediately and investigation in the corner should be made as soon as possible. On the other hand, touch voltages at some spots also exceed the limit, a mandatory examine is required at these locations.

Figure 2.18 is the field test data of soil resistivity in a 12-month study [46]. The resistivity was lower during the summer due to high precipitation, and it was higher during the winter with the frozen soil. Three locations are picked

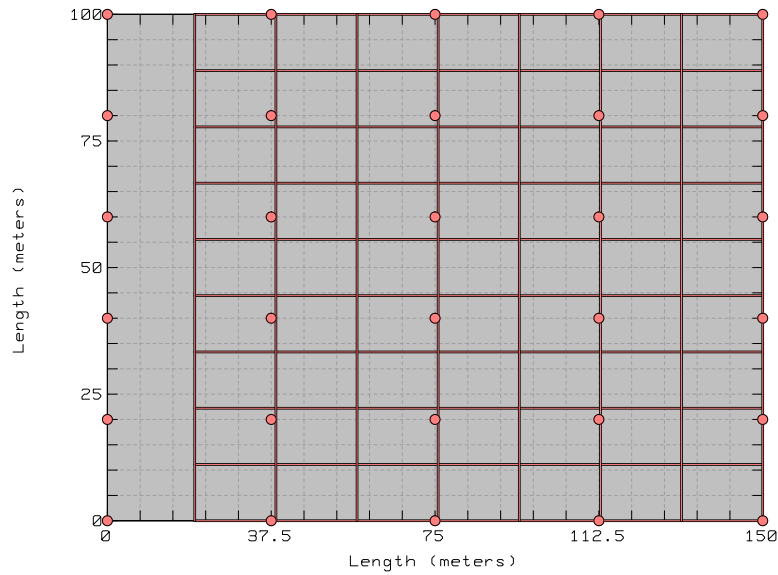


Figure 2.16: The conductors on the left edge are stolen.

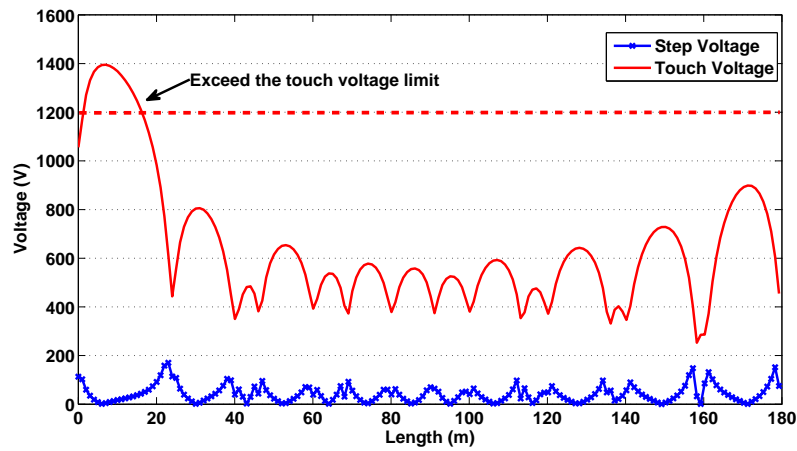


Figure 2.17: The potential profile after theft.

up from the diagonal line as shown in Figure 2.19 and the touch voltages are illustrated in Figure 2.20. When a fault occurs in June, all touch voltages are under the limit. However, if a fault happens in December, touch voltages rise due to the increase of soil resistivity, and some of them exceed the limit.

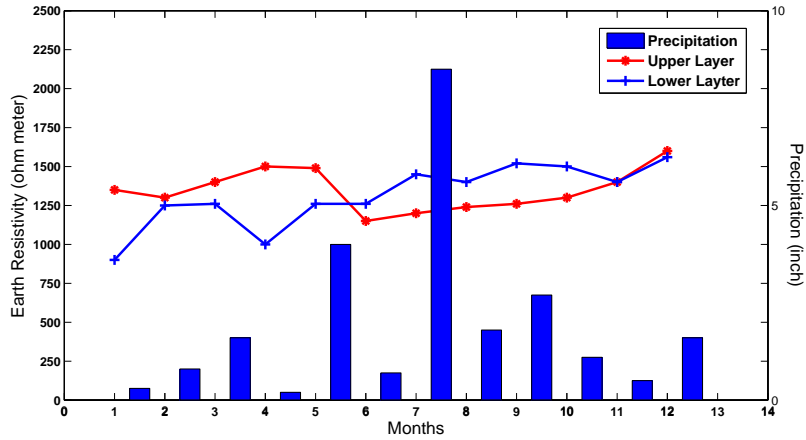


Figure 2.18: The soil resistivity in different seasons.

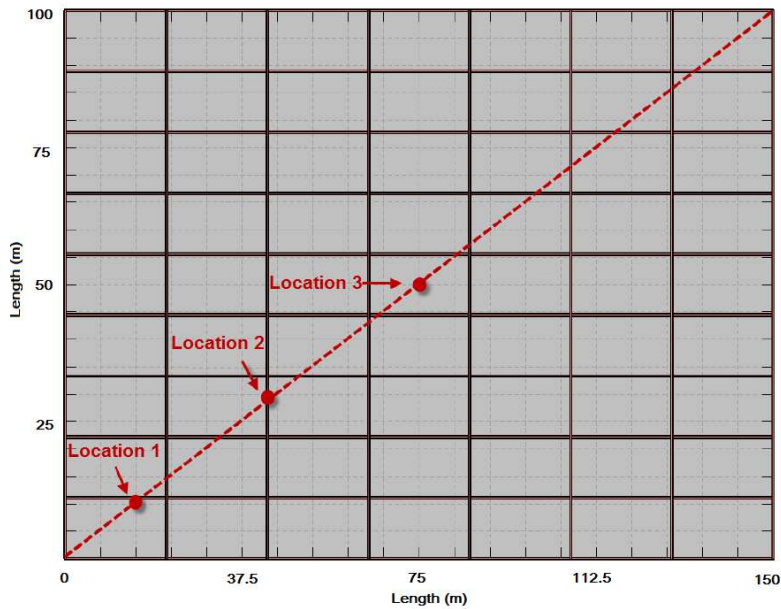


Figure 2.19: Three suspect spots are picked up from the diagonal line.

If an offline test is taken in June but not in December, these hazardous spots cannot be founded. In the proposed online monitoring, these spots can be reported in time with monthly evaluation. The frequency of measurements can be adjusted according to the requirement of utilities.

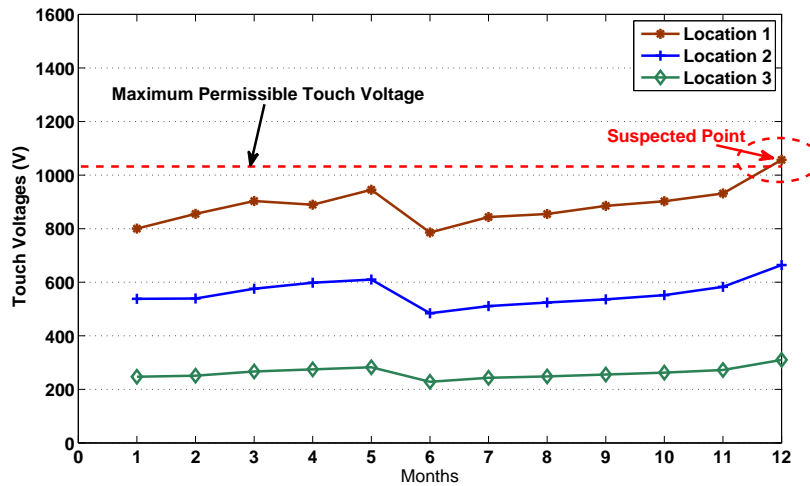


Figure 2.20: Touch voltages of three suspect spots in different seasons.

## 2.5 Conclusion

An online monitoring scheme for substation safety assessment is presented, which periodically measures touch and step voltages and evaluates the condition of a grounding grid with the help of an online database. The testing current is generated by firing a pair of thyristors for 50ms. This current can be injected remotely or locally. The local injection scheme has a larger portion of the injected current flowing through the grounding grid, but it costs more than the remote scheme due to high rating voltage and high capacity of the step-down transformer.

The condition monitoring is achieved with a network of wireless touch/step voltage sensors installed at various locations of a substation. These sensors are connected to a central database where an evaluation process is carried out by comparing the newly measured data to the limits from IEEE standard, or checking if the data variation at the same spot exceeds safety thresholds. Fur-

thermore, current distribution has been studied with computer simulations, which verified the effectiveness of the proposed local and remote schemes. From the case studies of conductor theft and seasonal influences, the advantage of online monitoring is very clear since some hazardous spots cannot be found in time without continuous measurements. Compared to offline methods, which at best gives one-shot assessment, the proposed online grounding grid monitoring scheme is more effective and reliable, and it could become an important component of a smart substation.



## Chapter 3

### Power Electronics Aided Fault Detection in De-Energized Feeders

When a circuit breaker is tripped or a recloser is lockout due to events such as repair, maintenance or storms, the downstream circuit is isolated from the energized circuit. After a feeder is de-energized for an extended period, there is always the possibility that humans or animals may be in contact with feeder conductors unknowingly. A re-closing action in such a situation can easily lead to fatality. Therefore, it is necessary to check if a fault still exists before re-energizing a feeder. A novel active method for fault detection in de-energized feeders is presented in this chapter. Thyristors are controlled to momentarily connect the energized upstream to the de-energized downstream. Various combinations of signals are created to detect different types of faults. The actual embodiment of the technique is a low voltage power electronics device connected to a medium voltage feeder through service transformers. The device is installed permanently at recloser or breaker locations and can be operated locally or remotely. As a result, there is no need to replace the existing breakers or reclosers.

### 3.1 Introduction of Fault Detection Methods

Fault detection in a de-energized system is more challenging than that in an energized system, as it requires the generation and application of a voltage signal to the de-energized feeder. Furthermore, the signal must be high enough to mimic the normal medium voltage stress experienced by a feeder. Especially in a long distribution line with several branches, high energy is necessary for the pulse to travel without significant attenuation. On the other side, the applied signal should be initiated as an alarm with low energy so that human or animals contacting with the conductors can sense it and get away to avoid injury. The injected current is therefore required to be very adaptive.

As shown in Figure 3.1, the existing fault detection schemes can be classified into two types according to the sources of current: self-powered and powered from the energized side.

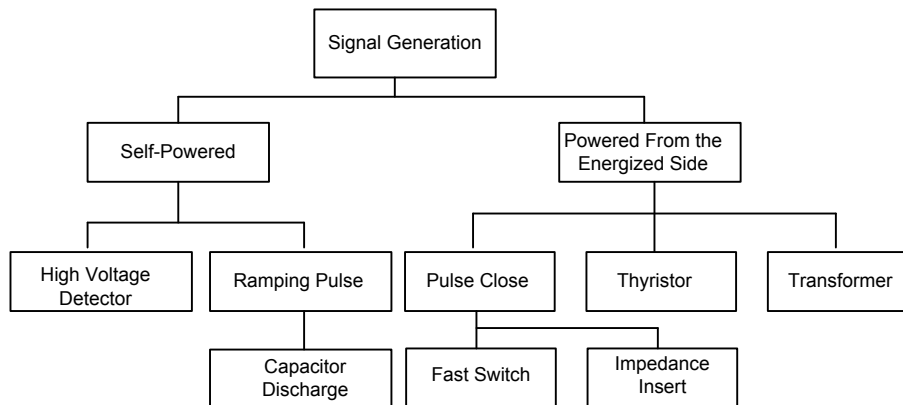


Figure 3.1: The review of the existing detection methods.

### 3.1.1 Self-Powered Signal Generation

In [38], a portable tester utilizes a capacitor to discharge a high voltage pulse into the de-energized line. It comprises two hook terminals connected between line to line or line to neutral in a de-energized feeder to detect either a phase-to-phase fault or a phase-to-neutral fault. The responses of voltage and current are analyzed to estimate the impedance of the line to determine the existence of a fault. A cable tester with a set of battery and capacitor is described in [48]. The principle is to use the capacitor to create a high voltage charging circuit between the inner and outer terminals of the tested cable. If there is a short-circuit, the voltage across the capacitor cannot attain a threshold value and give an indication of a fault.

These devices are portable and easy to use. However, they require maintenance of power source such as batteries. In addition, the energy of the injected pulse is usually fixed and limited, which means these devices cannot be adapted for different voltage ratings or used for a high impedance fault.

### 3.1.2 Powered From the Energized Side

Another way to generate the detection signal is to “borrow” energy from the energized upstream. Extra power supply is therefore not required. The fault detector in [49] produces a signal by closing the recloser for one cycle. If the current is too high, which indicates the presence of a downstream short circuit, a series impedance will be inserted to reduce the inrush cur-

rent. Like auto-reclosers, this method still injects significant inrush current into the downstream before the insertion of the series impedance. In [39], a short-duration voltage from a gate turn-off (GTO) thyristor is applied to the de-energized downstream, and the resulting current is integrated to compare with a threshold to determine if a fault exists. A transformer can also be used to generate a detection signal as illustrated in [50], where a step-up transformer convert power from 120V to 500V with limited output of 5mA. If an output current is larger than 3mA, the detection of an insulation failure is triggered. However, the device does not have enough power to work in a medium voltage system, and the strength of the pulse is not adjustable. Furthermore, another drawback for the above methods is that they cannot identify different types of faults in a single device.

Recently, a pulse-recloser technique has been developed for the purpose of reducing the inrush current caused by reclosing to a faulted feeder [80]. This technique uses specialized recloser and is intended for fuse-saving oriented feeder reclosing operations. In theory, the technique can be applied to the problem of concern to this work (i.e. detecting feeder faults after the feeder has been de-energized for an extended period). However, its application requires replacing the existing feeder breaker or recloser. This can be costly to utility companies if implemented on a large scale.

### **3.2 The Power Electronics Aided Fault Detection Method**

The single line representation of the proposed method is shown in Figure 3.2. A thyristor is connected in parallel to a circuit breaker or recloser by a

switch. The switch is off in the normal system operation. When maintenance or repair at downstream is completed and the de-energized feeder needs to be restored, the line operator can turn on the switch and control the thyristor to trigger at several degrees before the voltage crosses zero. The energized upstream line is thus momentarily connected to the de-energized side so that a detection pulse is created in the downstream. The thyristor automatically shut off when its current drops to zero [30] [81]. A step-down transformer is used to decrease the voltage of the distribution line to a low level for thyristor operation and then a step-up transformer is used to restore the signal back to the system voltage level. Point X in Figure. 1 is the location for measuring the stimulated voltage and current signals. The typical thyristor voltage, current and the measured waveforms at point X are shown in Figure 3.3.

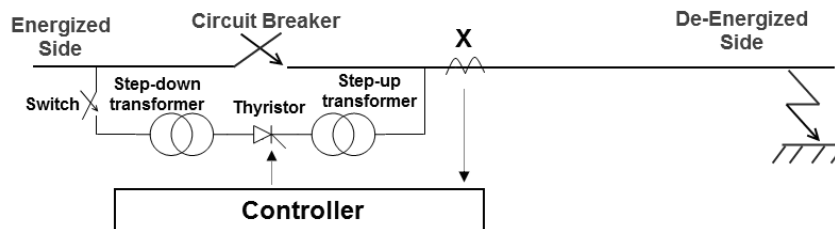


Figure 3.2: Single-line representation of the proposed fault detection method.

A significant feature of this technique is that the signal strength is adjustable by changing the firing angle of thyristors. For example, at the beginning, a low-strength signal is created with a large firing angle, which can be considered as an alarm so that human or animals contacting with the conductors can sense it and get away to avoid injury. Then, the signal strength increases gradually by reducing the firing angle to stimulate detectable electrical responses. This firing angle can be further reduced to reach a high voltage to break down an insulated gap if there is a high impedance fault.

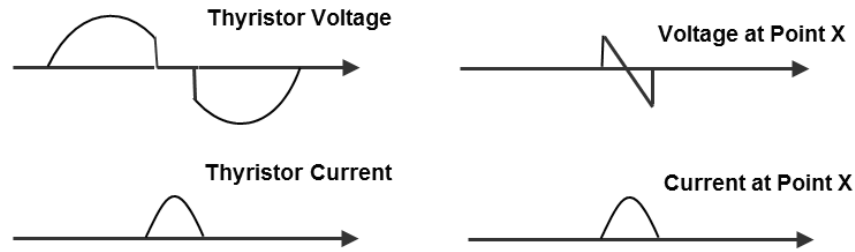


Figure 3.3: Waveforms of: (a) thyristor voltage and current, (b) measured voltage and current at the point X.

### 3.2.1 Three-Phase Thyristor Bridge Based Structure

In a three-phase four-line system, a fault can be symmetrical or asymmetrical and it may happen between phases or between a phase and ground. Therefore, the detection and classification of all kinds of faults is highly desired. A three-phase thyristor bridge based scheme is proposed for this purpose. As shown in Figure 3.4, a three-phase thyristor bridge circuit is connected in parallel to a circuit breaker. The upper thyristors are connected to one phase of the energized upstream and the bottom thyristors are connected to a neutral line. As mentioned earlier, to minimize the size and reduce the cost of power electronics devices, transformers are used to convert the voltage to a level suitable for thyristors. Even considering the added cost on transformers, the overall cost of this configuration will be lower. Once the detection signals are injected, voltage and current at point X are measured and analyzed in a signal detector to determine if a fault still exists. The detection for different kinds of faults depends on the combinations of gating signals.

Basically, there are two control modes as shown in Figure 3.5. In the first

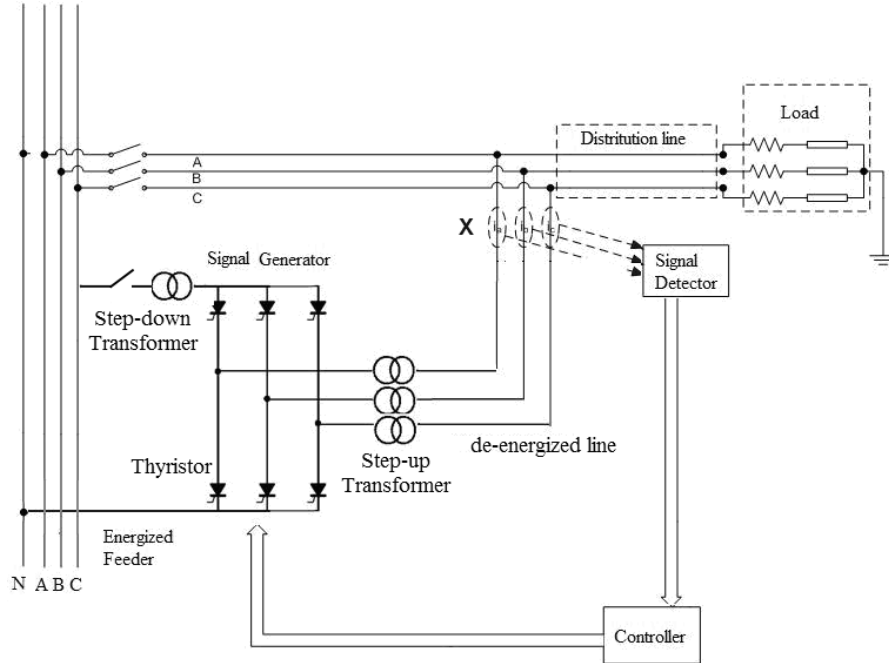


Figure 3.4: Three-phase thyristor bridge based fault detection scheme.

mode (Figure 3.5(a)), when an upper thyristor (T1) is turned on and all bottom thyristors are off, a detection pulse is injected to the corresponding phase of the de-energized line through the upper thyristor, creating a fault current if there is a phase-to-ground fault in that phase. In the other mode (Figure 3.5 (b)), T1 and T4 are fired simultaneously. If a fault between phase A and phase B exists, it provides a path for the fault current to flow from T1 and T4 to the neutral. The overall combinations of gating signals are listed in Table 3.1, which include three steps that can detect all types of faults.

### 3.2.2 Phase-to-Ground Faults Detection

Statistics has shown that single phase-to-ground fault is the most common fault in a distribution system, which accounts for 70% - 80% of distribution

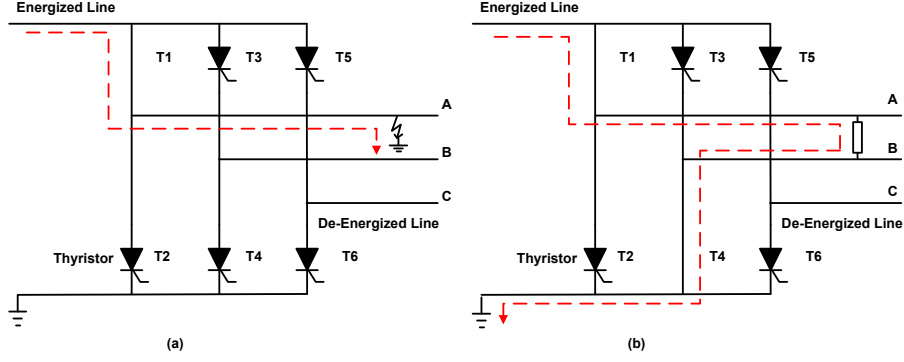


Figure 3.5: The gating control logic in two fault detection modes: (a) phase-to-ground fault, and (b) phase-to-phase fault.

Table 3.1: Overall control logic and detected fault types

Step No.	Control Logic	Fault Types
Step I	T1, T3, T5 On, Others Off	Single phase-to-ground fault Double phase-to-ground fault Three phase-to-ground fault
Step II	T1, T4, T6 On, Others Off	phase A to phase B fault phase A to phase C fault
Step III	T3, T6 On, Others Off	phase B to phase C fault

line faults. To the contrary, three-phase to ground fault with balanced three-phase currents only accounts for 5% of faults [82]. For this reason, the analysis in this section focuses on single phase-to-ground fault and other unbalanced phase-to-ground faults.

In Step I of the fault detection algorithm, when T1, T3 and T5 (upper switches in a thyristor bridge) are turned on simultaneously and T2, T4 and T6 (lower switches in a thyristor bridge) are off, a pulse is injected into all three phases simultaneously. This signal, which is from the same phase of the energized side, can be considered as a zero sequence voltage applied to the downstream. The equivalent circuit is illustrated as Figure 3.6.  $E$  is the rated phase-to-neutral voltage of the distribution line,  $Z_{load}$ ,  $Z_{line}$ ,  $Z_{sys}$ ,  $Z_{xform}$  are the impedance



of load, distribution line, system and transformer, respectively.

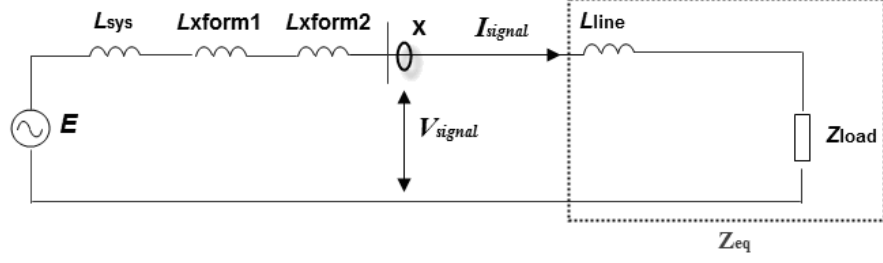


Figure 3.6: Single-line equivalent circuit with zero sequence current injection.

If the firing angle of the thyristors T1, T3 and T5 is  $\delta$ , the injected voltage distortion at point X can be expressed as

$$V_{signal}(t) = \frac{Z_{load} + Z_{line}}{Z_{load} + Z_{line} + Z_{sys} + 2Z_{xform}} \sqrt{2} E \sin(\omega t + \delta) \quad (3.1)$$

Since the system and transformers impedance is much lower than the load impedance, (3.1) can be simplified as

$$V_{signal}(t) \approx \sqrt{2} E \sin(\omega t + \delta) \quad \omega t \in [0, 2\pi - 2\delta] \quad (3.2)$$

Assuming the downstream impedance  $Z_{eq} = R_{eq} + j\omega L_{eq}$  and the relationship of (3.3)

$$L_{eq} \frac{di_{signal}(t)}{dt} + R_{eq} i_{signal}(t) = V_{signal}(t), \quad (3.3)$$

the injected current can be obtained as in (3.4).

$$i_{signal}(t) = \frac{\sqrt{2} E}{\sqrt{R_{eq}^2 + (\omega L_{eq})^2}} \left[ \sin\left(\omega t + \delta - \tan^{-1} \frac{\omega L_{eq}}{R_{eq}}\right) - e^{-R_{eq}t/L_{eq}} \sin\left(\delta - \tan^{-1} \frac{\omega L_{eq}}{R_{eq}}\right) \right] \quad (3.4)$$

The magnitude of the injected current can be further expressed as in (3.5),

which suggests that lower the downstream impedance give higher values of current magnitude.

$$|I_{signal}(t)| = \frac{\sqrt{2}E}{|Z_{eq}|} [\sin(\omega t + \delta_1) - e^{-R_{eq}t/L_{eq}} \sin\delta_1] \quad (3.5)$$

where  $\delta_1 = \delta - \tan^{-1}(\omega L_{eq}/R_{eq})$ . If there is no asymmetrical fault, the three-phase parameters should be balanced, and the impedance of each phase is determined by (3.6).

$$Z_{eq} = R_{eq} + jX_{eq} = R_{load} + j(X_{load} + X_{line}) \quad (3.6)$$

In this case, the injected three-phase current pulses should be in phase and have the same magnitude as shown in Figure 3.7 (a). However, if a single

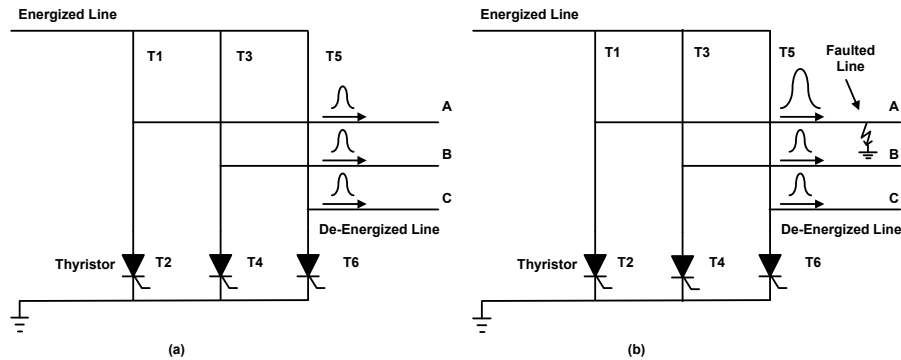


Figure 3.7: The current waveforms under (a) no fault with balanced three-phase currents, and (b) a single line-to-ground fault with unbalanced three-phase currents.

phase-to-ground fault exists, the fault resistance will be parallel to the circuit as shown in Figure 3.8. The equivalent impedance of the faulted phase is

smaller than that of other healthy phases as expressed in (3.7):

$$\begin{aligned} Z'_{eq} &= X_{line1} + R_f // (R_{load} + j(X_{load} + X_{line2})) \\ &< X_{line1} + (R_{load} + j(X_{load} + X_{line2})) = Z_{eq} \end{aligned} \quad (3.7)$$

where  $R_f$  is the fault resistance and the line reactance  $X_{line1} + X_{line2} = X_{line}$ .

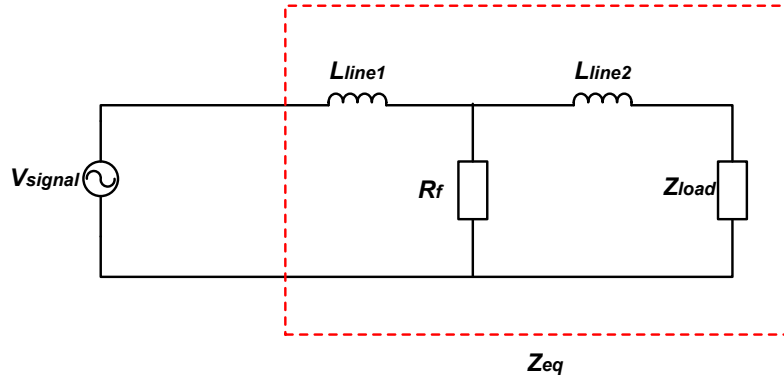


Figure 3.8: The equivalent impedance under a single phase-to-ground fault.

As a result, the current pulse in the faulted phase is higher according to (3.5). The current waveforms with a phase A-to-ground fault are illustrated in Figure 3.7 (b).

The severity of current imbalance is highly related to the resistance of the fault. From the statistical data, about 85% - 98% of the faults are low impedance fault [83]. With the increase of fault resistance, the imbalance of three phases becomes less severe. Thus, for high impedance fault detection, the firing angle should be small enough to create a high voltage on the de-energized side to produce a sufficient fault current that differs from an un-faulted line. The criterion for detecting an unbalanced phase-to-ground fault

is designed as following:

1. Measure all three-phase currents in Step I of Table 3.1.
2. Calculate the magnitude of the injected current in each phase ( $I_a, I_b, I_c$ ). Are they identical? If yes, there is no asymmetrical fault. If no, an asymmetrical fault exists.
  - (a) Among the three current magnitudes, if one of them is larger and the others are the same (e.g.  $I_a > I_b = I_c$ ), it indicates a single phase to ground fault and the faulted phase is identified.
  - (b) If two of them are the same and larger than the third one (e.g.  $I_a = I_b > I_c$ ), it indicates a double-phase to ground fault and then the two faulted phases are detected.

Note that the firing angle of the thyristors determines the pulse energy. Reducing the firing angle can increase the signal strength and extend the conduction period (See Figure 3.9). Therefore, an initial alarming pulse with a

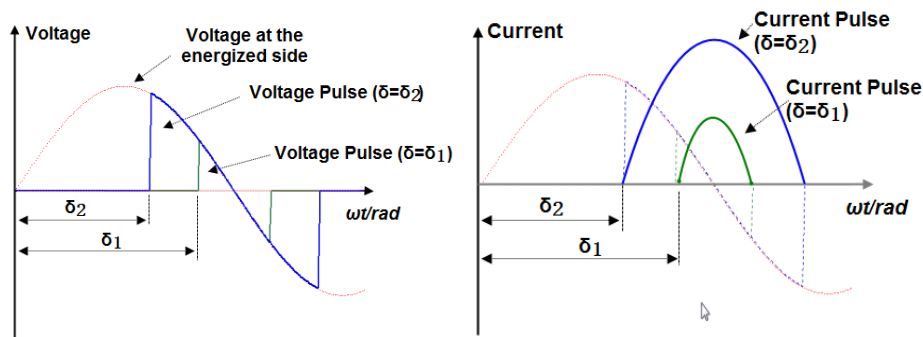


Figure 3.9: Voltage and current pulses generated with different thyristor firing angles.

small voltage is generated by controlling the firing angle close to  $180^\circ$ . After that, the firing angle decreases gradually to achieve high voltage for high impedance fault detection. If the device is fully turned on, the maximum amount of energy is essentially applied.

### 3.2.3 Phase-to-Phase Faults Detection

The detection signal for a phase-to-phase fault is created by simultaneously turning on one upper thyristor and one or two bottom thyristors from different legs. In this case, the phase of the upper thyristor is connected to the energized side and the others are connected to the neutral line. If a phase-to-phase fault exists, a current pulse will show up on both phases in reverse directions.

For example, as shown in Figure 3.10, T1, T4 and T6 are turned on and others are off. If there is no fault between phase A and phase B, the current in phase A is determined by (3.4) and no current flows in phase B and phase C. If a fault exists between phase A and phase B, the current will show up on both phases in reverse directions. The equivalent impedance of phase A is

$$Z_{eqa} = j\omega Z_{line_a} + Z_{load} // (R_f + j\omega Z_{line_b} // Z_{load}) \quad (3.8)$$

where  $R_f$  is the fault resistance,  $Z_{line_a}$ ,  $Z_{line_b}$  are the line impedance of phase A and B respectively.

Since a load impedance is much larger than a line impedance, most current from phase A flows back to neutral through the distribution line instead of

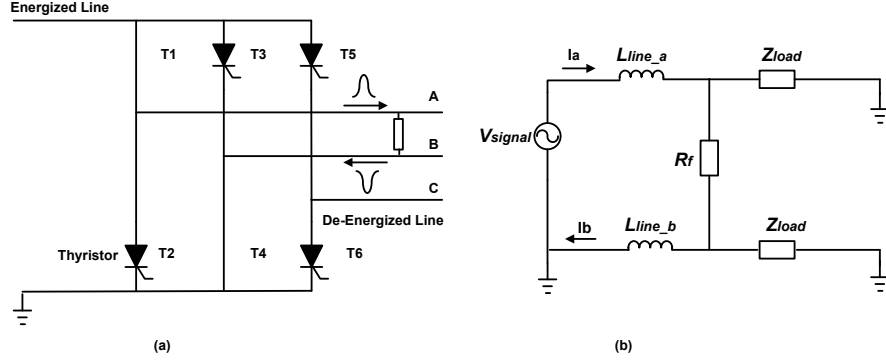


Figure 3.10: Signal injection for phase-to-phase fault detection.

the loads. The current of phase B can therefore be determined as:

$$\begin{aligned}
 I_b &= - \frac{Z_{load}}{Z_{load} + j\omega L_{line_b}} \frac{Z_{load}}{Z_{load} + R_f + (Z_{load} // j\omega L_{line_b})} I_a \\
 &\approx - \frac{Z_{load}}{Z_{load} + R_f} I_a
 \end{aligned} \tag{3.9}$$

The voltage and current waveforms of phase A and phase B with a phase A-to-phase B low impedance fault are shown in Figure 3.11.

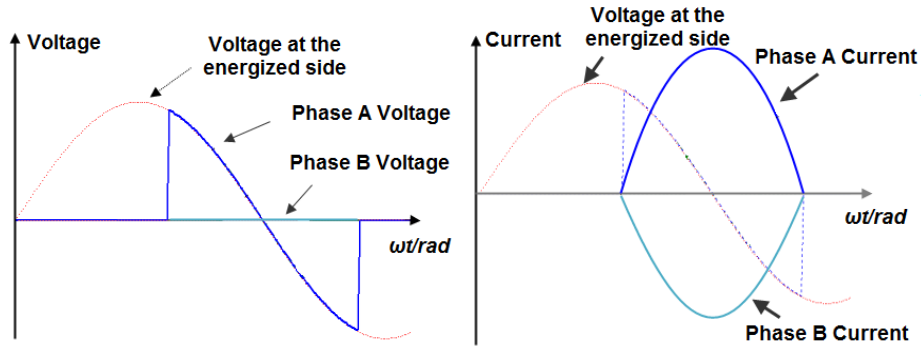


Figure 3.11: Voltage and current pulses when a phase A-to-phase B fault exists.

Based on the analysis of signal characteristics in a phase-to-phase fault, the presence of reverse signal can be used as an indicator. The criterion is therefore designed as following:

1. In Step II of Table 3.1, the magnitude of phase B and phase C currents are measured. If  $I_b < 0$ , a fault exists between phase A and phase B; If  $I_c < 0$ , a fault exists between phase A and phase C; Otherwise, there is no fault between phase A and any other phases.
2. In Step III, the magnitude of phase C current is measured. If  $I_c < 0$ , a fault exists between phase B and phase C; Otherwise, there is no fault between phase B and phase C.
3. All possibilities of phase-to-phase faults can be checked after Steps II and III.

Finally, combining both the phase-to-ground faults and phase-to-phase faults detection schemes, the overall fault detection algorithm is summarized in Figure 3.12. Different kinds of asymmetrical faults can be identified after conducting the three steps. If a large or small injection current is needed, the firing angle can be adjusted accordingly. Note that the neutral ground connection is important for the proposed scheme. A loose ground connection will not affect the line-to-ground fault detection, but it will affect the line-to-line fault detection as there is no current return path in this case. To check the ground connection, a simple procedure can be performed by firing T1 and T4 simultaneously at a very small angle before the voltage zero crossing. The present of a current pulse indicates a good grounding connection.

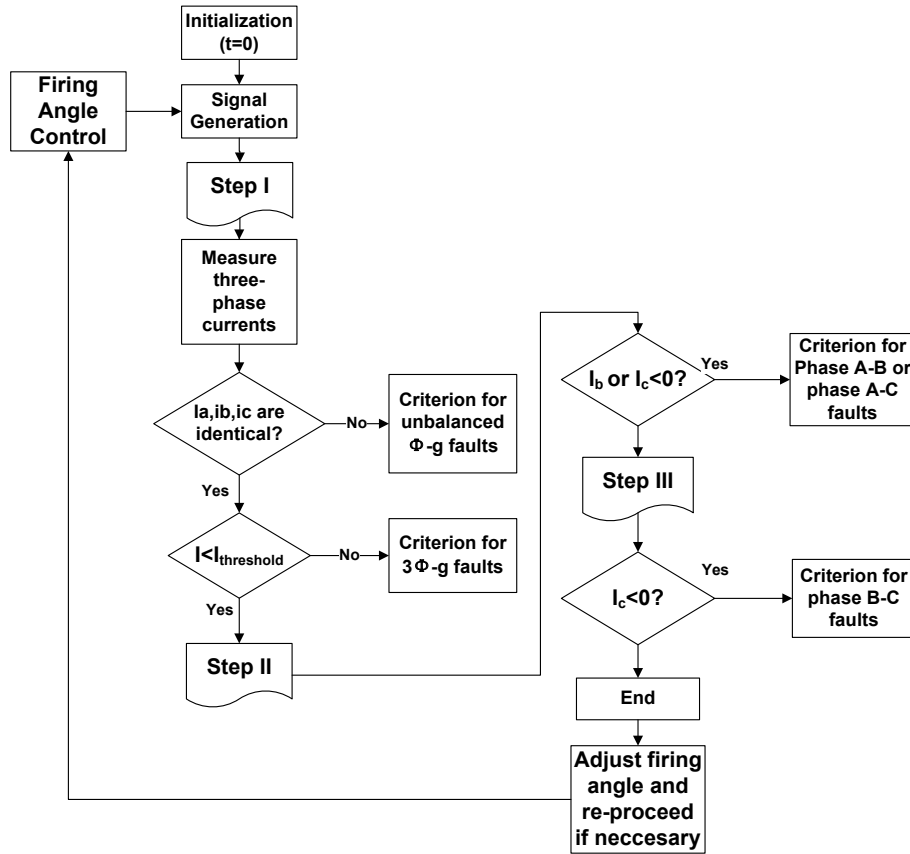


Figure 3.12: Details of the three-step fault detection algorithm.

### 3.3 Computer Simulation Results

Computer simulations are performed to verify the above analysis. The rated voltage of the distribution line is  $25kV$ . As shown in Figure 3.13, a three-phase thyristor bridge based signal generator is connected to the upstream phase A through a single phase transformer. The three bridge legs are connected to the de-energized downstream through step-up transformers. Three separate step-up transformers are used instead of a three-phase transformer to reduce the interference between phases. Other parameters used in the computer simulations are listed in Table 3.2.



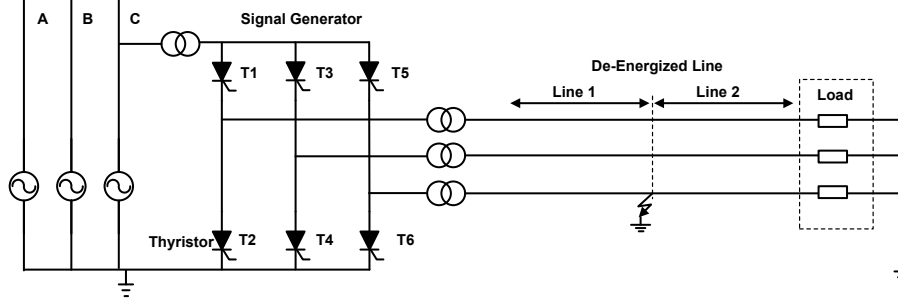


Figure 3.13: Configuration of the computer simulation system

Table 3.2: The system parameters of computer simulation

Utility	25kV, Yg-Yg connection.
Step-up Transformer	5MVA, 14.4kV/0.48kV.
Step-down Transformer	5MVA, 0.48kV/14.4kV.
Feeder	Both Line 1 and Line 2 are 5km, the positive sequence $R_1 = 0.2138\Omega/km$ , $X_1 = 0.3928\Omega/km$ , $B_1 = 4.2315\mu S/km$ ; the zero sequence $R_0 = 0.3875\Omega/km$ , $X_0 = 1.8801\Omega/km$ , $B_0 = 1.6058\mu S/km$ .
Load	4MVA, lagging, $p.f. = 0.95$ , Fed with a 5MVA, 25kV/0.6kV, Yg/Yg transformer ( $z=5\%$ ).
Fault Resistance	$R_f = 10 \sim 200\Omega$ , the default $R_f = 50\Omega$
Thyristor Firing Angle	$150^\circ \sim 180^\circ$

According to the gate signals control logic (See Table 3.1), three detection steps are carried out to detect different kinds of faults. These thyristors fire once in every four fundamental cycles. Shorter intervals for faster detection are also possible as the signal attenuate to zero within one fundamental cycle. The interference between different steps is negligible as shown in the results. Considering the three steps as one operation period, the firing angle reduces from  $180^\circ$  after each period until faults are identified. Most faults (except for some high impedance faults) can be detected within 1 second.

When there is no fault, the measured currents are shown in Figure 3.14. In

Step I, as a zero sequence voltage is applied to three phases, the currents are identical. In Step II, a signal is injected from phase A, and both phase B, C are connected to neutral. As there is no fault between A-B or A-C, the signal has no path to flow into phase B and C so that the currents of phase B and C are zero; Step III is similar to Step II, with the only difference being that the signal is injected from phase B rather than from phase A.

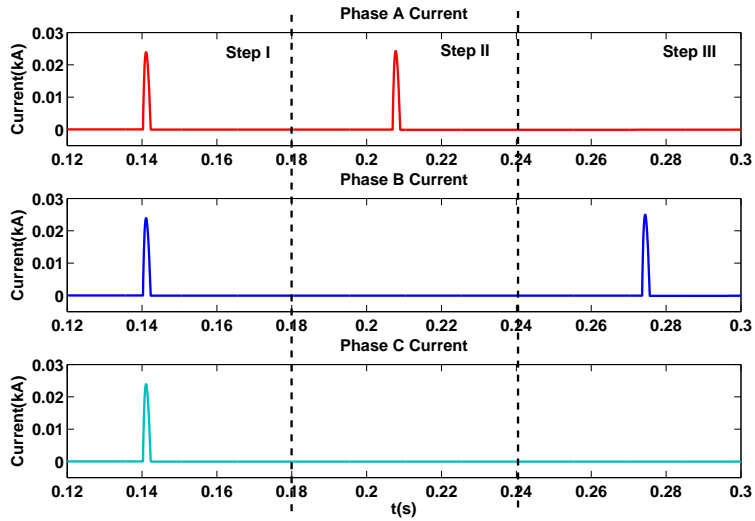


Figure 3.14: Three-phase currents in three steps without fault.

### 3.3.1 Phase-to-Ground Fault

If a single phase to ground fault exists in phase C and ground, the current in Step I will change. As shown in Figure 3.15, the current of phase C increase significantly due to the fault. The magnitude of the current is also affected by the fault resistance  $R_f$ . When the firing angle is  $150^\circ$ , the current waveforms with different fault resistances are shown in Figure 3.16. It is apparent that the magnitude of the fault current decreases with the increase of fault resistance. Therefore, if  $R_f$  is small, the thyristor firing angle should

be large enough to decrease the current to a safe value. On the other hand, If  $R_f$  is large, the current of faulted phase is comparable to the currents of unfaulted phase, which increase the difficulty of detection. Thus, the firing angle should be reduced to obtain an obvious difference between faulted and healthy phases.

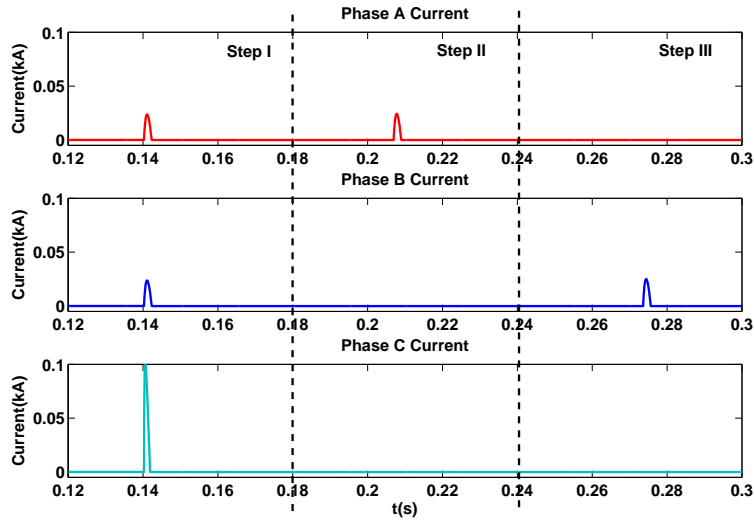


Figure 3.15: Three-phase currents in three steps under a phase C-to-ground fault.

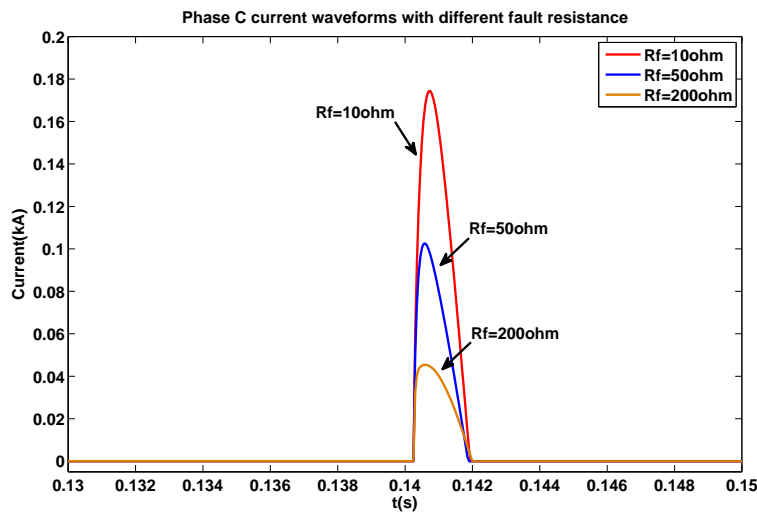


Figure 3.16: Current waveforms of phase C with different fault resistances.

According to the criterion of identifying an unbalanced phase-to-ground fault, the current difference between two phases is calculated. The single phase C-to-ground fault does not affect phase A and phase B, thus the currents of phase A and B are identical when a zero sequence voltage pulse applied to the downstream in Step I. As shown in Figure 3.17,  $|I_a - I_b|$  is almost zero regardless of firing angles and fault resistance. As the current of phase C is larger,  $|I_b - I_c|$  and  $|I_c - I_a|$  have almost the same values. As discussed, reducing the firing angle can make the difference of current between phases more significant.

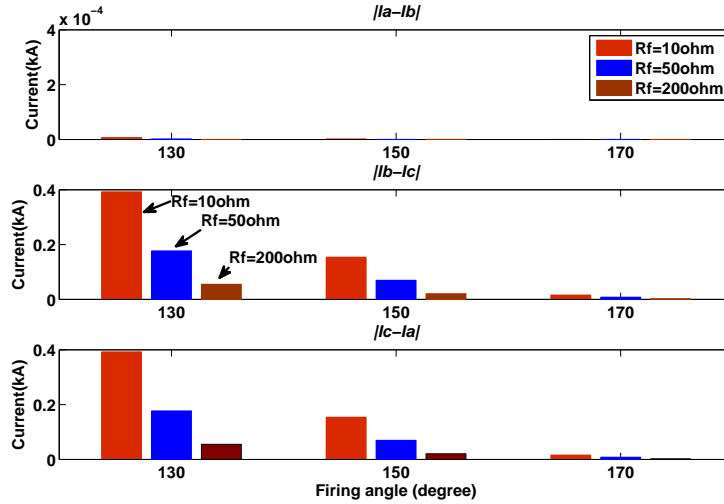


Figure 3.17: Current difference between phases under a phase C-to-ground fault.

### 3.3.2 Phase-to-Phase Fault

If there is a phase-to-phase fault between phase A and B, the three-phase current waveforms in three steps are shown in Figure 3.18. In Step I, all three-phase currents are identical but in Step II, a reverse signal shows up in phase B when a pulse is injected from phase A. The waveforms in Step III

verify the existence of a fault since a reverse signal shows up in phase A when a pulse is injected from phase B.

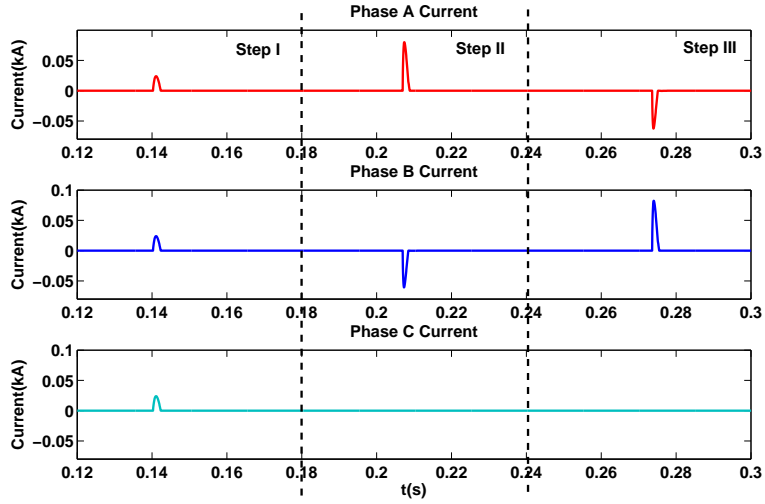


Figure 3.18: Three-phase currents in three steps under a phase A-to-phase B fault.

The current of phase B in Step II not only depends on the injected current from phase A, but it is also affected by other three parameters of power system as shown in (3.9): the fault location (the length from the fault detection point, which determines the line impedance of interest), the load and fault impedance.

Figure 3.19 shows the ratio of  $I_b/I_a$  with the different values of the three parameters in Step II with the bases of Line 1 length 5km, Load 4MVA,  $R_f = 200\Omega$ . Apparently, the fault resistance has a significant impact on current division. If the phase-to-phase fault has a high impedance, the current of phase B through the fault will be largely reduced. Another significant impact is from loads. A large load will lead more current flow through the load on phase B rather than from the grounded conductor of phase B where the measurement point X is located as shown in Figure 3.10 (b). However,

the impact of the Line1 length is very limited.

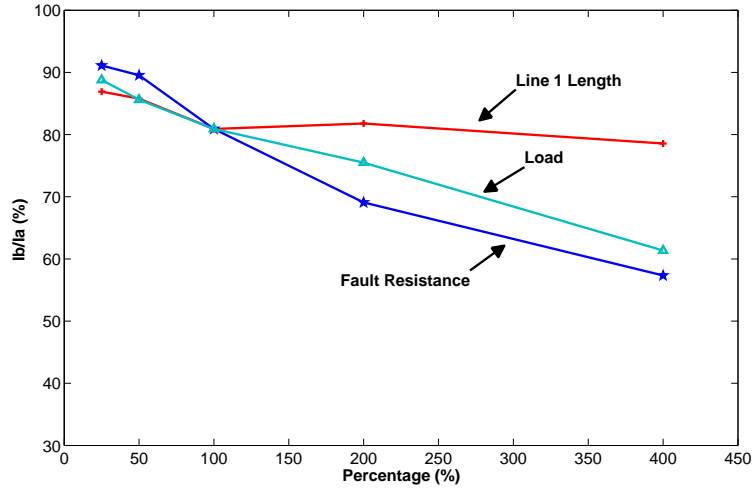


Figure 3.19: The sensitivity study of a phase-to-phase fault.

Multiple faults are also tested, including (1) a phase C-to-ground fault, (2) a phase A-to-phase B fault and (3) a phase A-to-phase C fault. The test results are shown in Figure 3.20. In Step I, phase C current is much larger than that of phase A and phase B, which indicates a phase C-to-ground fault. In Step II, a pulse is injected from phase A and reverses pulses show up on both phases B and C, meaning both a phase A-to-phase B fault and a phase A-to-phase C fault exist. Step III verifies that a fault between phase A and phase B exists.

### 3.4 Experiment Verifications

An experiment based on 120V single phase system is carried out in laboratory and the prototype comprises of (1) a thyristor-based signal generator; (2) a data acquisition system; and (3) a lumped model based equivalent circuit.

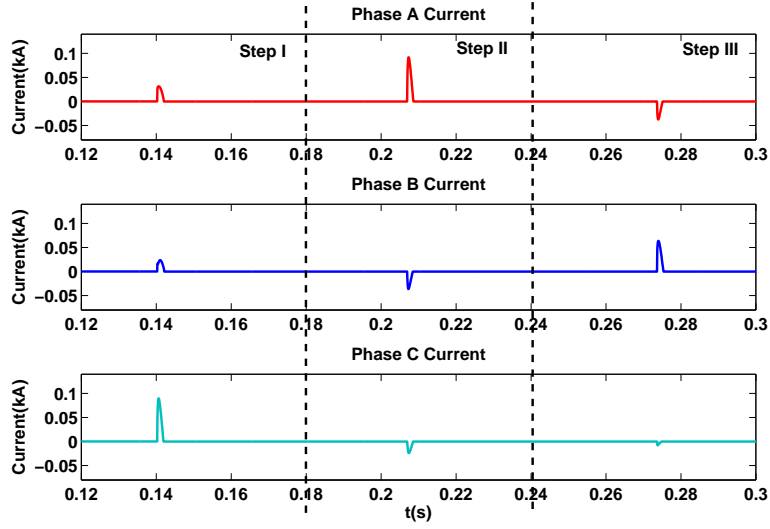


Figure 3.20: Three-phase currents in three steps under multiple faults.

The firing angle of the thyristor can be adjusted from  $180^\circ$  to  $150^\circ$  and the firing interval can be either 2 or 4 fundamental cycles. Six channels, including three voltage measurement channels and three current measurement channels are utilized. Due to the limitation of lab equipment, all the transmission lines and transformers are replaced by equivalent inductors. The loads are replaced by equivalent R-L model as well. The system parameters are listed in Table 3.3.

Table 3.3: The parameters of experiment verifications

Power source	120V
Transformer Impedance	$L_{xformer} = 0.76mH$
Line Impedance	$R_{line} = 0.08\Omega, L_{line} = 0.4mH$
Load Impedance	$R_{load} = 11.4\Omega, L_{load} = 10mH$
Fault Resistance	$R_f = 0 \sim 7.68\Omega$
Thyristor Firing Angle	$150^\circ \sim 180^\circ$

The equivalent circuit of the lab test prototype is shown in Figure 3.21. The fault resistance  $R_f$  and the load size ( $R_{load}, L_{load}$ ) are adjustable.

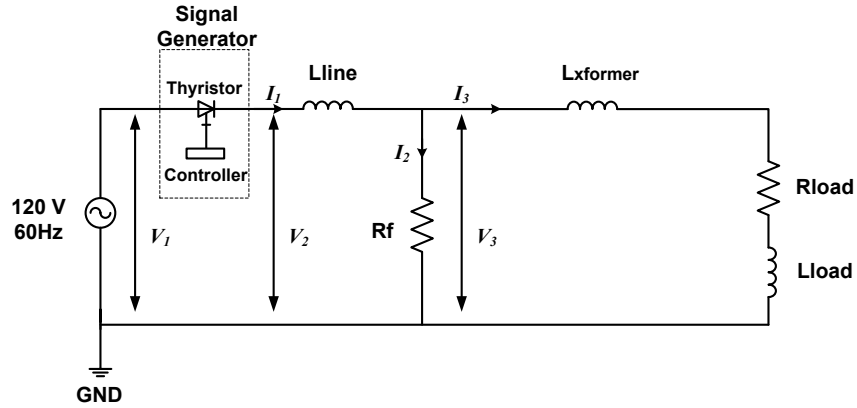


Figure 3.21: The equivalent circuit of the experimental testing system.

Figure 3.22 shows voltage waveforms.  $V_S$  represents the 120V, 60Hz single phase voltage source and  $V_{thyristor}$  is the voltage across the thyristor. When the thyristor is fired at a certain degree before the source voltage crosses zero,  $V_{thyristor}$  becomes zero instantaneously. At this moment, the de-energized part of the circuit is connected to the voltage source. When the thyristor current becomes zero, the thyristor turns off naturally and the passive circuit returns to its de-energized state.  $V_d$  is the voltage pulse created by the thyristor.

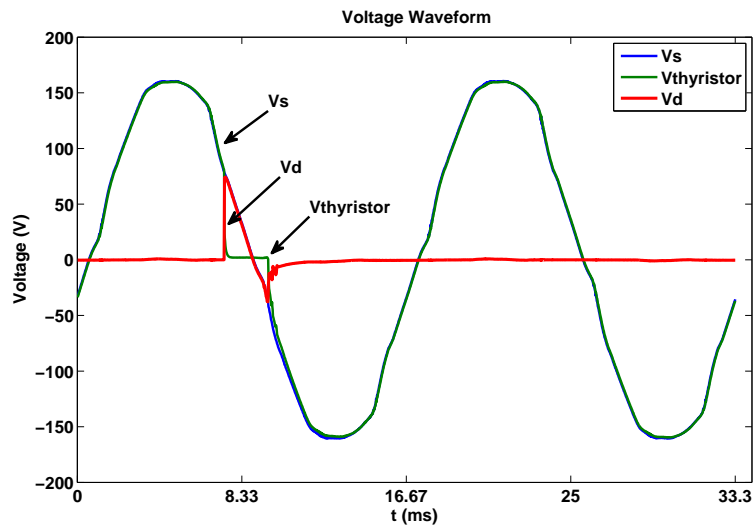


Figure 3.22: Measured voltage waveforms in the lab experiment.



The corresponding currents, including the load current  $I_{load}$ , the fault current  $I_{fault}$ , and the total current  $I_d$ , are shown in Figure 3.23. With a small fault resistance, the fault current  $I_{fault}$  is close to the total current  $I_d$  and the load current  $I_{load}$  is relatively small as the load impedance is much higher than the fault resistance.

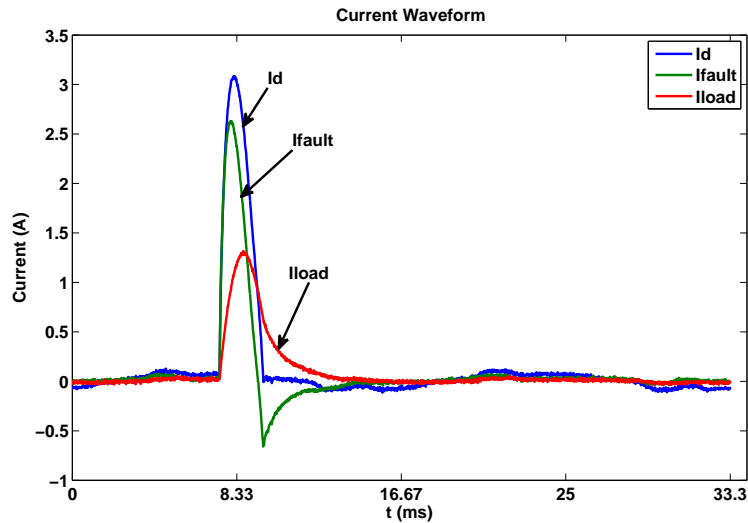


Figure 3.23: Measured current waveforms in the lab experiment.

The impact of fault resistance is illustrated in Figure 3.24. The fault current decreases with the increase of fault resistance. A bolted fault can result in a large current, which is easily detected by a signal with low strength. High impedance fault is more difficult to detect. However, in the proposed methods, asymmetrical high impedance faults can be identified by unbalanced fault currents.

Figure 3.25 shows the impact of the firing angle. For safety consideration, the firing angle is initiated at close to  $180^\circ$ , and then decreases gradually until all potential faults can be detected.

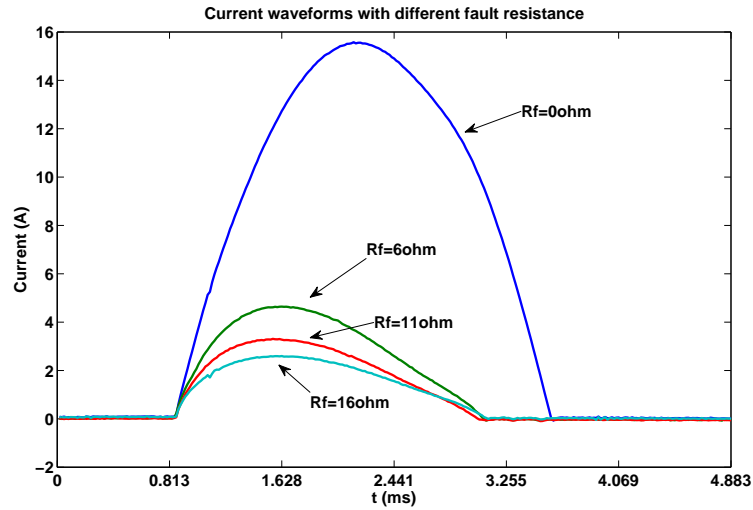


Figure 3.24: Measured current waveforms with different fault resistances.

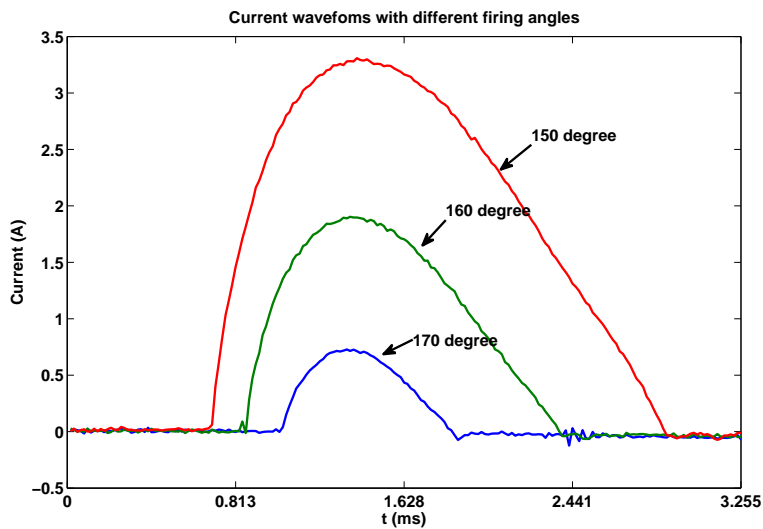


Figure 3.25: Measured current waveforms with different firing angles.

### 3.5 Alternative Cascaded Structure

An alternative signal generation structure is shown in Figure 3.26, which has four thyristors cascaded together. Similarly, the device is connected to an energized upstream phase line and the neutral through a transformer. In the

de-energized side, the phase conductors are connected to the joints between two thyristors. The cascaded structure only uses four thyristors rather than six thyristors in the previous structure.

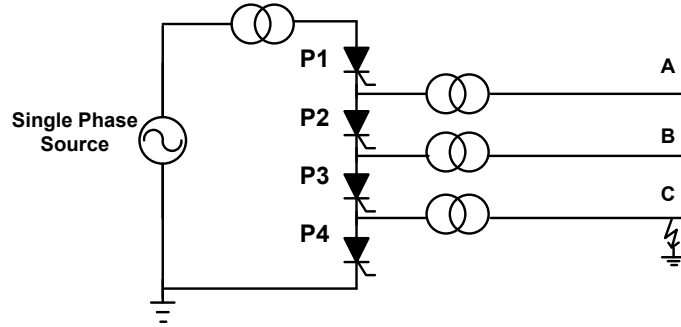


Figure 3.26: An alternative cascaded structure.

The control logic of gating signals is illustrated in 3.27. In Step I, a zero sequence signal is applied to three phases for phase-ground fault detection. In Step II, a signal is injected from phase A and returns to the neutral from phase B or C if there is any fault between phase A and other phases; There is a little difference from the bridge-based scheme in Step III, where the first thyristor must be turned on in order to connect phase B to the energized side. Faults between phase A and phase C or between phase B and phase C can be detected in Step III. The criteria for fault detection in this topology are the same as those in the bridge-based topology, as the signal responses under different types of faults are still the same.

### 3.6 Conclusion

A thyristor based fault detection scheme is presented to detect a fault in de-energized feeders, which can ensure a smooth and safe reclosing without caus-

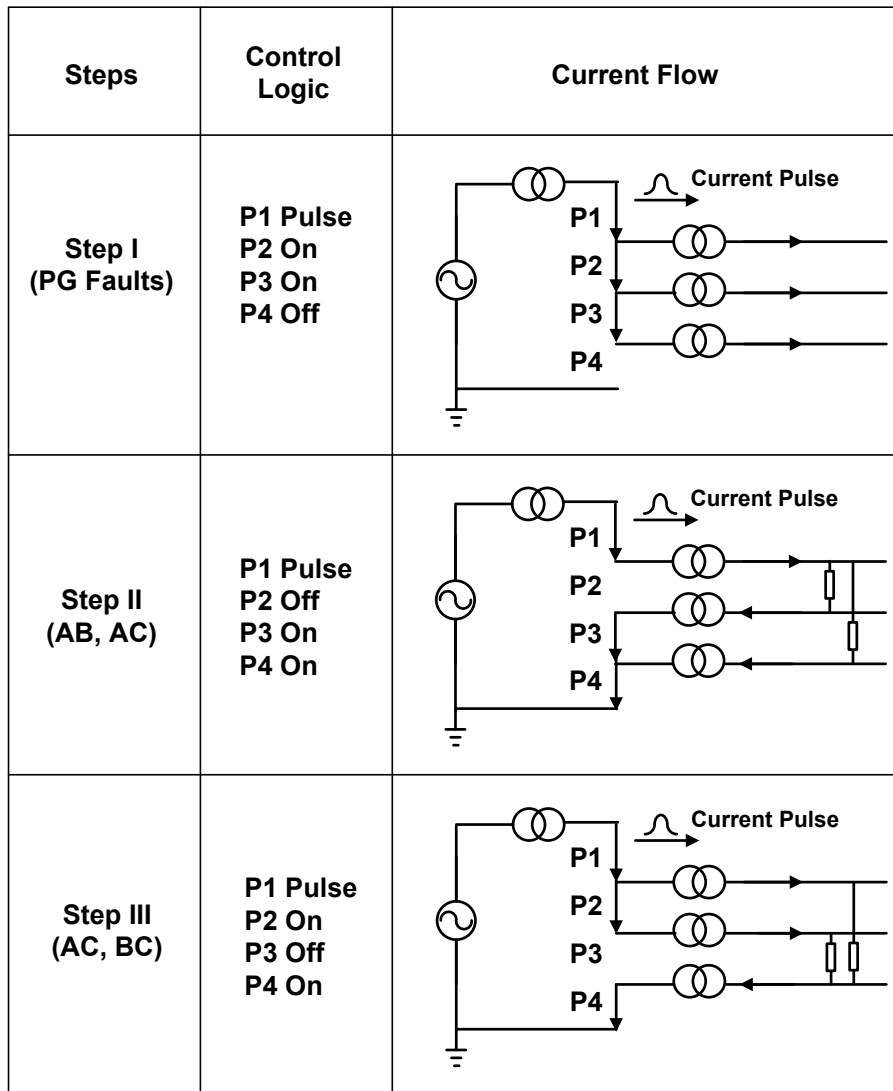


Figure 3.27: The control logic of the cascaded structure.

ing hazard to the downstream devices and personnel. The proposed technique functions by generating a controllable detection signal through the thyristor-based device connected in parallel with a recloser, and using the stimulated voltage and current signals to detect if a fault exists. The device can be run manually or automatically whenever reclosing is needed. For auto-operation, communication is not an issue since the recloser is linked with communication means if it can be reclosed remotely. To identify different types of faults, the

characteristics of injected signals under phase-to-ground faults and phase-to-phase faults are studied and the criteria for identifying a faulted line from healthy lines are developed accordingly. With the three-step fault detection algorithm, phase-to-ground faults are detected in Step I, and the phase-to-phase faults are detected in Steps II and III. The whole three-step testing procedure takes between one to a few seconds, which is sufficiently fast for fault detection in a de-energized system. An alternative structure with fewer thyristors is also presented.

## Chapter 4

### Harmonic Impedance Based Symmetrical Fault Detection in De-Energized Feeders

As a symmetrical fault affects three phases equally, the method based on the difference of three-phase currents for asymmetrical faults detection is not applicable here. In addition, when a voltage pulse is applied to a de-energized circuit, either a stalled motor or a capacitor bank can cause a large current like a short-circuit. This chapter describes a method based on analysis of harmonic impedance for symmetrical fault detection in de-energized feeders. By analyzing the differences of their harmonic impedances, this method can also be used to distinguish a real fault from a stalled motor or a capacitor bank.

#### 4.1 Characteristics of Symmetrical Fault in De-Energized Feeders

As shown in Figure 4.1, a voltage from one energized phase feeds three phases when the thyristors T1, T3 and T5 are fired simultaneously on a certain degree before a zero-crossing point. The corresponding current pulse in each phase depends on the line condition.

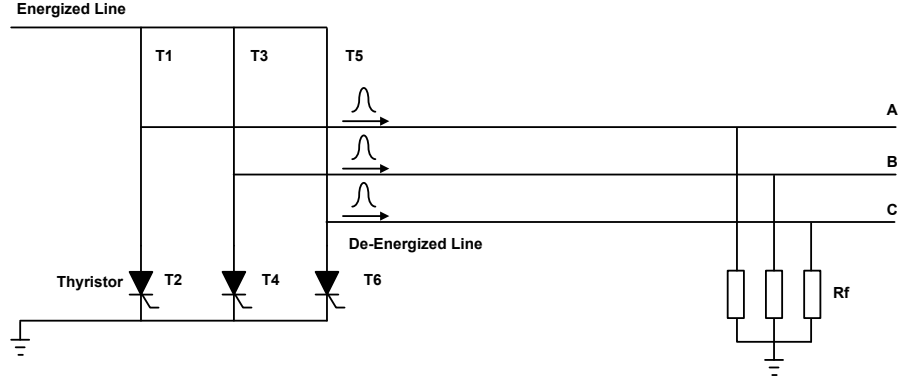


Figure 4.1: The proposed scheme for symmetrical faults detection.

In a normal condition, the injected currents are very small. However, if there is a symmetrical fault, inrush currents will show up in all phases at the same time. To illustrate this, a representative  $25kV$  system with  $10km$  distribution line is used as shown in Figure 4.2, and the parameters of the system are listed in Table 4.1.

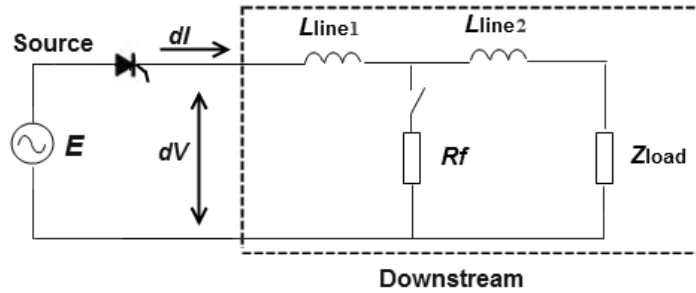


Figure 4.2: The equivalent circuit with a symmetrical fault.

To compare the difference of the faulted and unfaulted conditions, a symmetrical fault is created at  $5km$  away from the recloser. When the thyristor is fired at  $150^\circ$ , the voltage and current waveforms are shown in Figure 4.3. Apparently, a symmetrical fault increases the current magnitude. However, this fault current magnitude highly depends on the fault resistance  $R_f$ . It is therefore difficult to set up an appropriate threshold to detect if a fault exists, especially considering the possibility of a high impedance fault.

Table 4.1: The parameters of a representative 25kV system

Utility	$V_{pp} = 25kV, 60Hz, 50MVA$
Transformers	14.43kV/480V, 5MVA, $z=0.03pu$
Feeder Length	5km (Line1), 5km (Line2)
Line	$R_1 = 0.2138 \text{ ohm/km}, X_1 = 0.3928 \text{ ohm/km}$ and $B_1 = 4.2315 \text{ us/km}$ ; $R_0 = 0.3875 \text{ ohm/km}, X_0 = 1.8801 \text{ ohm/km}$ and $B_0 = 1.6058 \text{ us/km}$ .
Three-phase Load	4MVA, p.f.=0.95, lagging. 5MVA service transformer, 25kV/600V, $z=0.05$
Symmetrical Fault	$R_f = 20\Omega$

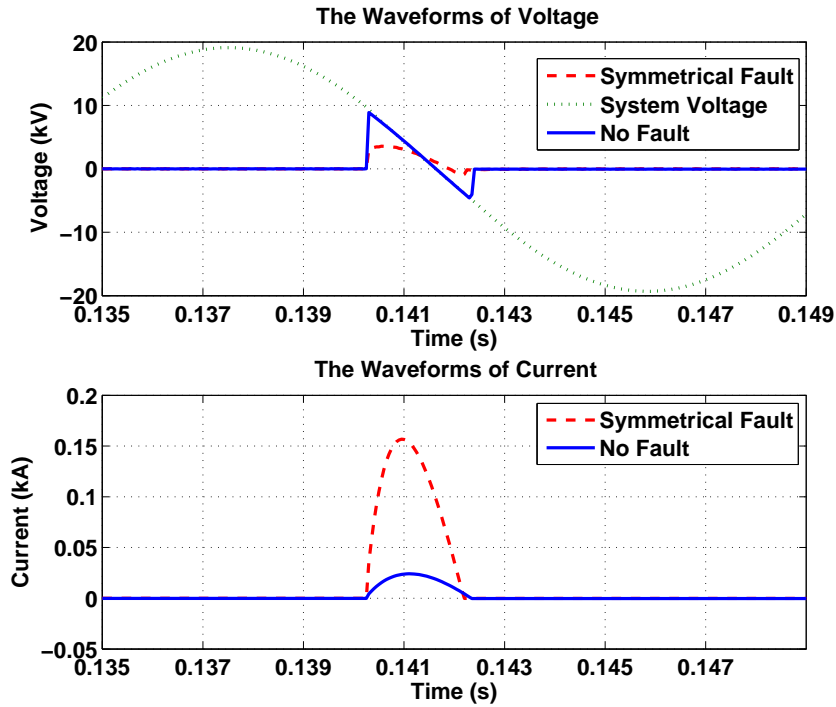


Figure 4.3: The voltage and current in different conditions.

Further considering stalled motors and shunt capacitor banks connected at downstream, a high current can be produced by applying the voltage  $V$ , similar to a short-circuit. Therefore, a fault detection method not just based on the current magnitude is required to distinguish a motor or a capacitor from a real fault.



## 4.2 Harmonic Impedance of A De-Energized Feeder

A de-energized downstream can be considered as a linear network as shown in Figure 4.4, and an equation is established according to the Fourier Transform of non-periodical signals [84],

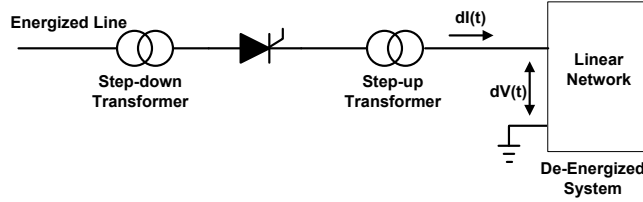


Figure 4.4: A de-energized downstream is considered as a linear network.

$$V(j\omega) = Z(j\omega) \times I(j\omega) \quad (4.1)$$

where  $V(j\omega)$ ,  $I(j\omega)$  are the Fourier Transform of transient voltage and current.  $Z(j\omega)$  is the harmonic impedance. The harmonic impedance can be further expressed as:

$$Z[jn\omega_1] = \frac{V[jn\omega_1]}{I[jn\omega_1]} \quad (4.2)$$

or

$$Z(f) = \frac{V(f)}{I(f)} \quad (4.3)$$

where  $\omega_1 = 2\pi f_1$ , and  $f_1$  is the fundamental frequency.

These equations imply that the harmonic impedance can be calculated by using an Fast Fourier Transform (FFT) algorithm. The basic principle of the proposed idea is to utilize the change of  $Z(f)$  in different conditions to detect a symmetrical fault. In normal condition, the harmonic impedance of

a de-energized feeder as shown in Figure 4.2 is

$$Z(f) = R(f) + jX(f) = R_{load} + j2\pi f(L_{load} + L_{line}) \quad (4.4)$$

where  $R_{load}$ ,  $L_{load}$  are the equivalent resistance and inductance of the load,  $L_{line} = L_{line1} + L_{line2}$ . The harmonic reactance  $X(f)$  is proportional to frequency, and the ratio  $k$  is

$$k = 2\pi(L_{load} + L_{line}) \quad (4.5)$$

However, if a symmetrical fault exists with fault resistance  $R_f$ , the harmonic impedance becomes

$$Z'(f) = X_{line1}(f) + R_f // (R_{load} + j(X_{load}(f) + X_{line2}(f))) \quad (4.6)$$

The harmonic resistance  $R(f)$  and harmonic reactance  $X(f)$  are changed to  $R'(f)$  and  $X'(f)$ .

$$R'(f) = \frac{R_f R_{load} (R_f + R_{load}) + R_f (L_{load} + L_{line2})^2 (2\pi f)^2}{(R_f + R_{load})^2 + (L_{load} + L_{line2})^2 (2\pi f)^2} \quad (4.7)$$

$$X'(f) = j(2\pi f L_{line1} + \frac{R_f^2 2\pi f L_{line2}}{(R_f + R_{load})^2 + (L_{load} + L_{line2})^2 (2\pi f)^2}) \quad (4.8)$$

Figure 4.5 and Figure 4.6 illustrate harmonic resistance and harmonic reactance, respectively.

Since  $(L_{load} + L_{line2})^2 (2\pi f)^2$  is much smaller than  $(R_f + R_{load})^2$  when frequency is low, one can obtain that  $R'(f) \approx R_f // R_{load}$  from (4.7) at low frequencies (such as 0 ~ 360Hz). On the other hand,  $X'(f)$  consists of two parts: the

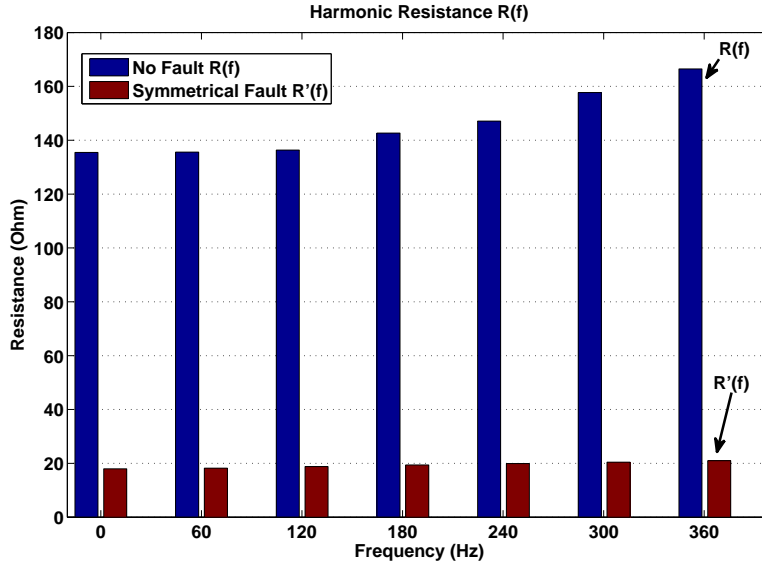


Figure 4.5: The harmonic resistance  $R(f)$  in unfaulted and faulted cases.

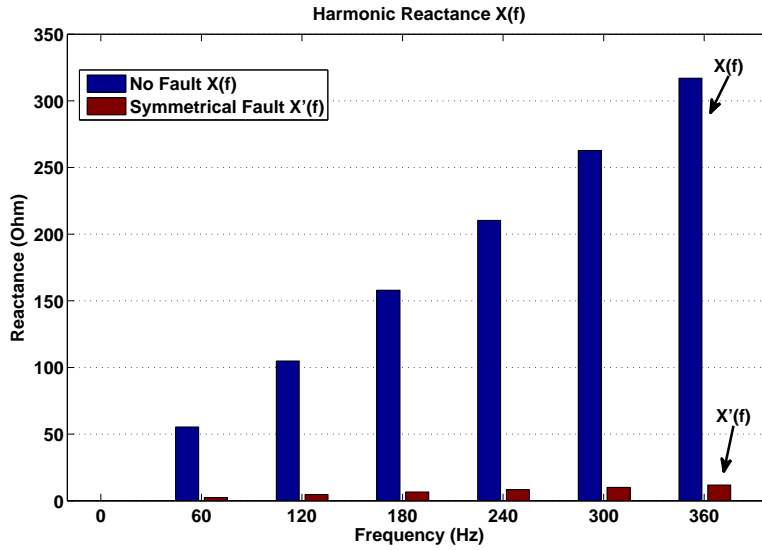


Figure 4.6: The harmonic reactance  $X(f)$  in unfaulted and faulted cases.

first part ( $2\pi f L_{line1}$ ) is proportional to the frequency but the ratio  $k'$  becomes much smaller as

$$k' = 2\pi L_{line1} \ll k = 2\pi(L_{load} + L_{line}) \quad (4.9)$$

And, the second part of  $X'(f)$  decreases with an increase in frequency. Thus, the overall effect is that  $X'(f)$  is much smaller than  $X(f)$  and it almost has no significant change at low frequencies.

Based on the above analysis, harmonic impedance can be utilized for symmetrical fault detection. The decision logic is therefore designed as following:

1. Measure the currents and voltages of three phases after T1, T3 and T5 are fired simultaneously.
2. Are currents the same? If No, turn to asymmetrical faults analysis. If Yes, estimate the  $X(f)$ .
  - (a) If  $X(f)$  is proportional to frequency, there is no fault.
  - (b) If  $X(f)$  has no significant change as frequency increases, there is a symmetrical fault.

### 4.3 The Impact of Stalled Motor

A stalled motor behaves like a short-circuit in a de-energized system. The equivalent circuit of a stalled motor is shown in Figure 4.7 [85]. The parameters  $R_1$  and  $X_1$  are the motor stator resistance and leakage reactance, and the locked-rotor resistance and leakage reactance referring to the stator side are denoted as  $R_2$  and  $X_2$ , respectively. The reactance  $X_m$  is the magnetizing reactance of the motor. The stator current is  $I_1$  and the rotor current is  $I_2$ .

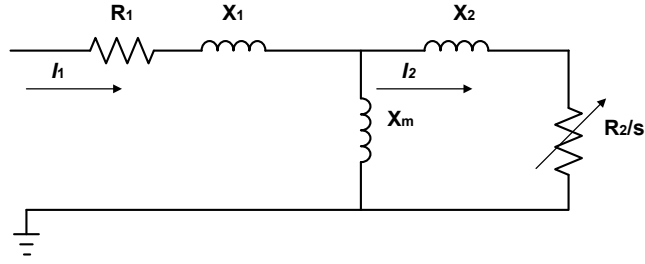


Figure 4.7: The equivalent circuit of a stalled motor.

The motor slip  $s = 1$  when the motor is stalled. Considering  $X_m \gg X_1$ , the impedance of a stalled motor is therefore expressed as

$$Z_M = R_M + jX_M = (R_1 + R_2) + j(X_1 + X_2) \quad (4.10)$$

Typically, power factor during motor starting is between  $0.2 \sim 0.3$ , and an inrush current can be up to  $600\% \sim 800\%$  of the rated current. As shown in Figure 4.8, a stalled motor can cause a large current pulse when a voltage is applied. The currents in different conditions are illustrated in Figure 4.9, in which the current pulse with a stalled motor connected is comparable to the fault current. This also indicates that the current magnitude is not a good indicator to distinguish a fault from a stalled motor. From the aspect

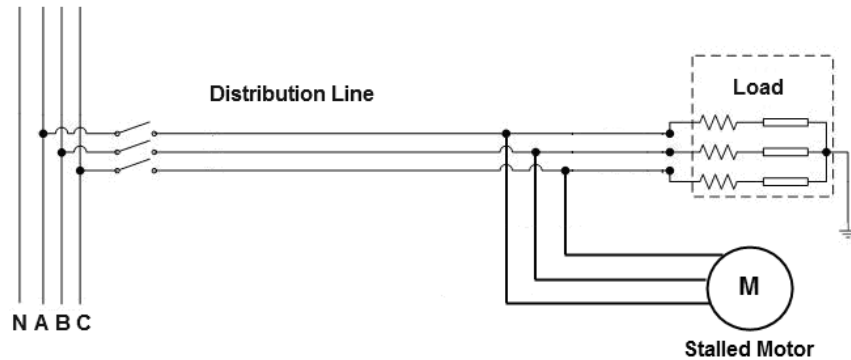


Figure 4.8: (Note: the stalled motor: 5000hp, starting p.f.=0.2, inrush current 700%, fed with a three-phase 5MVA transformer, 25kV/4.16kV,  $z=0.05$ )

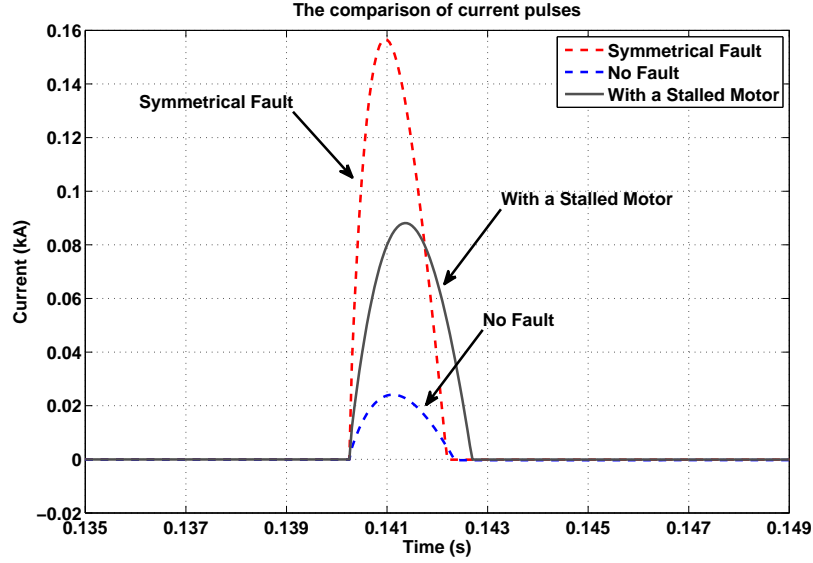


Figure 4.9: The effect of a motor on the current pulse.

of frequency domain, the impedance of a stalled motor is more inductive so that the resistance  $R_M$  in (4.10) can be ignored in a simplified model. When a stalled motor is connected parallel to a load as shown in Figure 4.8, the reactance of the downstream becomes:

$$X_{D.M}(f) = j(2\pi f L_{line} + \frac{R_{load}^2 L_M (2\pi f) + L_{load} L_M (L_{load} + L_M) (2\pi f)^3}{R_{load}^2 + (L_{load} + L_M) (2\pi f)^2}) \quad (4.11)$$

where  $X_{D.M}$  is the reactance of downstream with a stalled motor,  $L_M$  is the inductance of a stalled motor. The first part of the  $X_{D.M}(f)$  is proportional to frequency  $f$  and the ratio  $k_{DM} = 2\pi L_{line} > k' = 2\pi L_{line1}$ ; the second part of the  $X_{D.M}(f)$  increases with an increase in frequency.

As shown in Figure 4.10,  $X_{D.M}(f)$  increases significantly as the frequency increases. This scenario is clearly different from the reactance  $X'(f)$  in a faulty condition. Similar to the detection of symmetrical faults,  $X(f)$  versus

frequency can be used to distinguish a fault from a stalled motor. Note that

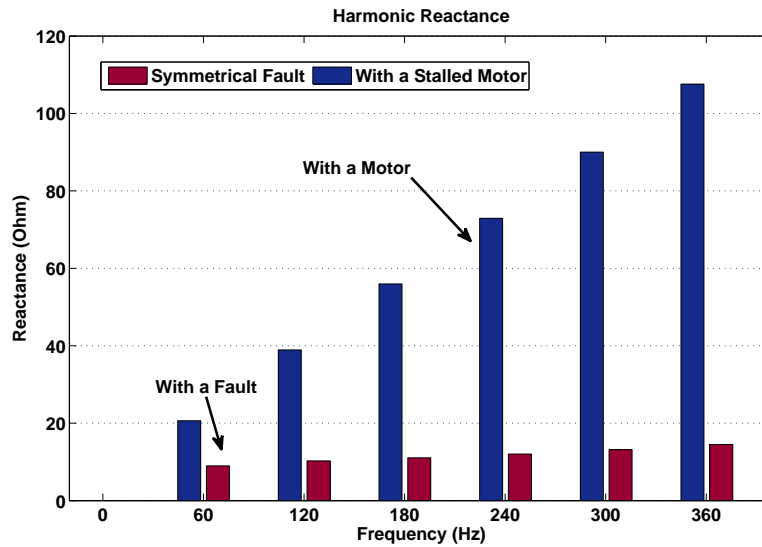


Figure 4.10: The harmonic reactance  $X_f$  with a stalled motor.

using the reactance vs. frequency criterion can effectively distinguish a fault from a stalled motor situation, but it cannot distinguish a stalled motor from a normal condition as they both have similar  $X/f$  ratio. However, detecting the existence of a stalled motor is not really the purpose of this work. As long as a fault can be effectively detected, the proposed detection scheme works as expected.

#### 4.4 The Impact of Capacitor Bank

As shown in Figure 4.11, a shunt capacitor is usually connected in a distribution system to provide reactive power compensation and improve the quality of the electrical supply. However, energizing a capacitor bank also causes a high inrush current which is similar to a fault. When a voltage pulse is ap-

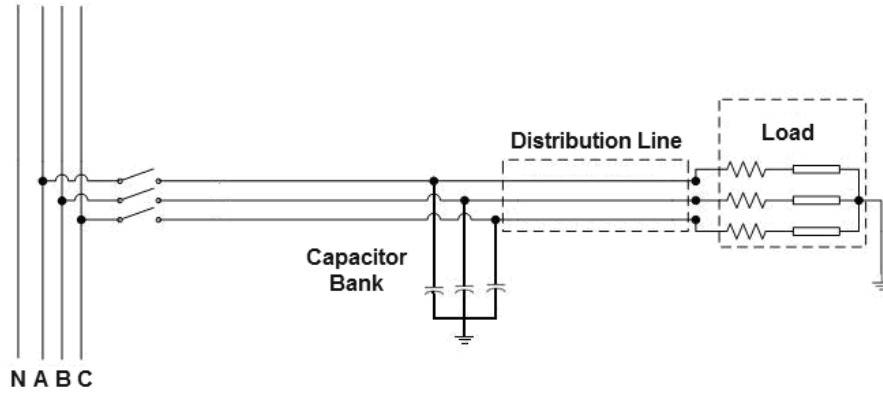


Figure 4.11: A three-phase shunt capacitor bank is connected to a distribution system.

plied to a downstream with a  $2.5\text{MVar}$  shunt capacitor, the produced current pulse is shown in Figure 4.12. This current has a comparable magnitude as

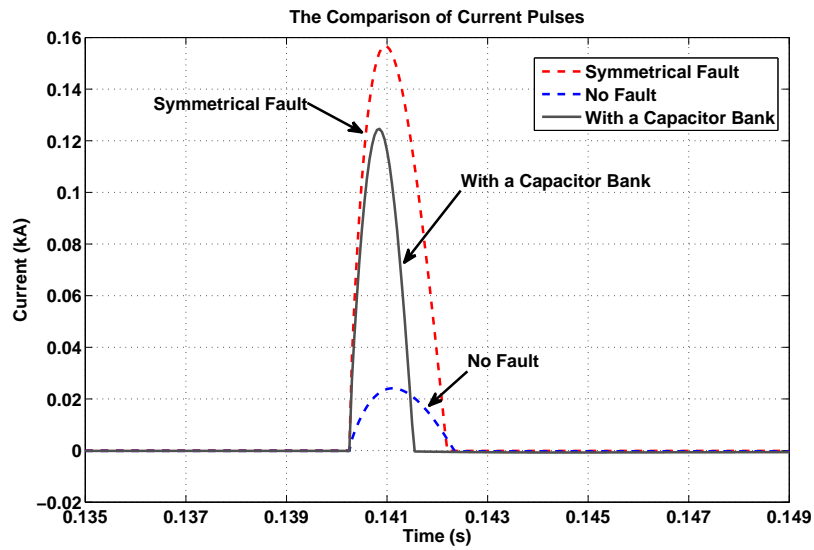


Figure 4.12: The effect of a capacitor on the current pulse.

a fault current. It is therefore difficult to distinguish a fault from a capacitor bank if only comparing the waveforms of current.

In the frequency domain, the capacitor almost has no contribution in DC component (0 Hz) and its harmonic impedance  $1/j\omega C$  decreases as frequency



increases. After installing a capacitor bank in a distribution system, the harmonic resistance  $R(f)$  is changed to  $R_{D-C}(f)$  as in (4.12).

$$R_{D-C}(f) = \frac{R_{load}}{R_{load}^2(2\pi fC)^2 + ((2\pi f)^2 L_{load}C - 1)^2} \quad (4.12)$$

$R_{D-C}(f)$  decreases rapidly with the increase of frequency. Contrast to this, the resistance  $R'(f)$  in a faulted condition almost has no change in low frequencies. Comparison of harmonic resistance in a faulted condition and a normal condition are shown in Figure 4.13. The difference between  $R_{D-C}(f)$

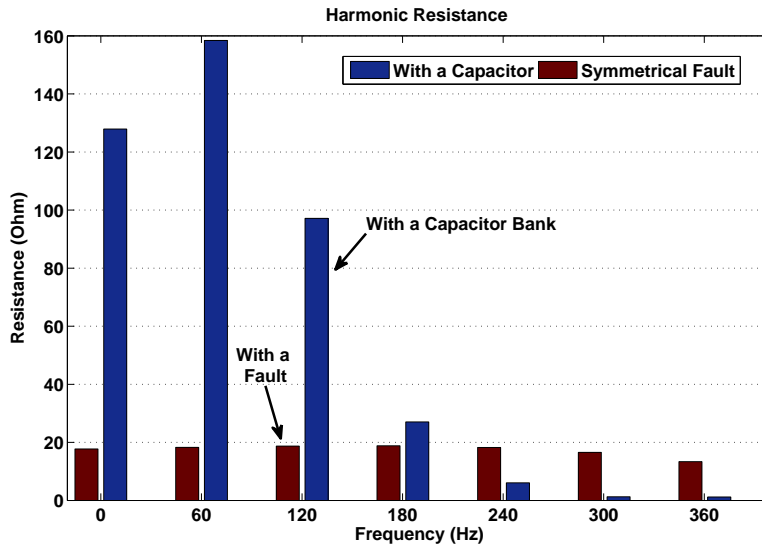


Figure 4.13: Harmonic resistance with a capacitor.

and  $R'(f)$  provides a criterion for distinguishing a fault from a capacitor bank.

Furthermore, if both a stalled motor and a capacitor bank exist in the downstream, the harmonic impedance will not follow the patterns discussed above since parallel resonance could happen. For example, if the motor in Figure 4.8 and the capacitor in Figure 4.11 are both connected to a de-energized

system in parallel, the harmonic impedance is changed as shown in Figure 4.14. Apparently, the parallel resonance happens at the frequency of 180 Hz.

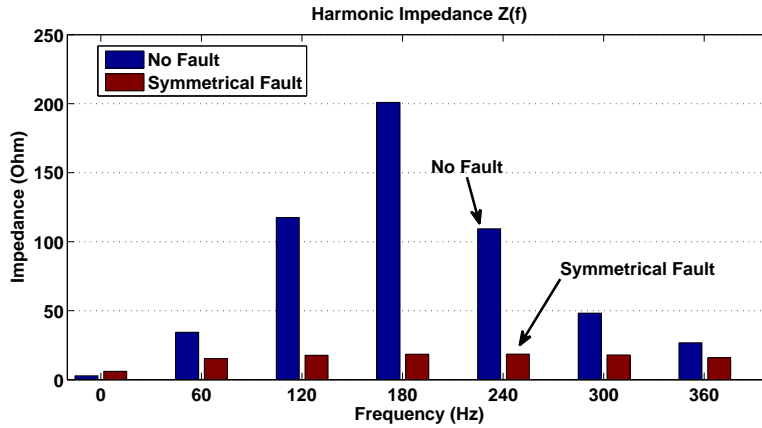


Figure 4.14: The harmonic impedance when both a 2.5MVA capacitor and a 5000hp motor connected.

The magnitude of the impedance at resonance frequency is limited due to the existence of resistance.

Generally, the resonance frequency depends on the system capacitance and reactance. If capacitance is small, a resonance will happen at higher frequency. Figure 4.15 shows the simulation result when the 2.5MVar capacitor is replaced by a 0.25MVar capacitor. Within the frequencies between 0 ~ 360Hz, the scenario of parallel resonance is not observed. However, the difference between the faulted and the unfaulted cases is significant in both Figure 4.14 and Figure 4.15. A symmetrical fault can still be detected even though there is a parallel resonance introduced by a capacitor and a stalled motor. The overall symmetrical fault detection procedure is updated as following. A flow chart is also presented in Figure 4.16.

1. Measure the currents and voltages of three phases after T1, T3 and T5 are fired simultaneously.

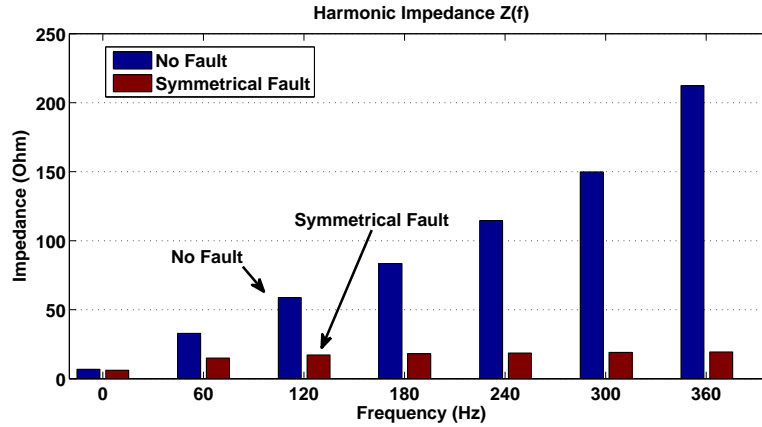


Figure 4.15: The harmonic impedance when both a 0.25MVA capacitor and a 5000hp motor are connected.

2. Are currents the same? If No, turn to asymmetrical faults analysis (as presented in Chapter 3). If Yes, calculate  $Z(f)$ ,  $X(f)$  and  $R(f)$  by using the Fourier Transform of current and voltage with an FFT algorithm.
  - (a) If harmonic resonance is observed in  $Z(f)$ , it indicates both a capacitor and a motor are connected and the line is healthy.
  - (b) Otherwise, if  $X(f)$  has a large increase with the increase of a frequency and it is almost proportional to the frequency, it indicates a normal condition or a stalled motor exist.
  - (c) Otherwise, if  $R(f)$  decays as frequency increase, a capacitor is connected without fault.
  - (d) If both  $X(f)$  and  $R(f)$  have no significant change as frequency increase in the observed frequencies ( $0 \sim 360\text{Hz}$ ), it indicates a symmetrical fault exist.

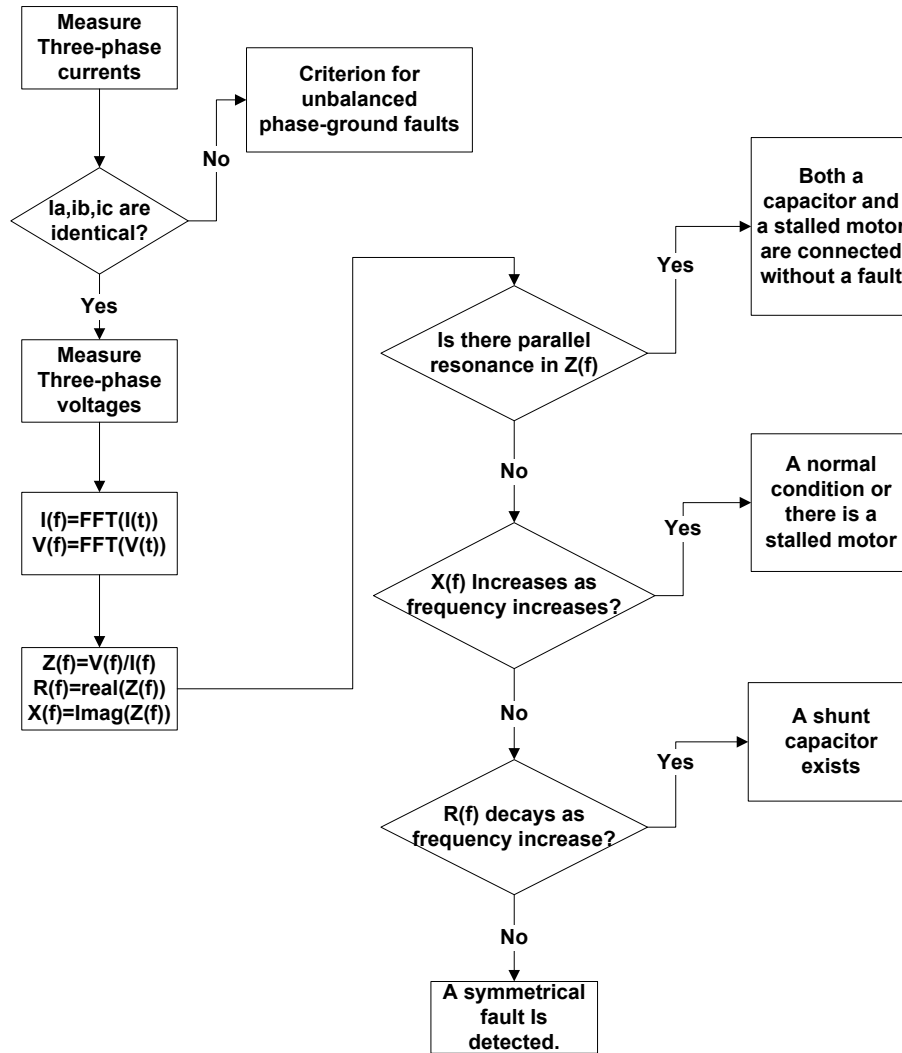


Figure 4.16: The overall logic for symmetrical fault detection.

## 4.5 Lab Experiment

A lab experiment based on a single-phase low voltage system has been carried out to verify the proposed method. The laboratory prototype comprises of (1) a thyristor-based signal generator, (2) a data acquisition system and (3) a lumped model based equivalent circuit. As the injected current is from an energized phase in the proposed scheme, a single-phase system can effectively represent a balanced three-phase system for the research of symmetrical fault

detection. In the data acquisition device, six channels are utilized, three of them for voltage measurement and the other three for current measurement. The sampling rate is 1024 points every cycle, and 1024-point FFT is performed for harmonic impedance analysis based on 60Hz fundamental. This sampling rate is fast enough since the signal frequencies of interest are between  $0 \sim 360$  Hz. In some cases such as high impedance fault detection, higher frequencies components are also considered as will be discussed later. The system parameters in this test are listed as following.

Table 4.2: The parameters of the lab experiment

Power source	120V
Transformer Impedance	$L_{xformer} = 0.76mH$
Line Impedance	$R_{line} = 0.08\Omega, L_{line} = 0.4mH$
Load Impedance	$R_{load} = 11.4\Omega, L_{load} = 10mH$
Fault Resistance	$R_f = 0 \sim 11\Omega$
Thyristor Firing Angle	$150^\circ \sim 180^\circ$

The equivalent circuit of the lab test is shown in Figure 4.17. The fault

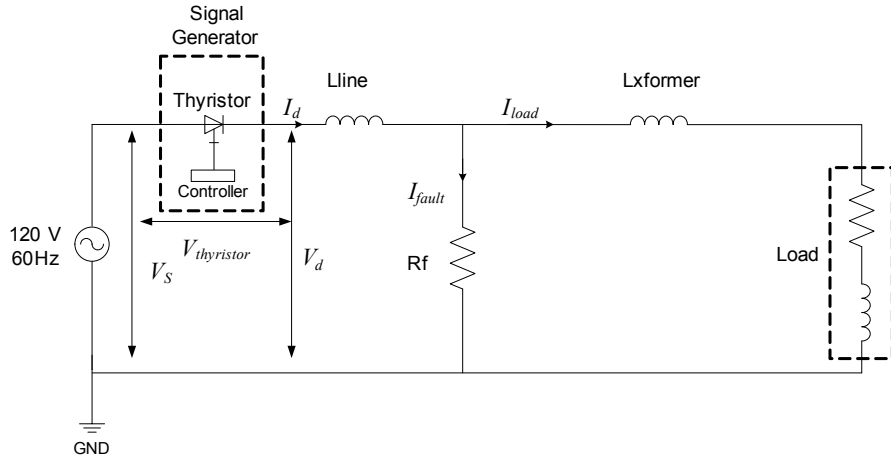


Figure 4.17: The diagram of the low voltage lab test setup.

resistance  $R_f$  is adjustable. The harmonic resistance  $R(f)$  and reactance  $X(f)$  are calculated by the measured  $V_d$  and  $I_d$ .

Figure 4.18 and Figure 4.19 show  $R(f)$  and  $X(f)$  in three different conditions: (a) a bolted fault; (b) a fault with resistance  $R_f = 6\Omega$ ; (c) No fault. It is

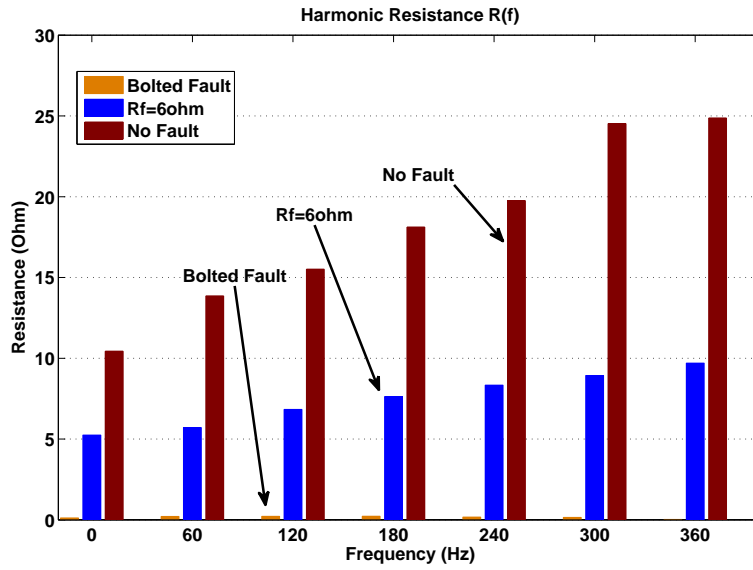


Figure 4.18: Comparison of harmonic resistance  $R(f)$ .

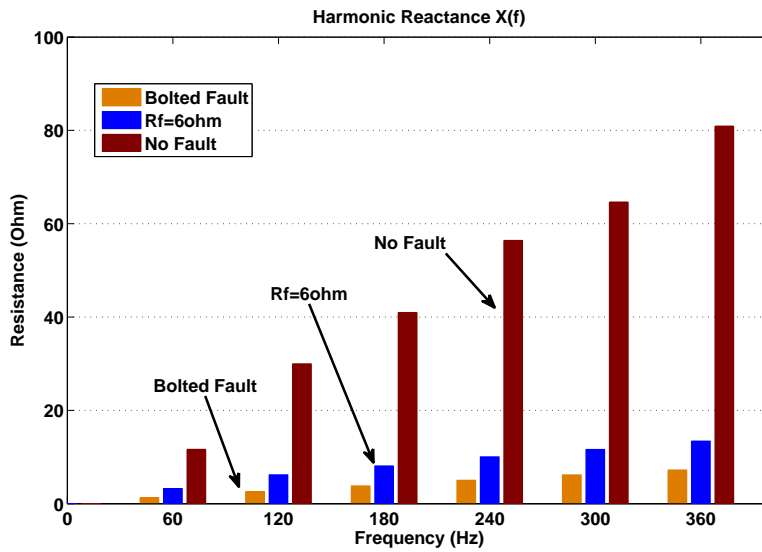


Figure 4.19: Comparison of harmonic reactance  $X(f)$ .

seen that  $R(f)$  with a bolted fault is almost zero at all frequencies, which can be easily detected. On the other hand,  $X(f)$  increases slowly in both faulted

situations but increase fast in a unfaulted situation, which is consistent with the theoretical analysis.

A single-phase induction motor is connected to the test circuit and the parameters of the motor are listed in Table 4.3. As the induction motor is just like

Table 4.3: The parameters of an induction motor

Parameters	Value
H.P.	1/12
Rated Voltage (V)	115
Rated Current (A)	2.8
Phase	1
R.P.M	1800

a short-circuit when it is stalled, it causes a high current which is even larger than the fault current as shown in Figure 4.20. To distinguish the stalled motor from a fault,  $X(f)$  in the two conditions are illustrated in Figure 4.21.

It is apparent that the reactance of the downstream with a motor increases

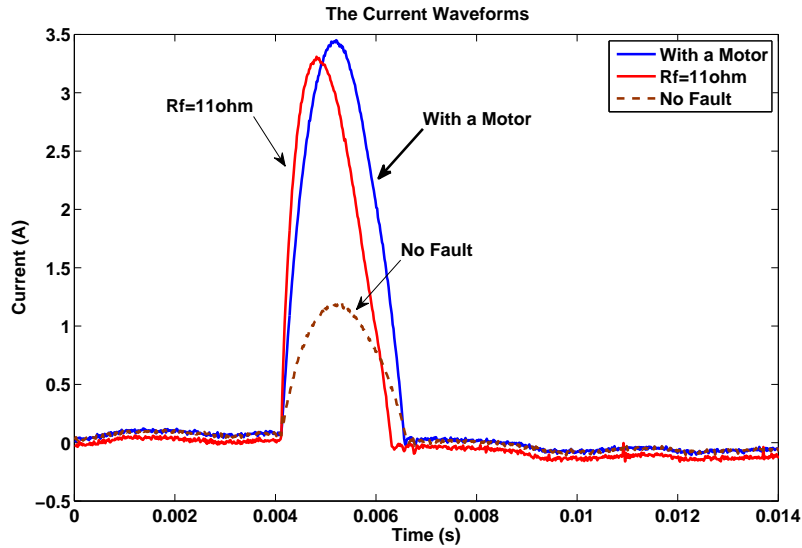


Figure 4.20: Current waveforms of the induction motor test.

in a normal condition, while this reactance with a fault is less affected by the

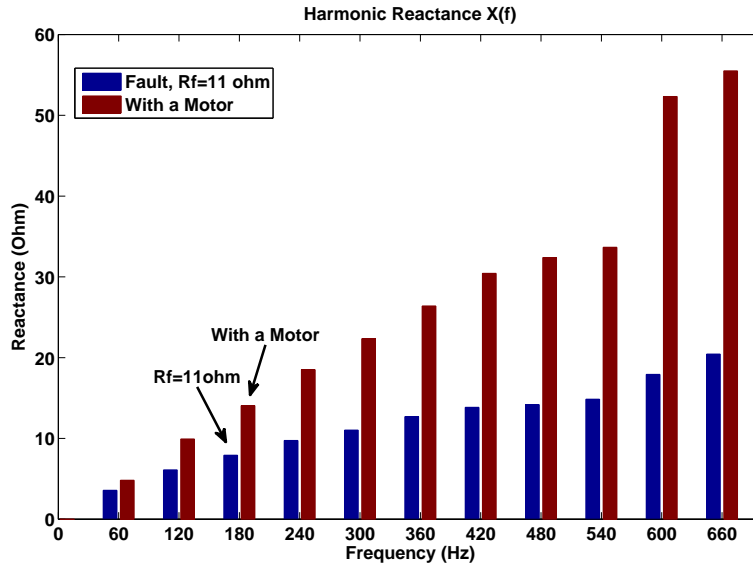


Figure 4.21: Harmonic reactance  $X(f)$  of the induction motor test.

increase of frequency.

In reality, a fault could happen on any ground condition, like tree branch, sand, mud and dirt. The ground conditions affect the characteristics of faults, and change the fault resistance. As shown in Figure 4.22, a tree branch is cut off from a live tree and its length is limited to 10cm to lower the impedance. However, its resistance still reaches  $16k\Omega$ , even though it is wet.

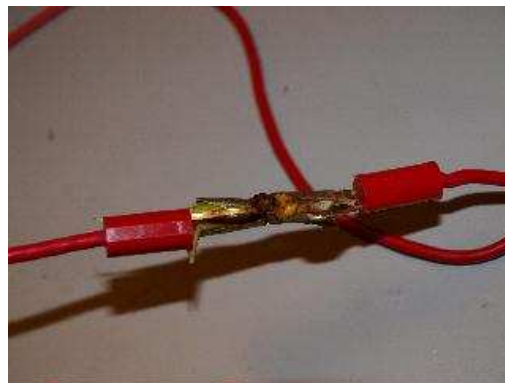


Figure 4.22: High impedance fault test with a tree branch.



Figure 4.23 shows the currents obtained from the tree branch test. The resis-

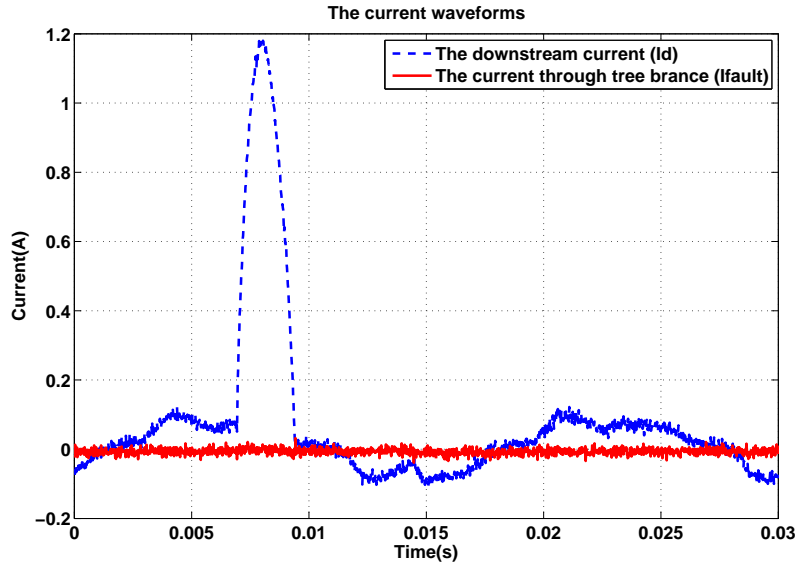


Figure 4.23: Current waveforms in a tree branch test.

tance of the branch is too high so that the fault current is almost zero.

Another high impedance fault test is with a box of dirt (Figure 4.24). The dirt comprises mud, little rocks, dead leaves and water. The resistance is  $5k\Omega$ , which is lower than the tree branch. The fault current is very low as shown in Figure 4.25, and most of the injected current  $I_d$  flows through the connected loads rather than the box of dirt with high impedance.

The harmonic reactance in two high impedance fault tests are shown in Figure 4.26. Since there is no electrical response on the tree branch, the measured harmonic reactance in the faulted line and the unfaulted line have almost no difference. The tree branch test is not effective due to the low voltage. In a real distribution system, a stronger voltage pulse could cause arcs through a tree branch, which essentially reduces the fault impedance and therefore help



Figure 4.24: High impedance fault test with a box of mud and dirt.

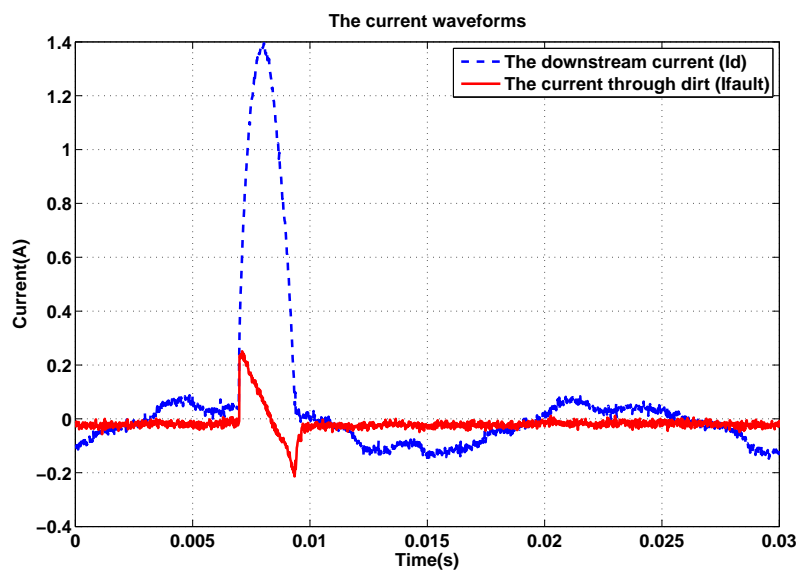


Figure 4.25: Current waveforms in a mud and dirt test.

high impedance fault detection. The mud and dirt test has better results despite the low magnitude fault current. The harmonic reactance in the faulted condition follows a flatter trend within a range of frequencies, such as

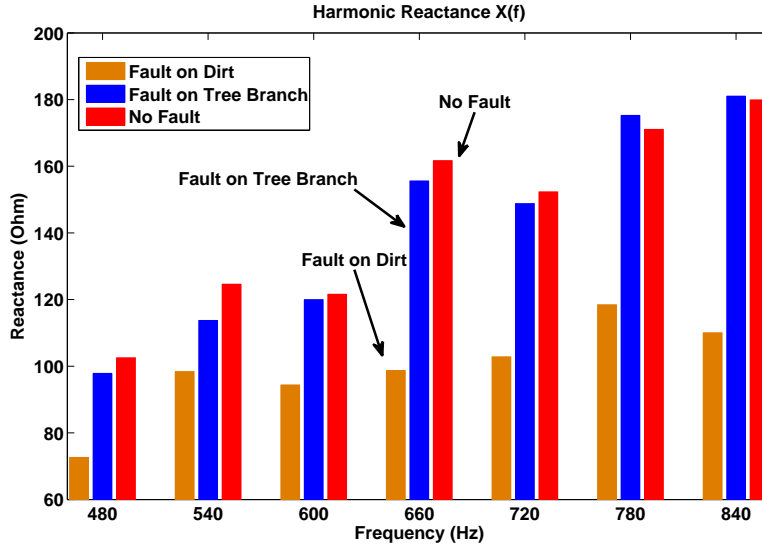


Figure 4.26: Harmonic reactance in the high impedance fault tests.

between 480 ~ 840 Hz, compared to the unfaulted condition.

## 4.6 Conclusion

An active method is presented for symmetrical fault detection in a de-energized system, where the existence of stalled motors or shunt capacitors make fault detection more challenging as they behave like short-circuits. A new detection algorithm based on analysis of harmonic impedance is proposed. This algorithm can effectively detect a symmetrical fault and distinguish a fault from a stalled motor or capacitor bank. The proposed method is verified in both computer simulations and lab tests.

## Chapter 5

### Monitoring of Neutral Grounding Integrity in Multi-Grounded Neutral System

A distribution system is not perfectly balanced due to several reasons, such as unbalanced three-phase loads, uneven distribution of single-phase loads and unsymmetrical system parameters. These unbalances lead current flowing through neutral and ground. When a neutral conductor is broken, it forces more current flowing into the earth which increases neutral-to-earth voltage (NEV) in normal situation or causes a large ground potential rise (GPR) during a fault. An active disturbance based method is presented in this chapter for the monitoring of neutral grounding integrity. A disturbance is created from the secondary neutral of a transformer, the current flow in the primary neutral is monitored to indicate the integrity of a neutral.

#### 5.1 Introduction of Multi-Grounded Neutral System

A distribution system can be either non-effectively grounded or effectively grounded. In some European and Asian countries, non-effectively grounded system is commonly used, in which a neutral line is unnecessary as no current is expected to flow in neutral [86]. On the other side, an effective grounding

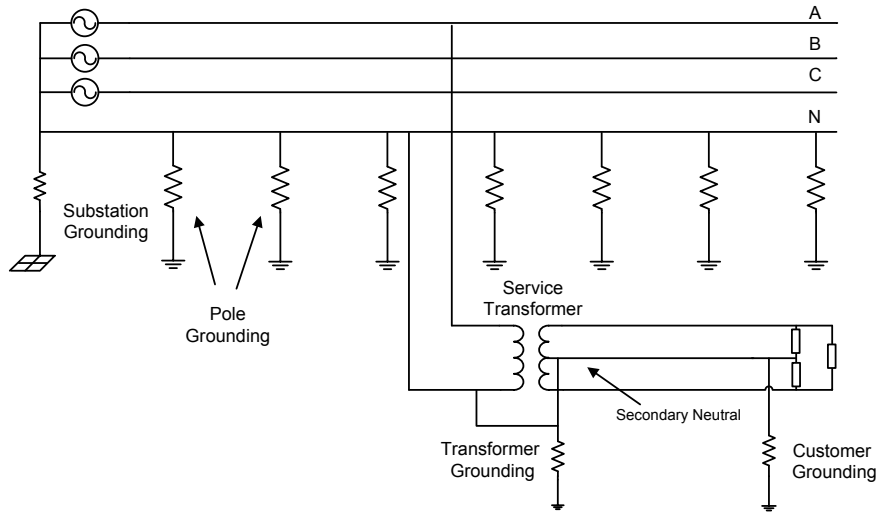


Figure 5.1: The typical structure of a MGN system.

system may have a single point grounded neutral or multi-grounded neutral (MGN). The latter is widely adopted in North America [51] due to safety and reliability. Each grounding system has its own pros and cons. This chapter only focuses on three-phase four-wire multi-grounded neutral system.

Figure 5.1 shows a typical MGN system. A primary feeder has three-phase conductors and a neutral conductor starting from a substation. The neutral line is grounded at several points along its route. The interval of grounding is at least three grounds per kilometer [52]. When a primary neutral reaches a service transformer, it is tied to a secondary neutral at the transformer grounding point. Secondary neutral is also grounded at service panels of customers.

One major advantage of a MGN system is that a high current will rise to trigger an over-current protection device in the case of a short circuit, so as to avoid the risk of electrical shock if a person touches an exposed conduc-

tive device. However, with this arrangement, unbalanced current can flow through neutral into ground. Ground current produces neutral-to-earth voltage, which can be transferred into customers' facilities. Moreover, MGN can cause significant ground potential rise (GPR) during a fault, which becomes a growing concern in power industry.

If a MGN network experiences a broken or loose-connected neutral, its negative effects on NEV and GPR will be amplified. Moreover, customers may experience bad power quality due to poor neutral conditions. As shown in Figure 5.2, when neutral is in a good condition, the unbalanced current  $I_u$  is split to  $I_n$  and  $I_g$ . The current  $I_n > I_g$  due to low neutral impedance. Accordingly, the neutral-to-earth voltage  $V_{NTE} = I_g \times R_g$ . However, if the neutral is broken, the current  $I_u$  is forced into ground, causing an increased  $V'_{NTE} = I_u \times R_g > V_{NTE}$ . To make sure a MGN system works as intended, it is necessary to routinely monitor its neutral condition.

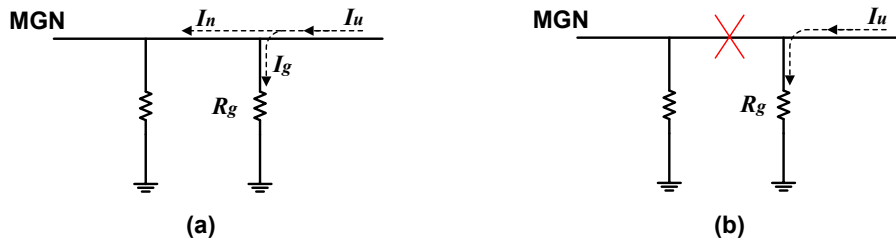


Figure 5.2: A broken neutral largely increases neutral-to-earth voltage.

## 5.2 Review of Neutral Monitoring Methods

Due to the complexity of a MGN network, the monitoring of neutral condition is quite difficult. Firstly, there is no accurate neutral model in computer simulation. Most of the existing power flow programs are designed to analyze

three-phase three-wire power system. The effects of neutral and grounding are either merged into phase wires or just neglected to simplify the simulation. Some researchers have introduced a full-scale model of a multi-grounded four-wire distribution system [87]. In this kind of model, the neutral wires and grounding can be represented explicitly, but the grounding electrodes are simplified and represented by unitary ones, which is not accurate in reality. Secondly, a neutral line is usually several kilometers or longer and there are a lot of different grounding connections along its route, such as substation grounding, pole grounding, equipment grounding and customer grounding. Each of them has different electrical characteristics and their performances also affect neutral condition. Thirdly, primary neutral has different features from secondary neutral. As shown in Figure 5.1, primary neutral is multi-grounded at poles and transformers, but secondary neutral is grounded only at service panels. In addition, an overhead primary neutral has certain distance from phase conductors, but it is hard to separate a secondary neutral from hot wires in a house or a commercial building.

After a comprehensive review of papers, patents and products, we found that although there are a number of publications and methods about condition monitoring of a secondary neutral, the research on primary neutral is very limited. The existing methods can be further categorized into two different types: passive schemes and active schemes, as shown in Table 5.1.

As monitoring of primary neutral condition is much more challenging, this chapter focuses on discussing the methods for the primary neutral monitoring, while the review of methods for secondary neutral monitoring are provided in the Appendix.

Table 5.1: The existing neutral condition monitoring methods

	Primary Neutral	Secondary Neutral
Passive Method	Visual Inspection	1.Capacitor Discharge 2.Leakage Current Measurement 3.Voltage Imbalance Detection 4. $V_{NTE}$ Measurement
Active Method	1.Fall-of-Potential 2.Staged Fault 3.RF signaling	1.Transient Signal Injection 2.RF Signal Injection

### 5.2.1 Neutral Impedance Measurement (NIM)

The impedance of a multi-grounded neutral is a critical parameter, and several monitoring schemes, including Fall-of-Potential based methods and staged fault based methods, measure neutral impedance to determine the condition of a neutral.

#### • Fall-of-Potential Based Methods

The Fall-of-Potential measurement based methods are widely used in grounding impedance measurement, which has been introduced in Chapter 2. Its principle is to inject a current into neutral and then measure the corresponding current and voltage. The neutral impedance is therefore obtained from the equation:

$$Z_{MGN} = \frac{V}{I} \quad (5.1)$$

Where  $Z_{MGN}$  is neutral impedance including all grounding connections,  $V$  is the voltage difference between neutral and the remote earth and  $I$  is the injected current as shown in Figure 5.3.



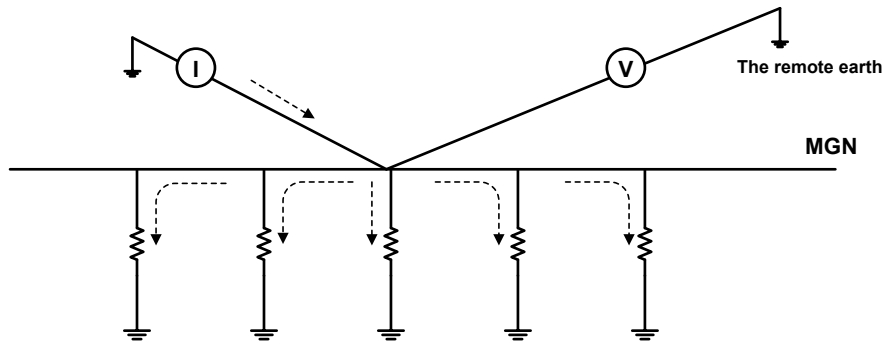


Figure 5.3: A typical Fall-of-Potential based method.

A typical FOP test system is at least composed of the following components:

- Current electrode. It is used to inject and collect current. Current electrode participates in a current return loop with the grounded neutral system together. Injected current will flow through the neutral line to the remote earth and back to current electrode.
- Potential electrode. It is used to locate the remote earth. Ideally, potential electrode should be located at an infinite distance from the injection point to obtain the true GPR of the neutral line. In reality, the electrode is placed in a location that can represent the remote earth approximately.
- Signal source. A signal source is necessary to produce a test current into the neutral line. Basically, the fundamental frequency current is chosen to obtain the corresponding grounding impedance. However, due to the interference from the fundamental frequency voltage and unbalance current in power system, variable frequency current is used in some schemes to eliminate the related noise.

## • Staged Fault Based Methods

Figure 5.4 shows a measurement method by creating a controllable fault. The test current is injected between a phase and neutral, which does not require the installation of additional current-injection circuit. Compared to FOP based methods, the negative impact on customers is reduced, but it requires strict procedures that must be implemented to ensure the safety of workers and the public.

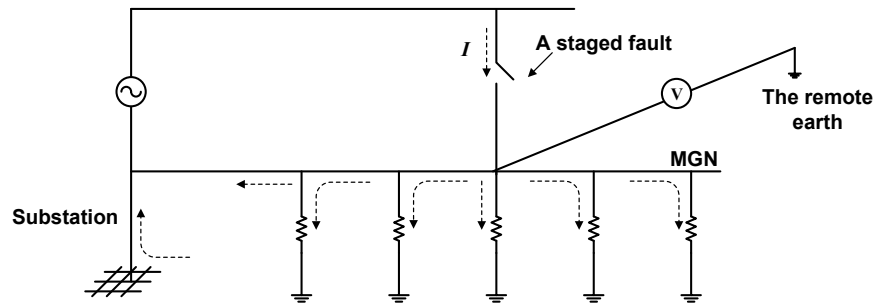


Figure 5.4: A typical staged single-phase fault based method.

### 5.2.2 RF Signal Injection

Rather than measuring neutral impedance, another approach for neutral condition monitoring is to utilize communication signal to monitor power line condition. An open phase conductor detector is described in [29]. The transmitter detects an open phase conductor by monitoring the phase conductor voltage. As shown in Figure 5.5, when an open phase conductor is detected, the transmitter injects a signal to the neutral conductor by means of a coupling current transformer. The signal is frequency and duration coded. The receiver decodes the signal and generates a trip signal which may activate a circuit breaker or a recloser causing isolation of the distribution line with the

open phase conductor.

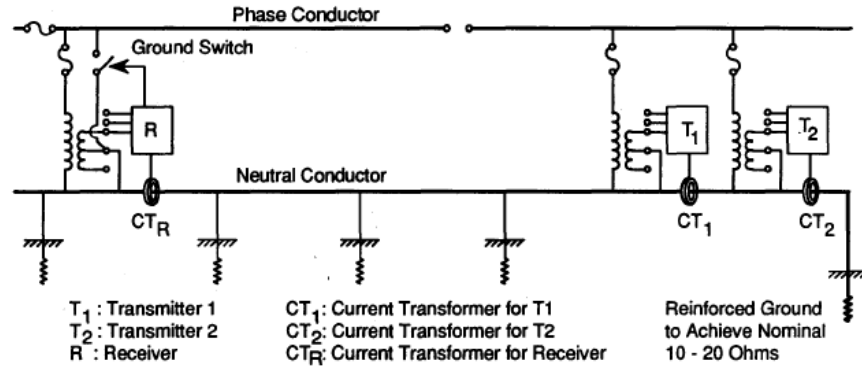


Figure 5.5: An open conductor detector system based on communication.

The power line signaling in this method can also be used for monitoring neutral condition. For example, a transmitter injects a signal to neutral line, and the receiver located at the far end monitors if the signal exists. The absence of the signal indicates a broken neutral. The main challenge for this scheme is that the communication signal is attenuated due to multiple grounds between transmitter and receiver. In the field test,  $1km$  neutral line made the signal attenuated to a level where the receiver did not respond.

### 5.3 Challenges of Neutral Impedance Measurement

To calculate neutral impedance, a reference ground is essential for  $V_{NTE}$  measurement. Unfortunately, this “true” earth point is hard to be located. Moreover, the installation of ground electrodes and a long wire test largely reduce the mobility of this method.

Another challenge is that even though  $Z_{MGN}$  can be calculated accurately,

it still cannot truly reflect neutral condition. A MGN system is naturally a ladder network and its neutral impedance is a constant value after certain distance. An equation for neutral impedance  $Z_{MGN.ladder}$  calculation is given in [88]:

$$Z_{MGN.ladder} = \sqrt{Z_{pn} \times R_{gn} \times S} \quad (5.2)$$

where  $Z_{pn}$  is the impedance of the neutral conductor between two grounding points,  $R_{gn}$  is pole grounding resistance, and  $S$  is grounding interval. A broken neutral does not change these three parameters so that it may not change the impedance, especially if the broken point is far away from the observation point.

Assuming  $Z_{pn} = 0.911 + 0.946j \Omega$ ,  $R_{gn} = 7\Omega$ ,  $S = 1km$ , the neutral impedance is shown in Figure 5.6 according to (5.2). It is apparent that the neutral impedance almost has no change when it is longer than  $5km$  from the test location.

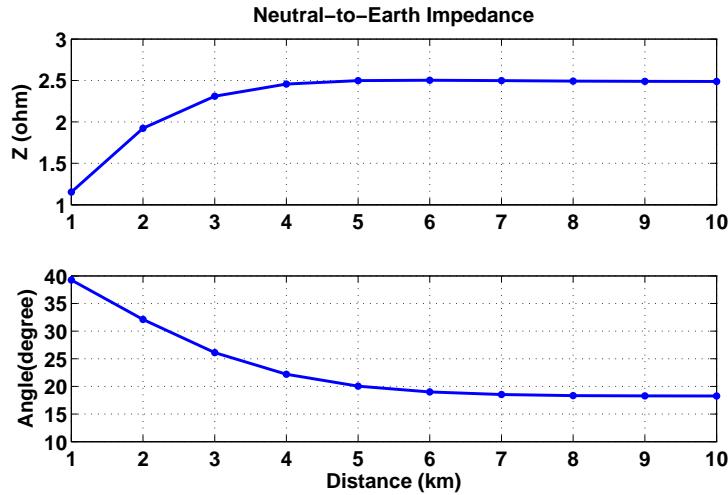


Figure 5.6: The magnitude and angle of the NTE impedance with different length.

Figure 5.7 illustrates a situation that a span of neutral is broken. From the

signal injection point, it marks the first span as “1”, the second span as “2”.

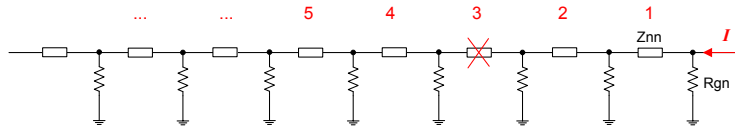


Figure 5.7: The neutral is broken at certain section.

The simulation results of  $Z_{MGN}$  with a broken span are shown in Figure 5.8. When the broken point is close to the current injection point, an increased neutral impedance is detected. However, if it is broken far away (5 km away in this simulation), the impedance is as same as that in a normal situation.

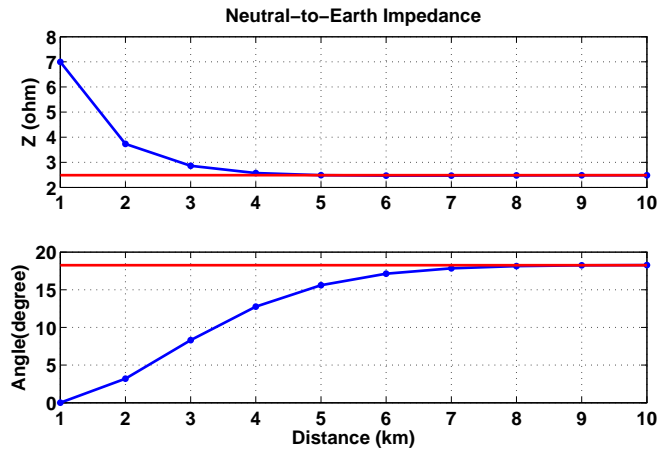


Figure 5.8: The neutral impedance when a section of the neutral is broken.

The simulation results suggest that a broken neutral does not necessarily change  $Z_{MGN}$  in a MGN system. When a neutral is broken, the multiple-grounded poles along the neutral line provide alternative routes for neutral current flow, which results in an insignificant change of neutral impedance. In other words, the change of neutral impedance caused by a broken neutral line is compensated by the multiple-grounded connections. Consequently, the

neutral impedance can be utilized as an indicator for broken neutral detection only if the test point is close to the broken point.

## 5.4 Active Disturbance Based Neutral Monitoring

To overcome the limitations of NIM based methods, an active neutral monitoring scheme is proposed which utilizes a signal generator to create current disturbance in the neutral system, and monitors the flow of this current disturbance. Compared to NIM based methods, it has several advantages:

- Portability. The new detector only measures the neutral currents at a service transformer. There is no need to install electrodes for voltage measurement. Moreover, the device is self-powered, no extra power is required.
- The neutral condition is indicated by analyzing the neutral current flow rather than measuring neutral impedance. Thus, the effort to find a reference ground is avoided.
- The “online” current injection accelerates the detection process. The condition of a neutral around the tested transformer can be verified quickly and conveniently.

This new approach transforms the detection of neutral condition into the analysis of unbalanced current flow in a MGN system. As shown in Figure 5.9, a signal generator is installed at the secondary side of the transformer.

It is made up of two variable loads. One is connected between hot wire A (+120V) and neutral and the other is connected between hot wire B (-120V) and neutral. By controlling the imbalance of the added AN and BN loads, neutral current is created. A signal detector is located at the transformer, which continuously monitors  $I_{np}$  and  $I_{ns}$ . The changes of  $I_{np}$  and  $I_{ns}$  caused by unbalanced loads are utilized to indicate the neutral condition.

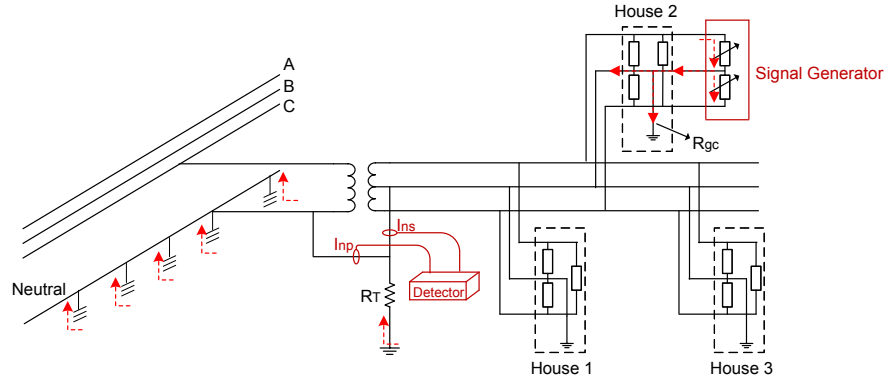


Figure 5.9: The new approach for monitoring primary neutral condition.

As primary neutral and secondary neutral is tied together at the transformer grounding point,  $I_{np}$  and  $I_{ns}$  always have two current sources at any moment. One is from secondary ground current caused by unbalanced loads, so called customer's contribution ( $I_{np\_Customer}, I_{ns\_Customer}$ ). The signal generator described in Figure 5.9 actually only creates disturbance on  $I_{np\_Customer}, I_{ns\_Customer}$ . The other is from primary neutral current, so called utility's contribution ( $I_{np\_Utility}, I_{ns\_Utility}$ ).  $I_{np}$  and  $I_{ns}$  can be expressed as:

$$\begin{aligned} I_{np} &= I_{np\_Utility} + I_{np\_Customer} \\ I_{ns} &= I_{ns\_Utility} + I_{ns\_Customer} \end{aligned} \quad (5.3)$$

The equivalent circuit of neutral current from the customer side is shown in Figure 5.10.  $Z_{sn}$  is the secondary neutral impedance.  $R_{gc}$  is customer

grounding resistance. The current source  $I_u$  is determined by the unbalanced voltage  $V_u$  and the equivalent unbalanced impedance  $Z_u$  which is caused by the imbalance of phase A loads  $Z_{an}$  and phase B loads  $Z_{bn}$ .  $I_u$  can be further expressed as:

$$I_u = V_u/Z_u \quad (5.4)$$

where

$$Z_u = Z_{an} // Z_{bn} = \frac{Z_{an} \times Z_{bn}}{Z_{an} + Z_{bn}} \quad (5.5)$$

$$V_u = \frac{Z_{bn} - Z_{an}}{Z_{bn} + Z_{an}} \times 120 \quad (5.6)$$

The Thevenin's equivalent circuit is shown in Figure 5.11. Due to its low

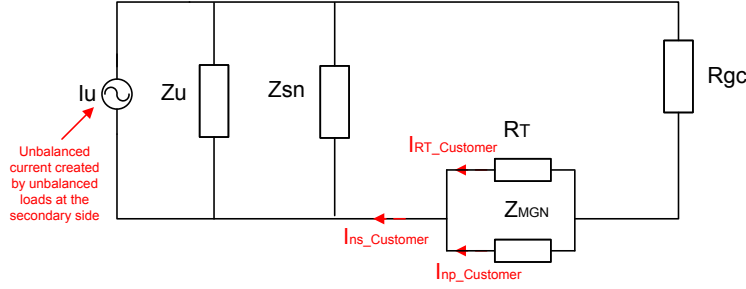


Figure 5.10: The equivalent circuit of unbalanced current caused by customer's loads.

impedance, most unbalanced currents flow through the secondary neutral  $Z_{sn}$  back to the source, and only a small amount flows via customer grounding  $R_{gc}$ . The neutral current  $I_{np\_Customer}$  can be expressed as:

$$I_{np\_Customer} = \frac{R_T}{Z_{MGN} + R_T} I_{ns\_Customer} = g \times I_{ns\_Customer}. \quad (5.7)$$

A factor  $g$  is then defined as:

$$g = \frac{R_T}{Z_{MGN} + R_T} = \frac{I_{np\_Customer}}{I_{ns\_Customer}}. \quad (5.8)$$



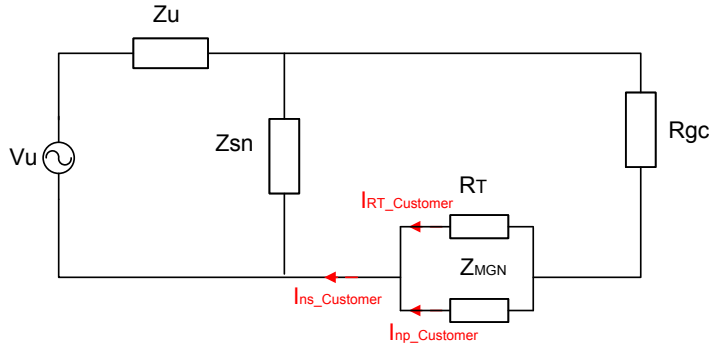


Figure 5.11: Redrawing the equivalent circuit by using virtual voltage source and impedance.

Normally, the transformer grounding connection  $R_T$  is solid. Thus, the value of the factor  $g$  highly depends on the MGN neutral impedance. If a neutral is broken close to the tested transformer, the increase of the  $Z_{MGN}$  will lead to a smaller  $g$ .

Due to the nature of MGN, a broken section far away from the test point may not change the neutral impedance. However, the purpose of this research is to study the safety issue caused by a broken neutral. Once the change of neutral impedance is compensated by multiple grounding connections, NEV will keep at the same level as a healthy line, which implies that a neutral broken far away will not affect the safety at the test point. Therefore, this research emphasizes on the cases where the neutral is broken around the test point.

From its definition, the factor  $g$  is valid only when considering customer's contribution, and the utility's contribution has to be eliminated. Equation

(5.9) is obtained from (5.7).

$$\begin{aligned}
 I_{np} &= I_{np\_Utility} + I_{np\_Customer} \\
 &= I_{np\_Utility} + g \times I_{ns\_Customer}
 \end{aligned} \tag{5.9}$$

When current disturbance is created, the variation of the neutral current  $\Delta I_{np}$  can be expressed as:

$$\begin{aligned}
 \Delta I_{np} &= \Delta I_{np\_Utility} + g \times \Delta I_{ns\_Customer} \\
 &= \Delta I_{np\_Utility} + g \times (\Delta I_{ns} - \Delta I_{ns\_Utility})
 \end{aligned} \tag{5.10}$$

If we can find an instant when it has  $\Delta I_{np\_Utility} = \Delta I_{ns\_Utility} = 0$ , the factor  $g$  can be calculated from

$$\begin{aligned}
 \Delta I_{np} &= \Delta I_{np\_Utility} + g \times (\Delta I_{ns} - \Delta I_{ns\_Utility}) \\
 &= 0 + g \times (\Delta I_{ns} - 0) \\
 \Rightarrow g &= \frac{\Delta I_{np}}{\Delta I_{ns}}
 \end{aligned} \tag{5.11}$$

The key point to calculate  $g$  is to find an instant when the current disturbance ( $\Delta I_{np}$  or  $\Delta I_{ns}$ ) is only from the secondary unbalanced loads but not from the utility side. This can be achieved when the total power of disturbance created by the signal generator keeps the same during the test so that it will not cause any difference on the primary current of the tested transformer. For example, if the loads switches are operated as shown in Table 5.2, different unbalanced currents are created from the customer side, and the disturbance from the utility can be considered as zero ( $\Delta I_{np\_Utility} = \Delta I_{ns\_Utility} = 0$ ).

Table 5.2: An example of loads switches in the proposed signal generator

Scenario	1	2	3	4	5
$P_{Z_a}$	1kVA	1.2kVA	1.4kVA	1.6kVA	1.8kVA
$P_{Z_b}$	1kVA	0.8kVA	0.6kVA	0.4kVA	0.2kVA
Total Power	2kVA	2kVA	2kVA	2kVA	2kVA

After  $\Delta I_{np}$  and  $\Delta I_{ns}$  are detected, the current ratio  $g$  can be calculated from (5.11). Furthermore, if the transformer grounding impedance  $R_T$  is measured, the primary neutral impedance can be obtained from

$$Z_{MGN} = \frac{(1-g)}{g} \times R_T \quad (5.12)$$

## 5.5 Computer Simulation of the Proposed Scheme

The simulated distribution system is a three-phase  $25kV$  MGN system. The span between two grounded points is 75 meters. The total length of the distribution line is  $15km$ . The customer side contains 10 houses which connected to a single-phase  $14.4kV/120V$  transformer. The interval between two houses is 20 meter. Each house is modeled separately and the loads vary with time to simulate the power consumption of a real house as illustrated in Figure 5.12.

Other parameters used in this computer simulation are listed as below.

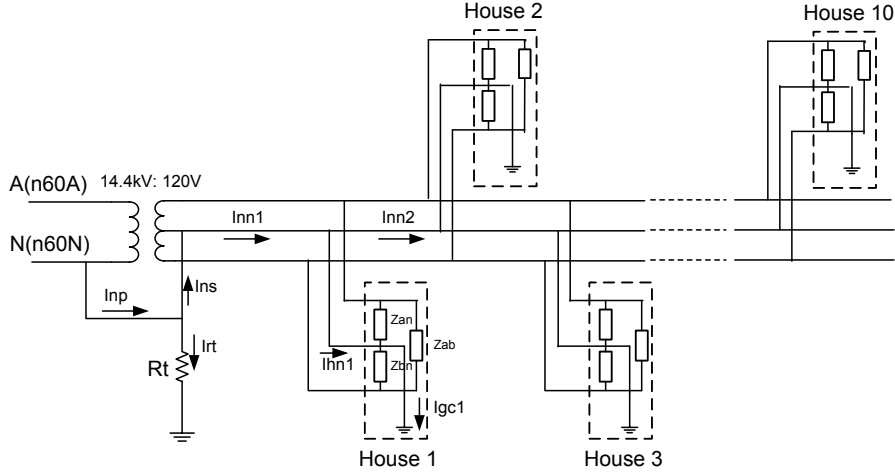


Figure 5.12: The customer side of the fully-simulated model.

Table 5.3: The system parameters of computer simulation

Parameter	Value
$R_{gs}$	0.15 $\Omega$
$R_{gn}$	15 $\Omega$
$Z_{line1}$	0.24940+j 0.8782 $\Omega/km$
$Z_{pn}$	0.42710+j 0.9609 $\Omega/km$
$Z_{mutual}$	0.05920+j 0.4905 $\Omega/km$
$R_T$	12 $\Omega$
$R_{gc}$	1 $\Omega$
$Z_{line2}$	0.2028+j 0.0936 $\Omega/km$
$Z_{sn}$	0.55+j 0.365 $\Omega/km$

$R_{gs}$ : Substation grounding resistance  
 $R_{gn}$ : Pole grounding resistance  
 $Z_{line}$ : Phase conductor impedance  
 $Z_{nn}$ : Primary neutral conductor impedance  
 $Z_{mutual}$ : Conductor mutual impedance  
 $R_T$ : Transformer grounding resistance  
 $R_{gc}$ : Customer grounding resistance  
 $Z_{line2}$ : Phase conductor impedance  
 $Z_{sn}$ : Secondary neutral conductor impedance

### • Simulation of Neutral Current Flow

To verify the equivalent circuit in Figure 5.11, unbalanced current is created by controlling  $Z_{bn}$  as one third of  $Z_{an}$  ( $Z_{bn} = 1/3 \times Z_{an}$ ). The neutral

currents, including  $I_{np}, I_{ns}, I_{RT}, I_{nn1}, \dots$ , can be calculated accordingly. The test results are summarized in the Table 5.4. The theoretical values which

Table 5.4: The verification of the neutral current flow model

Currents	Simulation Value	Theoretical Value	Error (%)
$I_{np}$ (A)	0.8368-0.0664i	0.7931-0.0381i	6.2
$I_{rt}$ (A)	0.0111+0.0008i	0.0106+0.0012i	5.4
$I_{ns}$ (A)	0.8256-0.0675i	0.7824-0.0396i	6.2
$I_{nn1}$ (A)	1.8006-0.7437i	1.8846-0.6400i	6.8
$I_{nn2}$ (A)	0.7138-0.0758i	0.6811-0.0505i	5.7
$I_{hn1}$ (A)	1.0868-0.6679i	1.2035-0.5895i	11.0
$I_{gc1}$ (A)	0.1084+0.0053i	0.1028+0.0084i	5.9

derived from the proposed model are highly consistent with the simulated values. As the impact of other houses at the secondary side are ignored in theoretical analysis, a slight error is introduced in the calculation.

To calculate  $g$ , loads  $Z_{an}$  and  $Z_{bn}$  are adjusted in sequence as shown in Table 5.5. At each scenario, the sum of power from  $Z_{an}$  and  $Z_{bn}$  is always the

Table 5.5: The arrangement of the varied loads

	Scenario 1	Scenario 2	Scenario 3	Scenario 4	Scenario 5
$Z_{an}$ (ohm)	50	50/6*5	50/7*5	50/8*5	50/9*5
$Z_{bn}$ (ohm)	50	50/4*5	50/3*5	50/2*5	50/1*5

same.

The test results of  $\Delta I_{np}$  and  $\Delta I_{ns}$  are shown in Figure 5.13. According to the Least Square Method (LSM), the factor  $g$  can be calculated as:

Calculated $g$ (LSM)	0.9897-0.0183i
Theoretical $g$	0.9896-0.0066i
Error (%)	1.18%

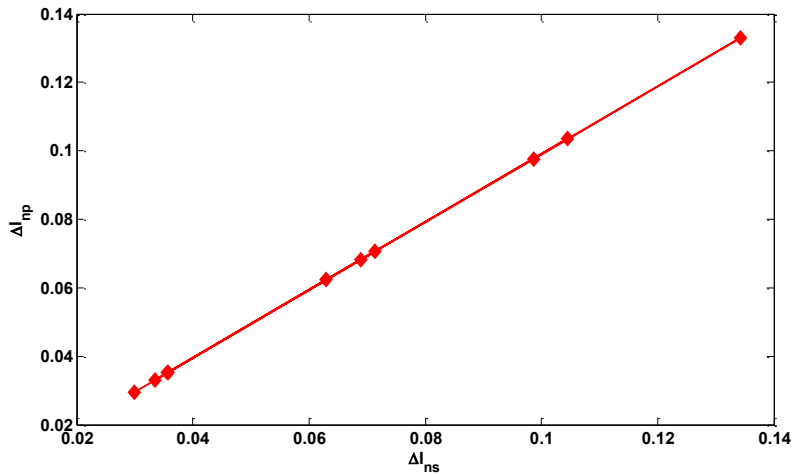


Figure 5.13: Test results for the factor  $g$  calculation.

The purpose of the factor  $g$  calculation is to indicate the condition of neutral impedance. If a largely reduced  $g$  is observed, the most possible reason is the neutral impedance  $Z_{MGN}$  increases due to a broken primary neutral nearby, which forces more unbalanced current flows through the  $R_T$  to back the source rather than from the MGN system.

### ● Cases Study of Broken Neutral

Figure 5.14 shows a case that a neutral line is broken at both sides of the test point. The neutral system suddenly changes from a ladder network to a single point grounding system. In this case, the neutral impedance largely increases, which results in a much smaller  $g$ . The error of 57% is a good indicator that a neutral is poorly-connected or broken at a location close to the transformer.

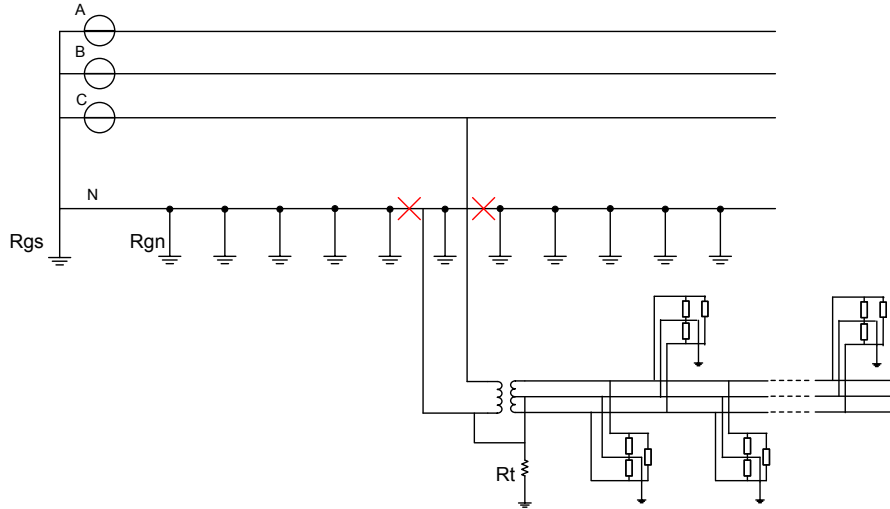


Figure 5.14: The primary neutral is broken at both sides of the transformer connection point.

Calculated $g$ (LSM)	$0.4255+0.0020i$
Theoretical $g$	$0.9896-0.0066i$
Error (%)	57%

However, if the neutral is not completely broken or the broken point is not close to the transformer as shown in Figure 5.15, the change of the impedance  $Z_{MGN}$  will be insignificant, which cause little change of  $g$ .

Calculated $g$ (LSM)	$0.9897-0.0264i$
Theoretical $g$	$0.9896-0.0066i$
Error (%)	0.4%

When a broken neutral does not cause a significant change of  $Z_{MGN}$ , safety is not an immediate concern. However, if the broken point is very close as shown in Figure 5.14, it is still hazardous for public safety. One solution to increase the sensitivity for the broken neutral detection is to estimate  $Z_{MGN}$  in (5.12). The test results are listed in Table 5.6. Even though the change

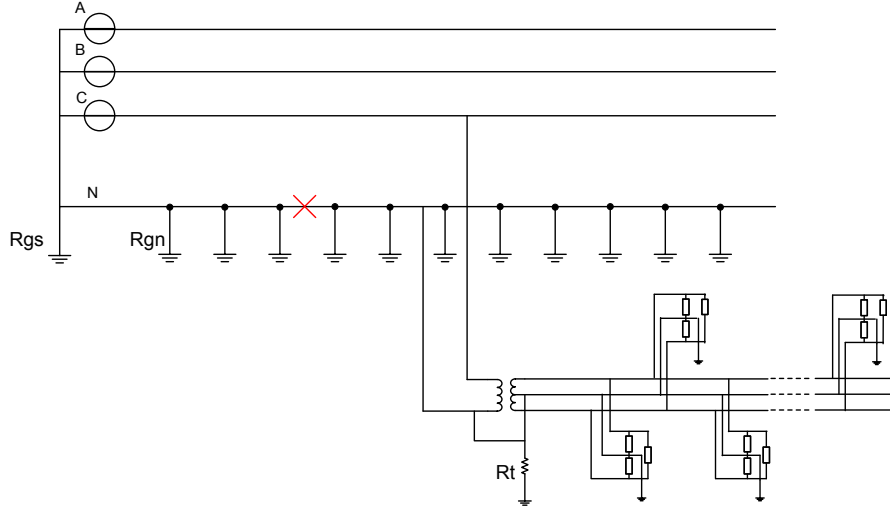


Figure 5.15: The primary neutral is broken far from the transformer connection point.

of  $g$  is little, the error of the estimated  $Z_{MGN}$  compared to the theoretical  $Z_{MGN}$  can indicate if a neutral line is abnormal.

Table 5.6: The calculated neutral impedance in different situations

	$g$	$Z_{MGN}(\Omega)$	Error*(%)
Normal	$0.9896-0.0066j$	$0.1256+0.0809j$	0.48
Figure5.14	$0.4255+0.0020j$	$16.2015-0.1326j$	10796
Figure5.15	$0.9897-0.0264j$	$0.1163+0.3232j$	162.6
* The theoretical value $Z_{MGN} = 0.1249 + 0.0811j$			

## 5.6 Conclusion

An active-disturbance based method is presented, in which the current flow in neutral system are analyzed to determine the neutral condition. Without the effort to find a “true” earth for neutral impedance measurement, this scheme is more practical compared to the NIM based methods.



In this method, two variable loads are used to create neutral current disturbance from the customer side. A current ratio of  $\Delta I_{np}/\Delta I_{ns}$ , defined as  $g$ , is used to indicate the neutral condition. A decreased  $g$  implies the increase of the neutral impedance  $Z_{MGN}$ , which is most likely caused by a broken neutral.

Due to the nature of MGN system, a broken point far away from the current injection point is compensated by multiple grounding connections, which makes it difficult to be detected. However, as long as it does not change the neutral impedance, it will not cause a safety problem at the test point.

## Chapter 6

### Identification of Neutral-to-Earth Voltage Contributors

Neutral current is an integral part of a three-phase four-wire MGN system. The current flowing from neutral into ground creates a neutral-to-earth voltage (NEV). NEV exists in a MGN system during normal operation. It may originally come from the primary distribution system, or from the secondary loads, or, in most cases, from both. This chapter presents a novel active method to identify the sources of NEV. Disturbances are created from the primary side and the secondary side of a service transformer separately. The contributions of the utility and customer are quantified based on analysis of corresponding neutral currents. In addition, this scheme can be used to monitor the condition of secondary neutral. Poor connections at the secondary side can be detected without extra visual inspection.

#### 6.1 The Sources of NEV

Through the neutral connection of a service transformer, NEV can be transferred from the primary neutral to the secondary neutral, and vice versa [89]. NEV at the secondary side causes stray voltage, which is defined as a voltage resulting from the normal delivery that may be present between two conductive surfaces that can be simultaneously contacted by members of the general

public and/or their animals [90]. Stray voltage has adverse effects on livestock production which results in economic losses of farmers. NEV can also be transferred into swimming pools and shower stalls [91]. There are growing public concerns on high NEV due to a few unfortunate accidents [92]. NEV is hard to be mitigated due to its complex causes. To solve the problems caused by NEV, it is necessary to identify its sources and quantify the contributions from the utility and customer sides.

One contributor to NEV is unbalanced current from the utility side of a service transformer. Assuming customers at the secondary side have perfectly balanced loads, the flow of neutral current is shown in Figure 6.1.  $I_{np\_Utility}$  consists of a current  $I_{np1}$  from unbalanced loads connected to the neutral. In addition, this single-phase service transformer also contributes a neutral current  $I_{np2}$  from its primary side.  $I_{ns\_Utility}$  is a part of  $I_{np\_Utility}$  flowing through the secondary neutral into customer grounding  $R_{gc}$ , and the rest of  $I_{np\_Utility}$  flows into ground through the transformer grounding  $R_T$ .

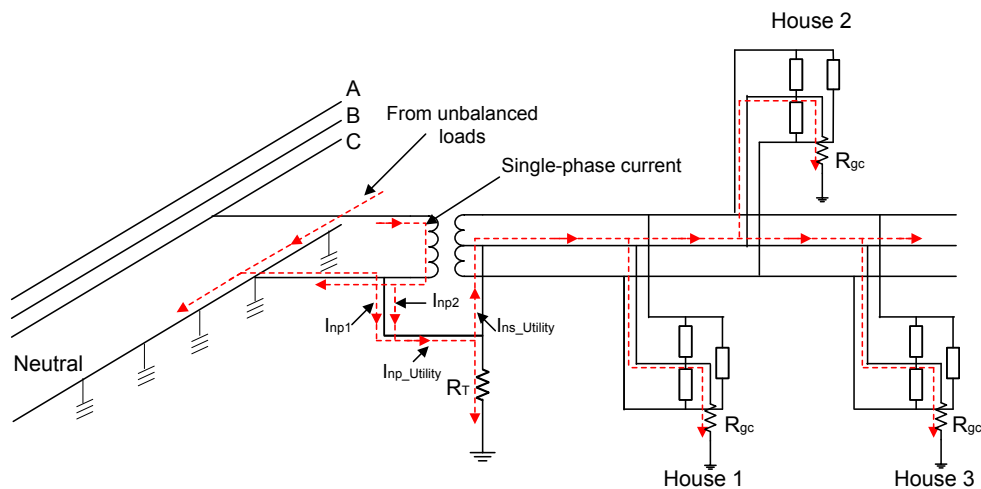


Figure 6.1: The current flow when only utility contributes unbalanced current.

Unbalanced current from customers is another contributor to NEV. Assum-

ing the utility side is perfectly balanced, the flow of neutral current is shown in Figure 6.2. In normal condition, most current flows back to the transformer through a neutral conductor, and a small portion flows into earth through customer grounding  $R_{gc}$ . The ground current circulates back to the service transformer through multiple grounded poles  $Z_{MGN}$  and the transformer grounding  $R_T$ .  $I_{np\_Customer}$  is the neutral current from all ground currents at the primary side.  $I_{ns\_Customer}$  is the sum of  $I_{np\_Customer}$  and the ground current from  $R_T$ .

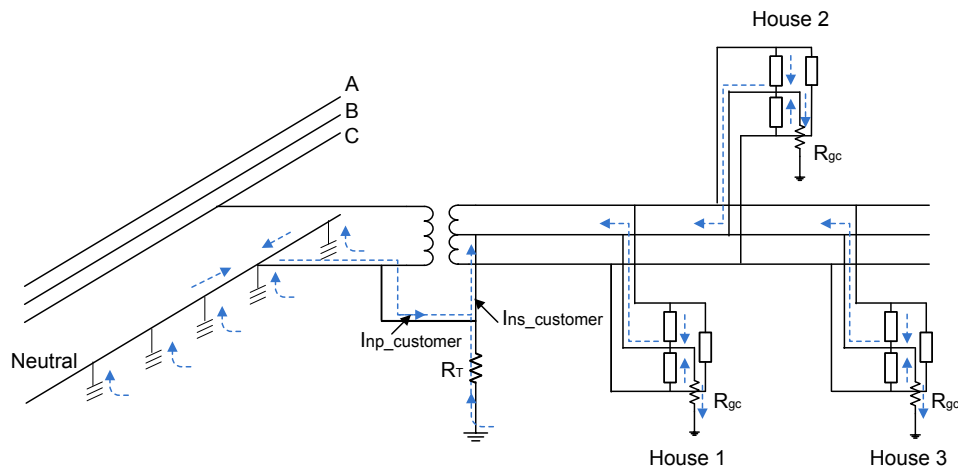


Figure 6.2: The current flow when only customer contributes unbalanced current.

In reality, these two sources always exist and it is impossible to separate one from the other. Figure 6.3 shows a measured neutral current from a house test. This current varied in a day due to the changes from distribution system and loads. It is almost impossible to separate the contribution of a customer from that of a utility based on this measured data.

The current practice to identify NEV sources is physically disconnecting the tie of utility and customer as following [93]:

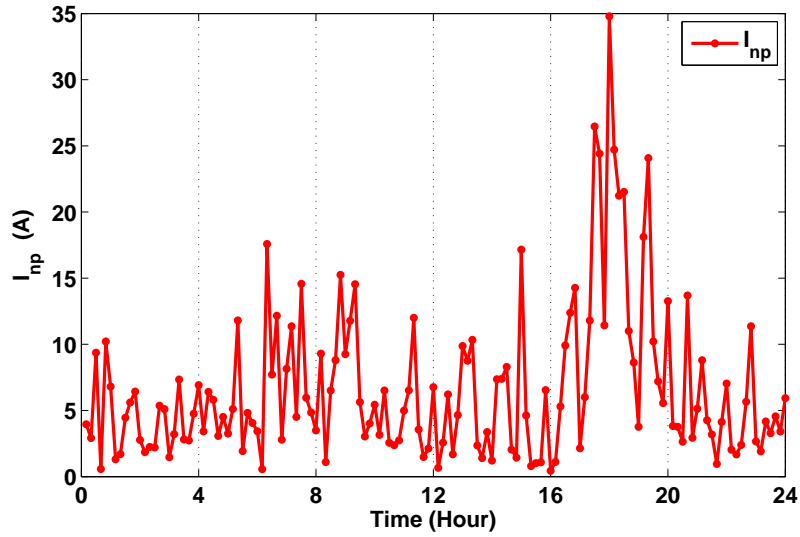


Figure 6.3: Neutral current in one day from a house test.

1. Measure neutral-to-earth voltage  $V_{NTE_C}$  at the customer's premise. Then, de-energize the customer by opening the main switch and measure  $V'_{NTE_C}$  again.  $V'_{NTE_C}$  is considered as utility contribution and the difference between  $V_{NTE_C}$  and  $V'_{NTE_C}$  is considered as customer contribution.
  
2. Measure NEV at the service transformer with the main switch close and open.  $V_{NTE_T}$  and  $V'_{NTE_T}$  are obtained respectively. If the difference  $\Delta V' = V'_{NTE_T} - V'_{NTE_C}$  is larger than  $1V$ , the connection between primary neutral and secondary neutral must be checked. If  $V_{NTE_T}$  is larger than  $10V$ , a visual inspection of the network near the customer's premise must be conducted.

This practice is very straightforward, but it has significant drawbacks. Firstly, it has a large negative impact on the customer. The site needs to be de-energized for several times during the test. Secondly, visual inspection is time

consuming and its reliability is easily affected by terrace, weather and climate. Thirdly, similar to all passive off-line measurements, the measured results depend on the condition when the test is conducted. Since power system is dynamic, any problem developed between two tests cannot be found in a timely manner.

## 6.2 Active Disturbance Based NEV Monitoring Scheme

If only utility has contribution on unbalanced current, the equivalent circuit of current flow is shown in Figure 6.4.

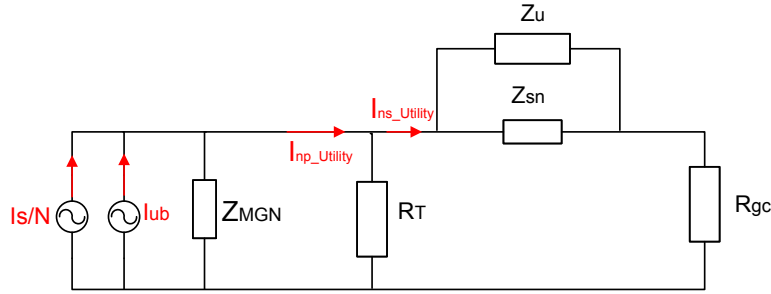


Figure 6.4: An equivalent circuit of Figure 6.1.

One current source  $I_{ub}$  is associated with unbalanced loads linked in the neutral, another source  $I_s/N$  is from the tested single-phase transformer.  $I_s$  is the current of the secondary side and  $N$  is the ratio of transformer windings.  $Z_u = Z_{an} // Z_{bn}$  is the total phase-neutral loads at the secondary side.  $Z_{sn}$  is the impedance of the secondary neutral.  $R_{gc}$  represents the total customer grounding resistance at the secondary side. As the current sources are not concern in this work, they can be further simplified to an equivalent virtual voltage source  $V_{MGN}$  as shown in Figure 6.5. As  $Z_u$  is much larger than  $Z_{sn}$ ,

the current flowing through  $Z_u$  is neglected. Solving the equivalent circuit,

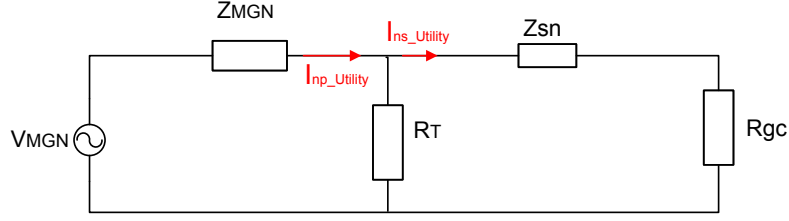


Figure 6.5: Another equivalent circuit of Figure 6.1 with a virtual voltage source.

we can obtain

$$I_{ns\_Utility} = \frac{R_T}{(Z_{sn} + R_{gc}) + R_T} I_{np\_Utility} = k \times I_{np\_Utility} \quad (6.1)$$

Thus, the factor  $k$  is defined as

$$k = \frac{R_T}{(Z_{sn} + R_{gc}) + R_T} = \frac{I_{ns\_Utility}}{I_{np\_Utility}} \quad (6.2)$$

Recall the analysis in Chapter 5, a factor  $g$  is defined as  $I_{np\_Customer}/I_{ns\_Customer}$  when only customer contributes to unbalanced current. Equation (6.3) is therefore obtained.

$$\begin{cases} I_{np} = I_{np\_Utility} + I_{np\_Customer} = I_{np\_Utility} + g \times I_{ns\_Customer} \\ I_{ns} = I_{ns\_Utility} + I_{ns\_Customer} = k \times I_{np\_Utility} + I_{ns\_Customer} \end{cases} \quad (6.3)$$

As  $I_{np}$  and  $I_{ns}$  are measurable, once  $k$  and  $g$  are obtained, the currents  $I_{np\_Utility}$  and  $I_{ns\_Customer}$  can be calculated. The contributions of utility and customer are therefore solved.

If a disturbance is created in a neutral system, (6.4) can be obtained from (6.3).  $\Delta I_{ns}$ ,  $\Delta I_{np}$ ,  $\Delta I_{np\_Utility}$ ,  $\Delta I_{np\_Customer}$ ,  $\Delta I_{ns\_Customer}$  are the correspond-

ing disturbances of  $I_{ns}$ ,  $I_{np}$ ,  $I_{np\_Utility}$ ,  $I_{np\_Customer}$ ,  $I_{ns\_Customer}$ , respectively.

$$\begin{aligned}\Delta I_{ns} &= k \times \Delta I_{np\_Utility} + \Delta I_{ns\_Customer} \\ &= k \times (\Delta I_{np} - \Delta I_{np\_Customer}) + \Delta I_{ns\_Customer}\end{aligned}\tag{6.4}$$

Assuming this disturbance is only from the primary side and customer has no additional contribution ( $\Delta I_{np\_Customer} = \Delta I_{ns\_Customer} = 0$ ), the factor  $k$  can be calculated from:

$$\begin{aligned}\Delta I_{ns} &= k \times (\Delta I_{np} - \Delta I_{np\_Customer}) + \Delta I_{ns\_Customer} \\ &= k \times (\Delta I_{np} - 0) + 0 \\ \Rightarrow k &= \frac{\Delta I_{ns}}{\Delta I_{np}}\end{aligned}\tag{6.5}$$

To calculate  $k$ , an active disturbance based method is illustrated in Figure 6.6. It utilizes a signal generator connected between two hot wires to produce a balanced current. With this arrangement, the secondary unbalanced current is not changed but a disturbance is created at the primary side.

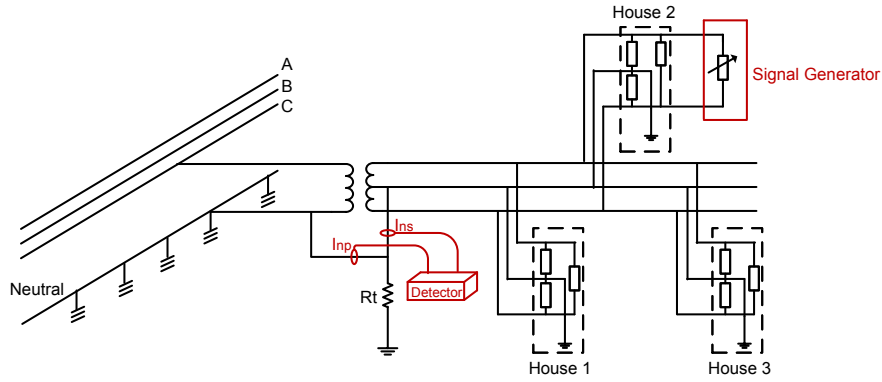


Figure 6.6: The proposed active method to calculate the factor  $k$ .

Figure 6.7 shows a complete scheme for NEV sources identification. As this signal generator is a combination of those in Figure 5.9 and Figure 6.6, it is



able to calculate  $g$  and  $k$ , respectively. The overall process to identify NEV sources is listed as following:

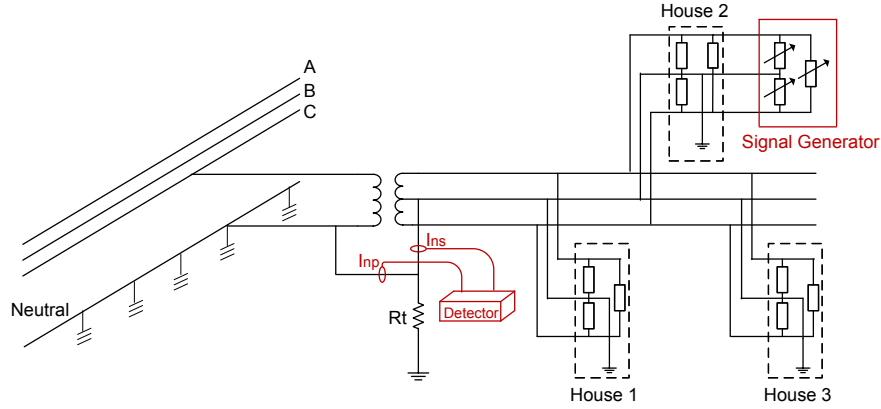


Figure 6.7: A complete signal generator for NEV source identification.

1. Turn on the signal generator between hot wires A and B to create a disturbance at the secondary side. Instantly, a neutral current is created at the primary side of the service transformer. Adjust the signal strength, a group of primary neutral disturbances is created with different magnitude. As this A-B signal generator has no contribution on secondary neutral current, the defined factor  $k$  is then can be calculated.
2. Turn off the A-B signal generator, and turn on other two signal generators A-N and B-N . With different combinations of AN and BN loads, a group of secondary neutral currents is created. To make sure the primary current has no change in this step, AN and BN signal generators must follow a rule - the total power of the AN and BN signals is always the same. Subsequently, the factor  $g$  is calculated.
3. From the measured  $I_{np}$ ,  $I_{ns}$  and calculated  $k$ ,  $g$ , currents  $I_{np\_Utility}$  and  $I_{ns\_Customer}$  can be calculated in the equation (6.3). Then,  $I_{ns\_Utility}$  and

$I_{np\_Customer}$  can be calculated from the following equations.

$$\begin{aligned} I_{np\_Customer} &= I_{np} - I_{np\_Utility} \\ I_{ns\_Utility} &= I_{ns} - I_{ns\_Customer} \end{aligned} \tag{6.6}$$

### 6.3 Computer Simulation

Computer simulations are carried out in order to verify the effectiveness of the proposed active method. The simulations consist of the following steps:

1. Simulate the proposed model of neutral current from distribution system. As the model for customer contribution has been verified in Chapter 5, this chapter only focuses on the simulation of unbalanced current from utility.
2. Simulate the process to calculate the factor  $k$ . It is required to have a disturbance of neutral current from the primary side of a service transformer but not from the secondary side.
3. Analyze the contributions from both utility and customer by using (6.3) with the calculated  $k$  and  $g$ .

#### 6.3.1 Verification of Utility Contribution Model

A fully-simulated model is built and tested in computer simulation as shown in Figure 6.8. The utility side is three-phase  $25kV$  distribution system with

a multiple grounded neutral line. The span between two grounded points is  $75m$ . The total length of the distribution line is  $15km$ . Loads are added with an interval of  $1km$ . The mutual impedance between phases and between phase and neutral are also considered. Other system parameters are listed in Table 6.1.

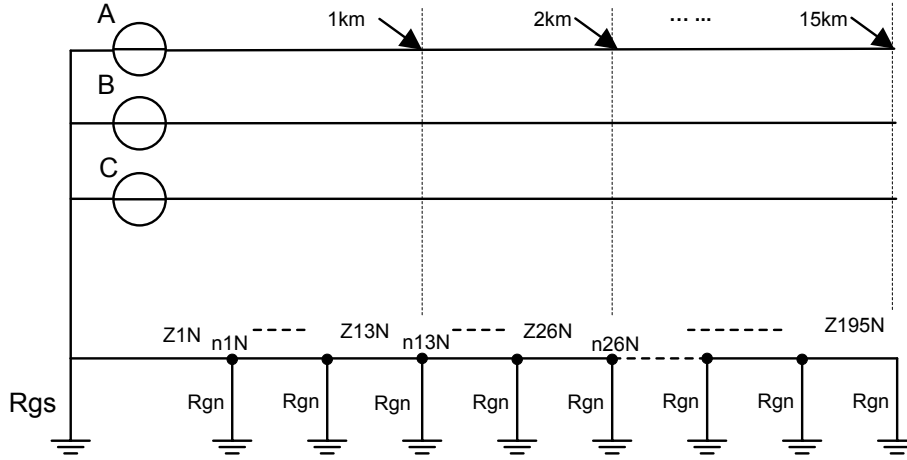


Figure 6.8: A fully-simulated model of the utility side.

Table 6.1: The system parameters of computer simulation

Parameter	Value
$R_{gs}$	$0.15 \Omega$
$R_{gn}$	$15 \Omega$
$Z_{line1}$	$0.24940+j 0.8782 \Omega/km$
$Z_{pn}$	$0.42710+j 0.9609 \Omega/km$
$Z_{mutual}$	$0.05920+j 0.4905 \Omega/km$
$R_{gs}$ : Substation grounding resistance $R_{gn}$ : Pole grounding resistance $Z_{line}$ : Phase conductor impedance $Z_{nn}$ : Primary neutral conductor impedance $Z_{mutual}$ : Conductor mutual impedance	

To consider the impact of loads along the simulated distribution line, a five-port load model is used in this work as shown in Figure 6.9. These loads vary with time to mimic a real distribution system.

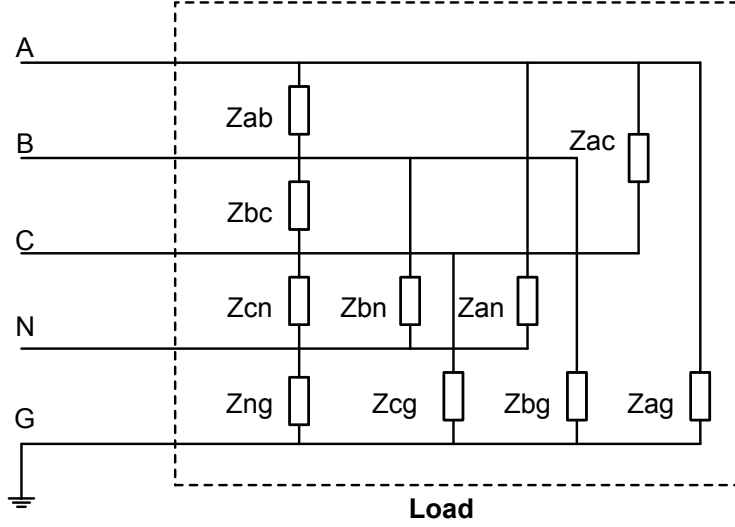


Figure 6.9: A five-port load model used in the simulation.

The simulated residential area has 10 houses. They are fed by a  $37.5kVA$  single-phase step-down transformer ( $14.4kV/120V$ ,  $z=2\%$ ), and the interval between houses is 20 meter. Other parameters are found in Table 6.2.

Table 6.2: The parameters at the customer side in computer simulation

Parameter	Value
$R_T$	$12 \Omega$
$R_{gc}$	$1 \Omega$
$Z_{line2}$	$0.2028+j 0.0936 \Omega/km$
$Z_{sn}$	$0.55+j 0.365 \Omega/km$
$R_T$ : Transformer grounding resistance $R_{gc}$ : Customer grounding resistance $Z_{line2}$ : Phase conductor impedance $Z_{sn}$ : Secondary neutral conductor impedance	

The loads of 10 houses are replaced by the same impedance to make sure that no unbalanced current is created by these houses. The simulation results are listed in Table 6.3. Theoretical values are calculated according to the proposed model (Figure 6.5). It is apparent that the simulated values are very close to the theoretical values with errors less than 1%, which proves the

accuracy of the proposed utility contribution model.

Table 6.3: The verification of the utility contribution model

Current	Simulation Value	Theoretical Value	Error (%)
Inp(A)	0.8943-0.06901j		
Irt(A)	0.0105+0.0009j	0.0105+0.0010j	0.58
InS(A)	0.8838-0.0701j	0.8838-0.0700j	0.01
Inn1(A)	0.8806-0.0746j	0.8838-0.0700j	0.63
Inn2(A)	0.7647-0.0805j	0.7678-0.0766j	0.65
Ihn1(A)	0.1158+0.0058j	0.1159+0.0065j	0.58
Igc1(A)	0.1159+0.0059j	0.1159+0.0065j	0.57

It is also found that the secondary neutral system has to be considered as a ladder network (Figure 6.10 (a)). If the secondary neutral impedance is considered as zero and the 10 houses groundings are paralleled as shown in Figure 6.10 (b), it will introduce large errors at the results. For example, the errors of  $I_{rt}$ ,  $I_{hn1}$  and  $I_{gc1}$  can be more than 20% as illustrated in Table 6.4. This further proves that even if the impedance of neutral conductor is very small, it cannot be ignored in the grounding modelling.

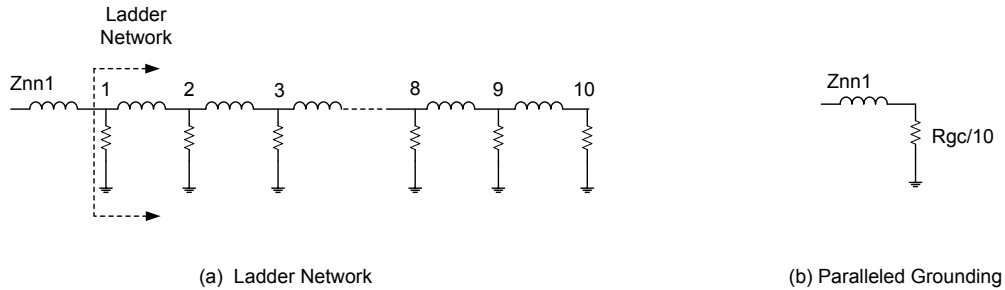


Figure 6.10: A ladder network compared to paralleled groundings.

### 6.3.2 Verification of The Proposed Active Method

After the models for unbalanced current flow are proved in the previous simulations, the active method to calculate  $k$  is also simulated. The process is

Table 6.4: The verification of the utility contribution model when simplified

Current	Simulation Value	Theoretical Value	Error (%)
Inp(A)	0.8943-0.06901		
Irt(A)	0.0105+0.0009j	0.0008-0.0001j	23.7
Ins(A)	0.8838-0.0701j	0.8861-0.0689j	0.29
Inn1(A)	0.8806-0.0746j	0.8861-0.0689j	0.89
Inn2(A)	0.7647-0.0805j	0.7975-0.0620j	4.89
Ihn1(A)	0.1158+0.0058j	0.0886-0.0068j	25.95
Igc1(A)	0.1159+0.0059j	0.0886-0.0068j	26.02

similar to the calculation of another factor  $g$ . Firstly, run a basic case to obtain  $I_{np1}$  and  $I_{ns1}$ , which is the total current from both utility and customer. Secondly, add a A-B load at House 1. For example, a load with impedance  $Z_{ab}$  is connected between A and B. Measure another set of  $I_{np2}$  and  $I_{ns2}$  after the load is added. As this A-B load does not change the customer side neutral current, the factor  $k$  is therefore obtained by

$$k = \frac{\Delta I_{ns}}{\Delta I_{np}} = \frac{I_{ns2} - I_{ns1}}{I_{np2} - I_{np1}}. \quad (6.7)$$

The test results are shown in Table 6.5. The calculated value with the proposed method matches the theoretical value very well.

Table 6.5: The simulation results for the calculation of  $k$ .

	Basic Case	Add a $Z_{ab}$	$\Delta I$
$I_{np}$ (A)	-1.5031+0.5649j	-1.3823+0.5528j	0.1207-0.0121j
$I_{ns}$ (A)	-1.5313+0.5485j	-1.4118+0.53659j	0.1194-0.0119j
Calculated $k$	0.9827-0.0002j		
Theoretical $k$	0.9908-0.0005j		
Error (%)	0.82%		

To make the calculated  $k$  more accurate, the added A-B load varies several time to get a group of  $I_{np}$  and  $I_{ns}$ . For example, if the  $Z_{ab}$  varies as following, the simulation results are shown in Figure 6.11.

Table 6.6: The phase-to-phase load Zab in different cases.

	Case 1	Case 2	Case 3	Case 4	Case 5
Zab(ohm)	70	60	50	40	30

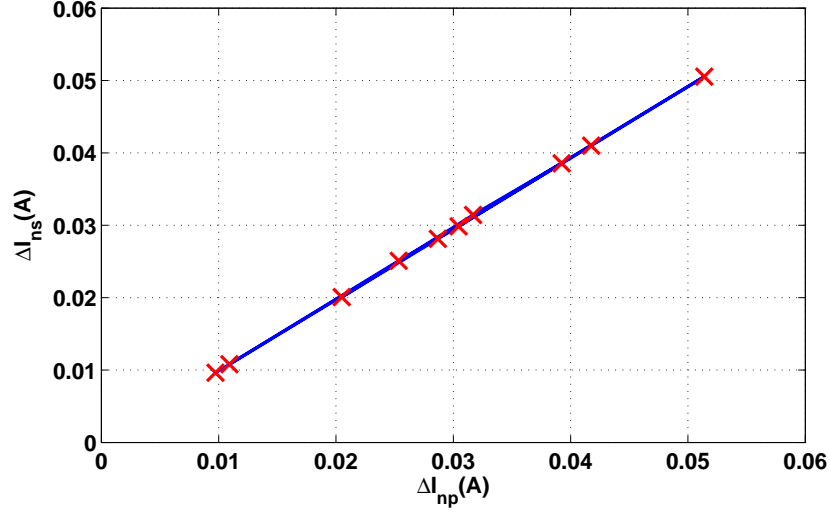


Figure 6.11: Simulation results for the calculation of  $k$ .

According to the Least Square Method (LSM),  $k$  can be calculated as:

Calculated $k$	$0.9852 - 0.0048j$
Theoretical $k$	$0.9908 - 0.0005j$
Error (%)	0.71%

Take the calculated  $k$  and  $g$  ( $g = 0.9897 - 0.0183j$  from Chapter 5) into (6.3),

we can get:

$$\begin{aligned}
 -1.5031 + 0.5649j &= I_{np\_Utility} + (0.9897 - 0.0183j) \times I_{ns\_Customer} \\
 -1.5313 + 0.5485j &= (0.9852 - 0.0048j) \times I_{np\_Utility} + I_{ns\_Customer}
 \end{aligned} \tag{6.8}$$

Solve the above equations,

$$I_{np\_Utility} = -0.0665 - 0.1780j,$$

$$I_{ns\_Customer} = -1.4649 + 0.7236j.$$

And,

$$I_{np\_Customer} = I_{np} - I_{np\_Utility} = -1.4366 + 0.7429j,$$

$$I_{ns\_Utility} = I_{ns} - I_{ns\_Customer} = -0.0664 - 0.1751j.$$

The utility contribution  $C_{Utility}$  and the customer contribution  $C_{Customer}$  are:

$$C_{Utility} = \frac{|I_{ns\_Utility}|}{|I_{ns\_Utility}| + |I_{ns\_Customer}|} = 10.3\% \quad (6.9)$$

$$C_{Customer} = \frac{|I_{ns\_Customer}|}{|I_{ns\_Utility}| + |I_{ns\_Customer}|} = 89.7\% \quad (6.10)$$

## 6.4 Field Test of the Proposed Active Method

A house test is shown in Figure 6.12. Three current probes are used to measure

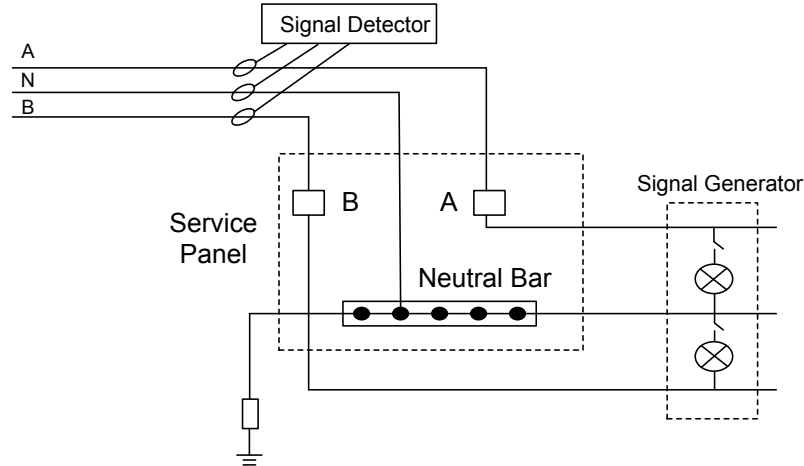


Figure 6.12: The house test arrangement.

the current of phase A, phase B and neutral. These probes are connected to a data collection system to record the current waveforms for post-processing.



The signal generator is made up by two sets of incandescent lights as shown in Figure 6.13. One set of lights is connected between phase A-N, and another

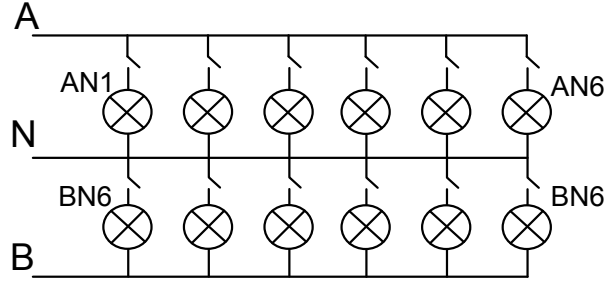


Figure 6.13: Two sets of light bulbs are used as an unbalanced current generator.

set is connected between phase B-N. Each set of the lights consists of six 60W light bulbs with independent switches.

Due to the limitation of the test, the transformer grounding point was not accessible, we cannot measure the currents  $I_{np}$  and  $I_{ns}$  as discussed. Alternatively, the currents in the service panel  $I_{ha}$ ,  $I_{hb}$  and  $I_{hn}$  were measured, and then the ground current in this house is calculated:

$$I_{hg} = I_{ha} - I_{hb} - I_{hn} \quad (6.11)$$

Before applying active disturbance to separate the contributions of the utility and customer on  $I_{hg}$  and  $I_{hn}$ , the equivalent circuits of the house test are illustrated. As shown in the Figure 6.14, the currents  $I_{hn}$  and  $I_{hg}$  are represented by  $I_{phn}$  and  $I_{phg}$  when there is only unbalanced current from the primary side. As the test location is at a service panel, it always has  $I_{phn} = I_{phg}$  regardless of the loads changes. Therefore, this house test is not able to verify the active method used for analyzing the utility's contribution as shown in Figure 6.6.

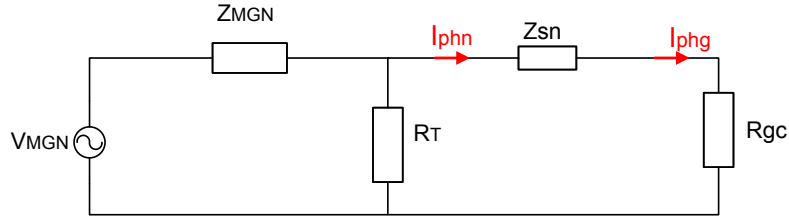


Figure 6.14: The illustration of the measured currents when only utility contributes unbalanced current.

Figure 6.15 shows  $I_{chn}$  and  $I_{chg}$  when only considering unbalanced current from customer. The system impedance of  $Z_{sn}$ ,  $R_{gc}$ ,  $R_T$  and  $Z_{MGN}$  determine the unbalanced current distribution between  $I_{chn}$  and  $I_{chg}$ . Thus, the active method can be verified by creating a group of  $I_{chn}$  and  $I_{chg}$ .

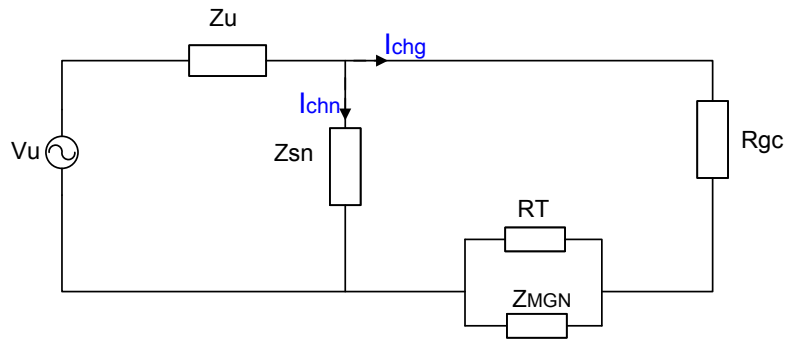


Figure 6.15: The illustration of the measured currents when only customer contributes unbalanced current.

To create neutral current from this device, the operation of the light bulbs is arranged as shown in Figure 6.16. Theoretically, the currents in phase A, phase B and neutral of each state are: The total power is always 360

Table 6.7: The arrangement of the varied loads

Scenario	1	2	3	4	5	6	7
$I_{an}(A)$	0	0.5	1	1.5	2	2.5	3
$I_{bn}(A)$	3	2.5	2	1.5	1	0.5	0
$ I_{an} - I_{bn} (A)$	3	2	1	0	1	2	3

Watt so that the variation of the primary current is zero from one scenario to another ( $\Delta I_{n.Utility} = 0$ ). The background currents before the test are shown in Figure 6.17. Phase B has more loads running than phase A, which results in significant neutral current. The purpose of this test is to use the current injection method to separate customer contribution from the measured neutral current, and calculate a new factor  $s$ , which is defined as the ratio of the neutral current  $I_{n.Customer}$  to the customer unbalanced currents ( $I_a - I_b$ ).

$$s = \frac{I_{n.Customer}}{I_a - I_b} = \frac{\Delta I_n}{\Delta(I_a - I_b)} \text{ when } I_{n.Utility} = 0 \quad (6.12)$$

The factor  $s$  represents the neutral condition at a house, but  $g$  defined in Chapter 5 is used to indicate the primary neutral condition of a service transformer. However, this test is to verify the active disturbance method, and the physical meaning of the  $s$  or  $g$  is not a concern here. The measured currents when the loads switching from Scenario 1 to Scenario 7 are shown in Figure 6.18.

By subtracting the background loads current, the magnitude of currents generated by the light bulbs is listed in the Table 6.8. Compared to the theoretical values in Table 6.7, the actual current for each bulb is not 0.5A, but 0.43A. The total current of added loads is always 2.594A in each scenario, leading to the same primary current.

To calculate  $s$ , the Least Means Squares (LMS) method is used for data fitting. The calculated result is shown in Figure 6.19. The neutral current caused by unbalanced load is extracted by the proposed active method, and the ratio of  $\Delta I_n / \Delta(I_a - I_b)$  is linear, which is consistent with (6.12).

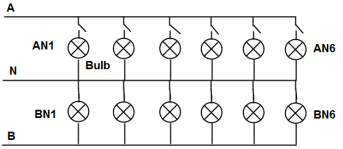
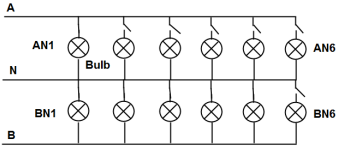
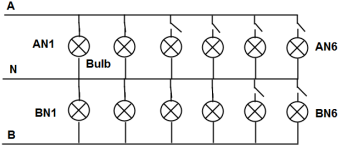
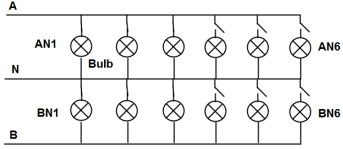
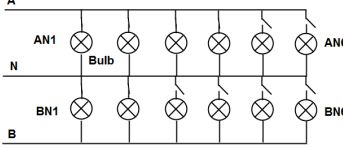
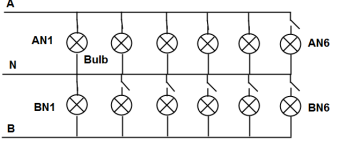
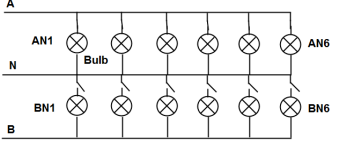
Scenario	Bulbs Status
<p style="text-align: center;"><b>1</b> AN: 0 BN: 6</p>	
<p style="text-align: center;"><b>2</b> AN: 1 BN: 5</p>	
<p style="text-align: center;"><b>3</b> AN: 2 BN: 4</p>	
<p style="text-align: center;"><b>4</b> AN: 3 BN: 3</p>	
<p style="text-align: center;"><b>5</b> AN: 4 BN: 2</p>	
<p style="text-align: center;"><b>6</b> AN: 5 BN: 1</p>	
<p style="text-align: center;"><b>7</b> AN: 6 BN: 0</p>	

Figure 6.16: Seven scenarios for creating neutral current disturbance.

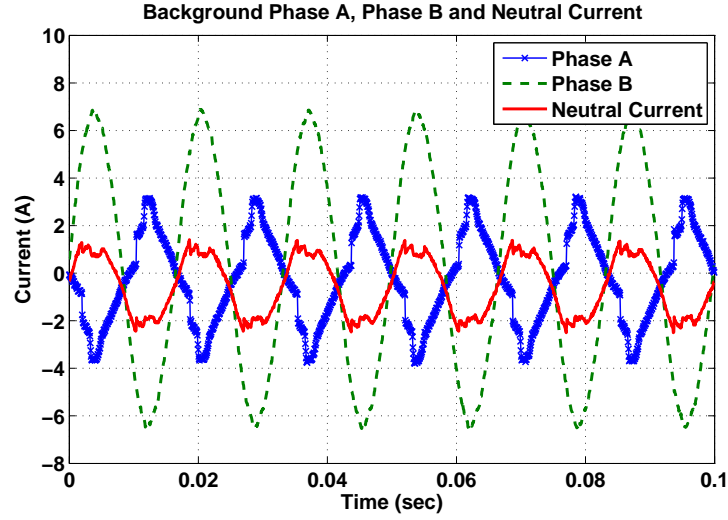


Figure 6.17: Background currents of phase A, phase B and neutral.

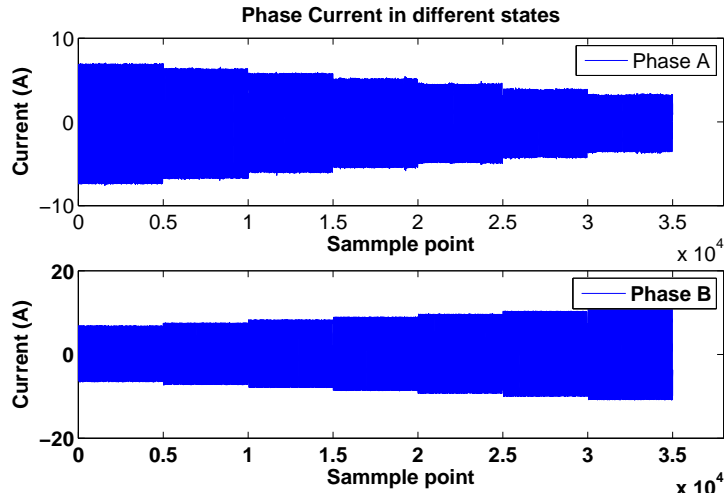


Figure 6.18: The phase currents when the loads switched from Scenario 1 to Scenario 7.

Table 6.8: The measured current in different scenarios

Scenario	1	2	3	4	5	6	7
$I_{an}(A)$	4.607	4.167	3.704	3.253	2.814	2.366	1.927
$I_{bn}(A)$	4.589	5.093	5.610	6.107	6.620	7.134	7.663
$*\Delta I_{an}(A)$	2.597	2.157	1.694	1.243	0.804	0.356	-0.082
$*\Delta I_{bn}(A)$	-0.002	0.437	0.900	1.351	1.790	2.238	2.677
$\Delta I_{an} + \Delta I_{bn}(A)$	2.594	2.594	2.594	2.594	2.594	2.594	2.594

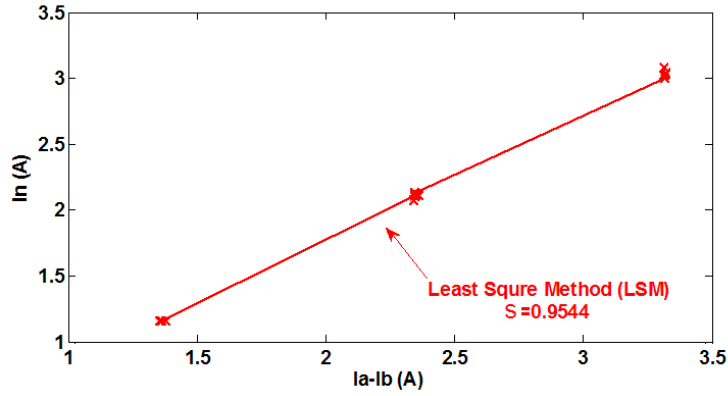


Figure 6.19: LMS method used for the calculation of  $s$ .

In addition, we adjusted other loads in the house to mimic the actual house loading in a long period to estimate the performance of a passive method. The waveforms of phase A, phase B and neutral currents are shown in Figure 6.20.

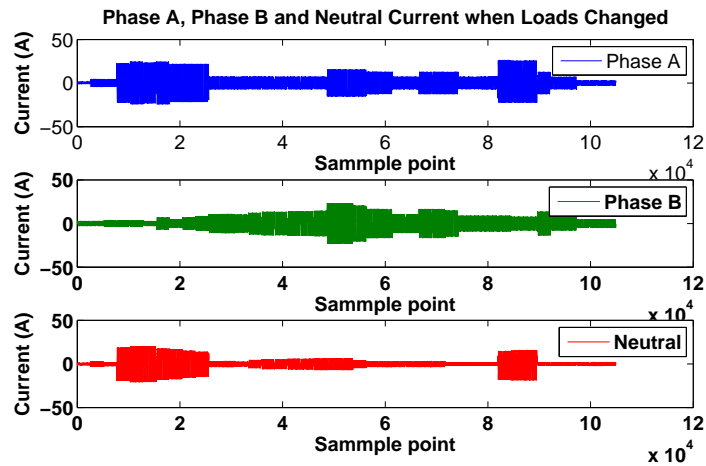


Figure 6.20: The currents of phase A, phase B and neutral when loads changed.

By using the same LMS method, the results of the passive method are shown in Figure 6.21. It is seen that  $\Delta I_n$  and  $\Delta(I_a - I_b)$  are not linear, which

suggests that the passive method is not valid here \*. This is because the random changes of loads caused the primary current changes, which result in ( $I_{n\_Utility} \neq 0$ ).

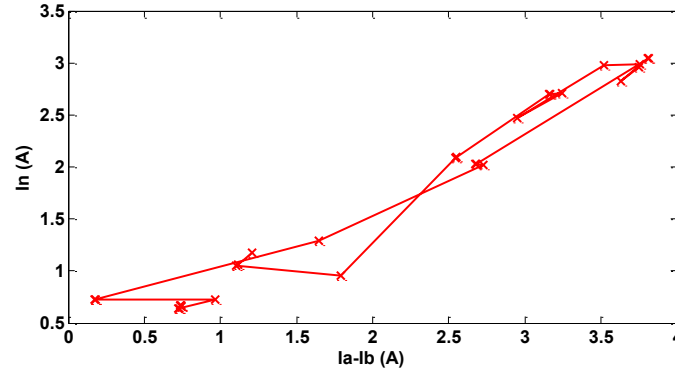


Figure 6.21: LMS method used for the calculation of  $s$  when loads change.

## 6.5 Secondary Neutral Condition Monitoring

Secondary neutral  $Z_{sn}$  has one end tied to a transformer grounding with primary neutral, and the other end grounded in a customer service panel. It has no other grounding point in between. A broken secondary neutral is more dangerous than a broken primary neutral, as the latter is compensated by multiple grounded connections. The proposed method is also able to monitor neutral impedance change to detect a broken secondary neutral.

---

\*The latest research on the passive method shows that the factor  $s$  can also be successfully calculated by selecting proper data with load changes. However, the passive monitoring based method may take hours to obtain an accurate value of  $s$ .

Recall the definition of  $k$ :

$$k = \frac{R_T}{(Z_{sn} + R_{gc}) + R_T}$$

which suggests that  $k$  decreases with the increase of  $(Z_{sn} + R_{gc})$ . For example, a section of the secondary neutral is broken as shown in Figure 6.22, the calculated  $k$  will decrease about 10%.

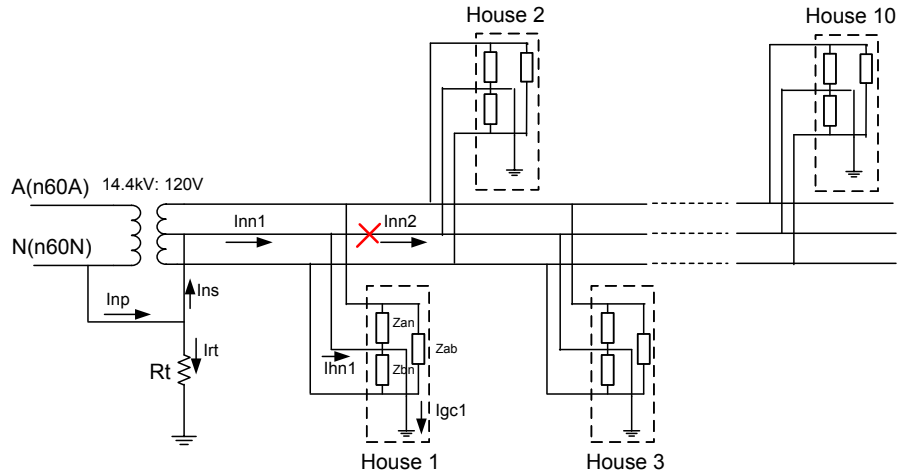


Figure 6.22: The secondary neutral is broken.

Calculated k	0.9498 - 0.0956i
Theoretical k	0.9908-0.0005i
Error (%)	10.1%

## 6.6 Conclusion

An active disturbance based method is presented to identify the contributions of the utility and customer to NEV. A fully-modeled simulation is conducted to verify the proposed scheme. The distribution system is made up of a



MGN network with varied loads to mimic a real situation. The primary neutral current model is proved that it is effective to analyze the flow of the unbalanced current from the utility. It is also proved that a MGN system must be considered as a ladder network. The neutral impedance cannot be ignored, even though it is very small compared to the grounding impedance. The active method by creating primary neutral current but not secondary neutral current has also been verified in this simulation.

Furthermore, a house test has also been conducted to prove the proposed active method. Due to the limitation of the test, a new factor  $s$  is introduced to replace  $k$  and  $g$  to represent the ratio of current return from neutral line  $I_{hn\_Customer}$  to the total unbalanced current  $I_{hab}$  in a house. From the test results, the active method is valid to calculate the desired  $s$ . The application of this active method can also be extended for secondary neutral condition monitoring.

## Chapter 7

### Conclusions and Future Work

#### 7.1 Conclusions and Contributions

Condition monitoring in distribution systems has played an important role in safety, reliability and system efficiency. Passive methods are the mainstream of condition monitoring, in which different types of sensors are used to monitor voltage, current and other parameters, such as temperature, moisture and vibration. The measured data is evaluated online or offline to indicate the status of the monitored device. However, applications of passive methods are constrained with the limitation of existent signals in power systems, some challenges faced by condition monitoring cannot be fulfilled by passive methods. Active methods are then developed to solve the challenges by creating the desired signals in accordance with monitoring tasks.

This thesis presents three challenges of condition monitoring related to substation grounding grid, de-energized line and multi-grounded neutral system. The main conclusions and contributions are summarized as follows:

1. An extensive review of condition monitoring in distribution systems is given. These monitoring methods are categorized into two groups: passive methods and active methods. Each group has two subcategories:

offline and online, according to monitoring continuity. Challenges faced by condition monitoring are presented, which cannot be solved by the existing passive methods or active offline methods. The thesis seeks solutions to fulfill these monitoring requirements by using active disturbance based methods.

2. Evaluation of a substation grounding grid is a necessary practice to sustain substation safety and protect electrical equipment. However, current methods cannot provide continuous and reliable assessments. An active online monitoring is therefore developed, which has the following features:

- Scalable current injection. The required current can be injected locally or remotely. The firing angles of thyristors are adjustable to create suitable current flowing into the tested grid. Without installing any extra electrode, this power electronics based signal generator can be easily controlled and maintained.
- Touch and step voltage sensors. Touch voltage and step voltage are directly related to substation safety. Monitoring touch and step voltages instead of grid impedance make the safety evaluation more accurate. The concept of a sensor network is proposed to monitor touch and step voltages at suspected spots in or outside of a substation.
- Online database. The measured data from sensors are transmitted to a database in real-time. A rapid decision is made according to

the comparison of the measured data with pre-determined thresholds or historical data. This online data processing largely reduces the response time so that an unperceived hazard can be identified in time.

3. A short-circuit in a de-energized system cannot be detected by passive methods, due to the fact that all electrical signals are zero after breakdown. A power electronics aided active method is described to address this challenge. The proposed scheme has the following advantages:

- Adaptive signal. The injected detection signal is required to be low enough at the beginning as an alarm for safety consideration. On the other hand, the injected signal is required to have voltage close to the operating line voltage to mimic the normal stress. This is achieved by controlling the firing angles of thyristors.
- Different types of faults are detected in a single device. With the help of three-phase thyristor bridge, the detection signals can be combined to detect different types of faults, including phase-to-ground faults and phase-to-phase faults. It also can be rapidly switched between different detection modes, without the change of any mechanical contact or switch.
- Harmonic impedance based symmetrical fault detection. The characteristics of harmonic impedance in a normal situation and in a symmetrical fault are analyzed. Then, an algorithm is developed to identify a symmetrical fault in a de-energized line. Moreover, this

algorithm is capable to distinguish a fault from a shunt capacitor bank or a stalled motor, which behaves like a short-circuit when a voltage is applied. Therefore, nuisance trips of circuit breakers can be minimized when energy is restored.

4. Neutral-to-Earth Voltage is a growing concern for utility and customers. A broken or poorly-connected neutral in a MGN system forces more current flowing into ground, which results in increased NEV. A method based on analysis of neutral current flow is presented for neutral condition monitoring, in which a unbalanced current is created from the secondary side, and the distribution of the created neutral current is analyzed to indicate neutral condition. As neutral impedance calculation is not required, the effort of looking for a zero potential point is avoided. This method is further extended to analyze the contributions of utility and customer to NEV by adding another disturbance created from the primary side. The two current disturbances can be created in a single unit. The effectiveness of this active method is verified by an experiment test in a residential house.

## **7.2 Recommendations for Future Work**

To further improve or verify the active methods described in this thesis, several extensions work can be explored as following:

1. Develop an algorithm in grounding grid monitoring to locate broken sections or missing grounding electrodes based on step/touch voltage

profiles obtained from sensors. To carry out an onsite measurement, a staged fault can be created by controlling a thyristor connected between a phase and ground. A prototype of the touch/step voltage sensor can be built based on Figure 2.5. The magnitude of the fault current should be adjusted in accordance with the sensitivity of the sensors. This test should last at least 6 months to consider the seasonal influences.

2. Conduct a field test of fault detection in a de-energized line. Different types of faults and their combinations should be simulated including: 1) phase-to-ground fault and phase-to-phase fault, 2) symmetrical fault and asymmetrical fault, 3) low impedance fault and high impedance fault. A prototype of signal generator has been built in PDS-LAB, University of Alberta. This prototype can be used to inject the desired detection signal between phases or between phase to ground in a field test. In addition, more studies are needed to verify if the three step-up transformers in Figure 3.4 can be replaced by one step-up transformer with switches.
3. Develop a current coupling scheme to induce current into neutral for a NEV test. From the literature review presented in Chapter 1, it is found that current coupling has better mobility for neutral current injection compared to power electronics. For example, current coupling does not need to find an exposed point for connecting a power electronics based device. A current coupler can be easily clipped on a neutral wire to induce current into power system. However, more research is needed to understand the mechanism of current coupling and the relation of the injected energy and signal frequencies.

## References

- [1] S. Tso, J. Lin, H. Ho, C. Mak, K. Yung, and Y. Ho, "Data mining for detection of sensitive buses and influential buses in a power system subjected to disturbances," *IEEE Trans. Power System*, vol. 19, no. 1, pp. 563–568, Feb. 2004.
- [2] J. Choi, Y. Ahn, H. Ryu, G. Jung, B. Han, and K. Kim, "A new method of grounding performance evaluation of multigrounded power systems by ground current measurement," in *Proc. 2004 International Conference on Power System Technology*, vol. 2, Nov. 2004, pp. 1144–1146.
- [3] B. Zhang, Z. Zhao, X. Cui, and L. Li, "Diagnosis of breaks in substation's grounding grid by using the electromagnetic method," *IEEE Trans. Magnetics*, vol. 38, no. 2, pp. 473–476, Mar. 2002.
- [4] D. Kasten, S. Sebo, and J. Lauletta, "Laboratory measurements for power system condition monitoring," in *Proc. 2012 IEEE International Symposium on Electrical Insulation*, Jun. 2012, pp. 113–116.
- [5] J. Wischkaemper, C. Benner, and B. Russell, "A new monitoring architecture for distribution feeder health monitoring, asset management, and real-time situational awareness," in *Proc. 2012 IEEE PES Innovative Smart Grid Technologies*, Jan. 2012, pp. 1–7.
- [6] S. Bagley and D. Branca, "A new approach to find fault locations on distribution feeder circuits," in *Proc. 2007 IEEE Rural Electric Power Conference*, May 2007, pp. 1–4.
- [7] J. Frate, D. Gagnon, R. Vilandre, and R. Dansereau, "Evaluation of overhead line and joint performance with high-definition thermography," in *Proc. 2000 IEEE 9th International Conference on Transmission and Distribution Construction, Operation and Live-Line Maintenance*, 2000, pp. 145–151.
- [8] W. Wang and L. Wang, "A temperature remote monitoring system of cable joint," in *Proc. 2010 2nd International Conference on Signal Processing Systems*, vol. 1, Jul. 2010, pp. 690–694.

- [9] D. Fournier and N. Amyot, “Diagnostic of overheating underground distribution cable joints,” in *Proc. 2001 CIRED 16th International Conference and Exhibition on Electricity Distribution, Part 1: Contributions*, 2001, p. 87.
- [10] J. Sato, T. Shioiri, T. Imai, O. Tagaya, Y. Takei, T. Kuriyama, and M. Homma, “Investigation of long-term reliability for solid insulated switchgear,” in *Proc. 2012 IEEE PES Transmission and Distribution Conference and Exposition*, May 2012, pp. 1–4.
- [11] A. Antur, D. Benenson, V. Demjanenko, D. Hess, H. Naidu, S. Park, A. Soom, M. Soumekh, M. Tangri, R. Valtin, and S. Wright, “A noninvasive diagnostic instrument for power circuit breakers,” in *Proc. 1991 IEEE Power Engineering Society Transmission and Distribution Conference*, Sep. 1991, pp. 508–515.
- [12] M. Runde, T. Aurud, L. E. Lundgaard, G. Ottesen, and K. Faugstad, “Acoustic diagnosis of high voltage circuit-breakers,” *IEEE Trans. Power Delivery*, vol. 7, no. 3, pp. 1306–1315, Jul. 1992.
- [13] S. Birlasekaran, S. Choi, and A. Liew, “Overview of diagnostic and condition monitoring techniques for in-service power apparatus,” in *Proc. 1998 EMPD International Conference*, vol. 2, Mar. 1998, pp. 673–678.
- [14] M. Jain, M. Srinivas, and A. Jain, “A novel web based expert system srchitecture for on-line and off-line fault diagnosis and control (fdc) of transformers,” in *Proc. 2008 IEEE Region 10 TENCON Conference*, Nov. 2008, pp. 1–5.
- [15] I. Metwally, “Failures, monitoring and new trends of power transformers,” *IEEE Potentials*, vol. 30, no. 3, pp. 36–43, May 2011.
- [16] M. Cabanas, M. Meler, F. Pedrayes, C. Rojas, G. Orcajo, J. Cano, and J. Iglesias, “A new online method based on leakage flux analysis for the early detection and location of insulating failures in power transformers: application to remote condition monitoring,” *IEEE Trans. Power Delivery*, vol. 22, no. 3, pp. 1591–1602, Jul. 2007.
- [17] F. Poza, P. Marino, M. Ubeira, and F. Machado, “Programmable electronic instrument for condition monitoring of in service power transformers,” in *Proc. 2004 IEEE 21st Instrumentation and Measurement Technology Conference*, vol. 3, May 2004, pp. 2126–2131.



- [18] J. K. Pylvanainen, K. Nousiainen, and P. Verho, "Studies to utilize loading guides and ann for oil-immersed distribution transformer condition monitoring," *IEEE Trans. Power Delivery*, vol. 22, no. 1, pp. 201–207, Jan. 2007.
- [19] T. Leibfried, "Online monitors keep transformers in service," *IEEE Trans. Computer Applications in Power*, vol. 11, no. 3, pp. 36–42, Jul. 1998.
- [20] J. Erbrink, E. Gulski, J. Smit, J. Aditya, L. Chmura, R. Leich, P. Seitz, and B. Quak, "Test procedure and test circuit considerations for on load tap changer dynamic resistance measurement," in *Proc. 2010 International Conference on High Voltage Engineering and Application*, Oct. 2010, pp. 317–320.
- [21] A. Zobaa and C. Cecati, "A comprehensive review on distributed power generation," in *Proc. 2006 International Symposium on Power Electronics, Electrical Drives, Automation and Motion*, May 2006, pp. 514–518.
- [22] M. Abdolrasol and S. Mekhilef, "Hybrid anti-islanding algorithm for utility interconnection of distributed generation," in *Proc. 2009 International Conference for Technical Postgraduates*, Dec. 2009, pp. 1–5.
- [23] T. Skocil, O. Gomis-Bellmunt, D. Montesinos-Miracle, S. Galceran-Arellano, and J. Rull-Duran, "Passive and active methods of islanding for PV systems," in *Proc. 2009 13th European Conference on Power Electronics and Applications*, Sep. 2009, pp. 1–10.
- [24] T. Radil, P. Ramos, F. Janeiro, and A. Serra, "PQ monitoring system for real-time detection and classification of disturbances in a single-phase power system," *IEEE Trans. Instrumentation and Measurement*, vol. 57, no. 8, pp. 1725–1733, Aug. 2008.
- [25] R. Chen and S. Sabir, "The benefits of implementing distribution automation and system monitoring in the open electricity market," in *Proc. 2001 Canadian Electrical and Computer Engineering Conference*, vol. 2, 2001, pp. 825–830.
- [26] Y. Ye and Y. Liu, "Monitoring power system disturbances based on distribution-level phasor measurements," in *Proc. 2012 IEEE PES Innovative Smart Grid Technologies*, Jan. 2012, pp. 1–8.

- [27] A. Kingsmill, S. Jones, and J. Zhu, “Application of new condition monitoring technologies in the electricity transmission industry,” in *Proc. 2003 ICEMS Sixth International Conference on Electrical Machines and Systems*, vol. 2, Nov. 2003, pp. 852–855.
- [28] L. Olsson and G. Bengtsson, “PD-mapping of paper insulated mv cables in gothenburg,” in *Proc. 1997 CIRED 14th International Conference and Exhibition on Electricity Distribution. Part 1: Contributions*, vol. 3, 1997, pp. 12/1–12/5.
- [29] A. Westrom, A. P. S. Meliopoulos, G. Cokkinides, and A. Ayoub, “Open conductor detector system,” *IEEE Trans. Power Delivery*, vol. 7, no. 3, pp. 1643–1651, Jul. 1992.
- [30] W. Xu, G. Zhang, C. Li, W. Wang, G. Wang, and J. Kliber, “A power line signaling based technique for anti-islanding protection of distributed generators - part i: scheme and analysis,” *IEEE Trans. Power Delivery*, vol. 22, no. 3, pp. 1758 –1766, Jul. 2007.
- [31] V. Sule and A. Kwasinski, “Active anti-islanding method based on harmonic content detection from overmodulating inverters,” in *Proc. 2011 IEEE Twenty-Sixth Annual Applied Power Electronics Conference and Exposition*, Mar. 2011, pp. 637–644.
- [32] D. Velasco, C. Trujillo, G. Garcera, and E. Figueres, “An active anti-islanding method based on phase-PLL perturbation,” *IEEE Trans. Power Electronics*, vol. 26, no. 4, pp. 1056–1066, Apr. 2011.
- [33] A. Yafaoui, B. Wu, and S. Kouro, “Improved active frequency drift anti-islanding detection method for grid connected photovoltaic systems,” *IEEE Trans. Power Electronics*, vol. 27, no. 5, pp. 2367–2375, May 2012.
- [34] P. Mahat, Z. Chen, and B. Bak-Jensen, “A hybrid islanding detection technique using average rate of voltage change and real power shift,” *IEEE Trans. Power Delivery*, vol. 24, no. 2, pp. 764–771, Apr. 2009.
- [35] Y. Cern, “Inductive coupling of a data signal to a power transmission cable,” U.S. Patent 6 452 482, Dec 28, 2000.
- [36] M. Montreuil, “Magnetically coupled alternating stray current neutralizing method and system,” U.S. Patent 5 825 170, Jan. 24, 1997.

- [37] B. Johansson, “Active booster transformer system,” U.S. Patent 6 700 223, Nov. 26, 2001.
- [38] D. A. Rhein and L. R. Beard, “Fault detection system including a capacitor for generating a pulse and a processor for determine admittance versus frequency of a reflected pulse,” U.S. Patent 5,650,728, Jul. 22, 1997.
- [39] R. Maier and W. Roethlingshoefer, “Method and arrangement for detecting short-circuit in circuit branches of electrical power system networks,” U.S. Patent 5,345,180, Sep. 6, 1994.
- [40] *IEEE Guide for Safety in AC Substation Grounding*, IEEE Std. 80-2000, 2000.
- [41] I. Lu and R. Shier, “Application of a digital signal analyzer to the measurement of power system ground impedances,” *IEEE Trans. Power App. Syst.*, vol. 100, no. 4, pp. 1918–1922, Apr. 1981.
- [42] A. Meliopoulos, G. Cokkinides, H. Abdallah, S. Duong, and S. Patel, “A PC based ground impedance measurement instrument,” *IEEE Trans. Power Delivery*, vol. 8, no. 3, pp. 1095–1106, Jul. 1993.
- [43] L. S. Devarakonda, J. Moskos, and A. Wood, “Evaluation of ground grid resistance for inservice substations,” in *Proc. 2010 IEEE Power Engineering Society Transmission and Distribution Conf.*, Apr. 2010, pp. 1–4.
- [44] C. Chang and C. Lee, “Computation of ground resistances and assessment of ground grid safety at 161/23.9-kv indoor-type substation,” *IEEE Trans. Power Delivery*, vol. 21, no. 3, pp. 1250–1260, Jul. 2006.
- [45] A. Puttarach, N. Chakpitak, T. Kasirawat, and C. Pongsriwat, “Substation grounding grid analysis with the variation of soil layer depth method,” in *Proc. 2007 IEEE Power Tech Conf.*, Jul. 2007, pp. 1881–1886.
- [46] R. Gustafson, R. Pursley, and V. Albertson, “Seasonal grounding resistance variations on distribution systems,” *IEEE Trans. Power Delivery*, vol. 5, no. 2, pp. 1013–1018, Apr. 1990.

- [47] *IEEE Guide for Measuring Earth Resistivity, Ground Impedance, and Earth Surface Potentials of a Ground System*, IEEE Std. 81-1983, 1983.
- [48] A. T. Trihus, "Cable tester," U.S. Patent 4,254,374, Mar. 3, 1981.
- [49] D. Wilson and Hedman, "Fault isolator for electrical utility distribution systems," U.S. Patent 4,370,609, Jan. 25, 1983.
- [50] R. Elms, "Diagnostic wiring verification tester," U.S. Patent 6,765,390, Jul. 20, 2004.
- [51] J. Nelson, "Grounding power systems above 600 v," *IEEE Magazine Industry Applications*, vol. 12, no. 1, pp. 50–58, Jan. 2006.
- [52] *Grounding methods for electric supply and communications facilities. Section 9 - Interpretation . Rule 096C Ground resistance requirements C Multi-grounded systems*, National Electrical Safety Code Std., Oct. 2009.
- [53] *Downed power lines: why they cant always be detected.* IEEE Power Engineering Society, 1989.
- [54] B. Aucoin and R. Jones, "High impedance fault detection implementation issues," *IEEE Trans. Power Delivery*, vol. 11, no. 1, pp. 139–148, Jan. 1996.
- [55] D. Jeerings and J. Linders, "Unique aspects of distribution system harmonics due to high impedance ground faults," *IEEE Trans. Power Delivery*, vol. 5, no. 2, pp. 1086–1094, Apr. 1990.
- [56] A. Sultan, G. Swift, and D. Fedirchuk, "Detecting arcing downed-wires using fault current flicker and half-cycle asymmetry," *IEEE Trans. Power Delivery*, vol. 9, no. 1, pp. 461–470, Jan. 1994.
- [57] A. Lazkano, J. Ruiz, E. Aramendi, and L. Leturiondo, "A new approach to high impedance fault detection using wavelet packet analysis," in *Proc. 2000 IEEE Ninth International Conference on Harmonics and Quality of Power*, vol. 3, 2000, pp. 1005–1010.
- [58] R. Patterson, W. Tyska, B. D. Russell, and B. M. Aucoin, "A microprocessor based digital feeder monitor with high impedance fault detection,"

in *Proc. 2000 Forty Seventh Annual Conference for Protective Relay Engineers*.

- [59] Kunsman, “High impedance fault detection,” U.S. Patent 7069116, 2006.
- [60] M. Arshad and S. Islam, “Significance of cellulose power transformer condition assessment,” *IEEE Trans. Dielectrics and Electrical Insulation*, vol. 18, no. 5, pp. 1591–1598, Oct. 2011.
- [61] K. Elkinson, G. Topjian, M. Lawrence, and A. McGrail, “Aspects of power transformer asset management,” in *Proc. 2012 IEEE PES Transmission and Distribution Conference and Exposition*, May 2012, pp. 1–5.
- [62] P. Kang and D. Birtwhistle, “Condition monitoring of power transformer on-load tap-changers. Part II: Detection of ageing from vibration signatures,” *IEE Proc. Generation, Transmission and Distribution*, vol. 148, no. 4, pp. 307–311, Jul. 2001.
- [63] X. Long, M. Dong, X. W., and Y. W. Li, “Online monitoring of substation grounding grid conditions using touch and step voltage sensors,” *IEEE Trans. Smart Grid*, vol. 3, no. 2, pp. 761–769, Jun. 2012.
- [64] X. Long, W. Xu, and Y. Li, “A new technique to detect faults in de-energized distribution feeders - part I: scheme and asymmetrical fault detection,” *IEEE Trans. Power Delivery*, no. 3, pp. 1893–1901, Jul. 2011.
- [65] X. Long, Y. W. Li, W. Xu, and C. Lerohl, “A new technique to detect faults in de-energized distribution feeders - part II: symmetrical fault detection,” *IEEE Trans. Power Delivery*, vol. 26, no. 3, pp. 1902–1910, Jul. 2011.
- [66] L. Qi, X. Cui, Z. Zhao, and H. Li, “Grounding performance analysis of the substation grounding grids by finite element method in frequency domain,” *IEEE Trans. Magnetics*, vol. 43, no. 4, pp. 1181–1184, Apr. 2007.
- [67] J. Ma and F. Dawalibi, “Analysis of grounding systems in soils with finite volumes of different resistivities,” *IEEE Trans. Power Delivery*, vol. 17, no. 2, pp. 596–602, Apr. 2002.

- [68] J. Hu, R. Zeng, J. He, W. Sun, J. Yao, and Q. Su, “Novel method of corrosion diagnosis for grounding grid,” in *Proc. 2000 International Conference on Power System Technology*, 2000, pp. 1365–1370.
- [69] J. He, R. Zeng, Y. Gao, Y. Tu, W. Sun, J. Zou, and Z. Guan, “Seasonal influences on safety of substation grounding system,” *IEEE Trans. Power Delivery*, vol. 18, no. 3, pp. 788–795, Jul. 2003.
- [70] Y. Liu, X. Cui, and Z. Zhao. (2010, May) A magnetic detecting and evaluation method of substations grounding grids with break and corrosion. [Online]. Available: <http://www.springerlink.com/content/f71631x2733n7158/fulltext.pdf>
- [71] R. Verma and D. Mukhedkar, “Fundamental considerations and impulse impedance of grounding grids,” *IEEE Trans. Power App. Syst.*, vol. 100, no. 3, pp. 1023–1030, Mar. 1981.
- [72] P. Rush, *Network Protection & Automation Guide*. ALSTOM T&D Energy Automation & Information, 2002.
- [73] H. Sarmiento, J. Fortin, and D. Mukhedkar, “Substation ground impedance: comparative field measurements with high and low current injection methods,” *IEEE Trans. Power App. Syst.*, vol. 103, no. 7, pp. 1677–1683, Jul. 1984.
- [74] S. Patel, “A complete field analysis of substation ground grid by applying continuous low voltage fault,” *IEEE Trans. Power App. Syst.*, vol. 104, no. 8, pp. 2238–2243, Aug. 1985.
- [75] *IEEE Guide to Measurement of Impedance and Safety Characteristics of Large, Extended Or Interconnected Grounding Systems*, IEEE Std. 81.2, 1992.
- [76] P. Yi, A. Iwayemi, and C. Zhou, “Developing zigbee deployment guideline under WiFi interference for smart grid applications,” *IEEE Trans. Smart Grid*, vol. 2, no. 1, pp. 110–120, Mar. 2011.
- [77] R. Kosztaluk, R. Mukhedkar, and Y. Gervais, “Field measurements of touch and step voltages,” *IEEE Trans. Power App. Syst.*, vol. 103, no. 11, pp. 3286–3294, Nov. 1984.

- [78] P. Sen and N. Mudarres, "Corrosion and steel grounding," in *Proc. 1990 the Twenty-Second Annual North American Power Symposium*, 1990, pp. 162–170.
- [79] (2009, Dec.) CYMGRD - Substation grounding program. Cooper Power Systems. [Online]. Available: <http://www.cyme.com/software/cymgrd/B1100-09079-CYMGRD.pdf>
- [80] *S&C IntelliRupter PulseCloser : Outdoor Distribution 15.5 kV and 27 kV*, Descriptive bulletin 766-30 ed., S&C, Mar. 2010.
- [81] W. Wang, K. Zhu, P. Zhang, and W. Xu, "Identification of the faulted distribution line using thyristor-controlled grounding," *IEEE Trans. Power Delivery*, vol. 24, no. 1, pp. 52–60, Jan. 2009.
- [82] M. T. Aung, J. V. Milanovic, and C. P. Gupta, "Propagation of asymmetrical sags and the influence of boundary crossing lines on voltage sag prediction," *IEEE Trans. Power Delivery*, vol. 19, no. 4, pp. 1819–1827, Oct. 2004.
- [83] D. C. Yu and S. H. Khan, "An adaptive high and low impedance fault detection methodan adaptive high and low impedance fault detection method," *IEEE Trans. Power Delivery*, vol. 9, no. 4, pp. 1812 – 1821, Oct. 1994.
- [84] W. Wang, E. E. Nino, and W. Xu, "Harmonic impedance measurement using a thyristor-controlled short-circuit," *IET Generation, Transmission and Distribution*, vol. 1, no. 5, pp. 707–713, Sep. 2007.
- [85] J. C. Gomez and M. M. Morcos, "A simple methodology for estimating the effect of voltage sags produced by induction motor starting cycles on sensitive equipment," in *Proc. 36th IAS Annual Meeting*, Oct. 2001, pp. 1196–1199.
- [86] K. Zhu, W. Wang, and W. Xu, "A new faulted line identification method based on incremental impedances," in *Proc. 2007 IEEE Conference on Industrial Electronics and Applications*, May 2007, pp. 217–221.
- [87] T. H. Chen and W. C. Yang, "Analysis of multi-grounded four-wire distribution systems considering the neutral grounding," *IEEE Trans. Power Delivery*, vol. 16, no. 4, pp. 710–717, Oct. 2001.

- [88] J. Acharya, Y. Wang, and W. Xu, "Temporary overvoltage and GPR characteristics of distribution feeders with multigrounded neutral," *IEEE Trans. Power Delivery*, vol. 25, no. 2, pp. 1036–1044, Apr. 2010.
- [89] T. C. Surbrook, N. D. Reese, and A. M. Kehrlé, "Stray voltage: sources and solutions," *IEEE Trans. Industry Applications*, vol. IA-22, no. 2, pp. 210–215, Mar. 1986.
- [90] C. DeNardo, "Stray and contact voltage an update on IEEE PES P1695 working group activities," in *Proc. 2012 IEEE Rural Electric Power Conference*, april 2012, pp. A3–1 –A3–7.
- [91] J. Burke and C. Untiedt, "Stray voltage: two different perspectives," *IEEE Magazine Industry Applications*, vol. 15, no. 3, pp. 36–41, May 2009.
- [92] A. Hanes, "Walkers warned after stray voltage kills second dog," *National Post*, Jan. 2009.
- [93] A. Charette and G. Simard, "Stray voltage at farm site utilities practice and review," in *Proc. 2006 IEEE PES Transmission and Distribution Conference and Exhibition*, May 2006, pp. 260–262.
- [94] O. Glennon, "Loss of neutral or ground protection circuit," U.S. Patent 4,931,893, 1989.
- [95] R. H. Legatti, "Ground fault current interrupter circuit with open neutral and ground lead protection," U.S. Patent 4,598,331, 1984.
- [96] W. R. Clark, "Open neutral protection," U.S. Patent 3,987,341, 1975.
- [97] J. Duve, "Conversion of standard class a ground-fault circuit-interrupters (GFCI), to a class a ground-fault circuit interrupter with open neutral protection," U.S. Patent 6,697,237, 2000.
- [98] D. T. Corner, "Power line communication system using anti-resonance isolation and virtual earth ground signaling," U.S. Patent 6,417,762, 2001.
- [99] R. Goldstein, "Apparatus and method for continuously monitoring grounding conductor resistance in power distribution system," U.S.



Patent 5,278,512, 1992.

# Appendices

## Appendix A

### Broken Neutral Detection On the Secondary Side

The secondary side of a residential service transformer typically has two hot wires and one neutral line. If a neutral line is broken, unequal loading may cause damage due to over-voltage or under-voltage. As illustrated in Figure A.1, if  $Z_1 > Z_2$ , then  $V_{Z_1} > 120V > V_{Z_2}$ . Additionally, many large home appliances utilize the neutral line as shock-protective means connected to the equipment case. An open neutral line to such installation creates a severe personnel shock hazard.

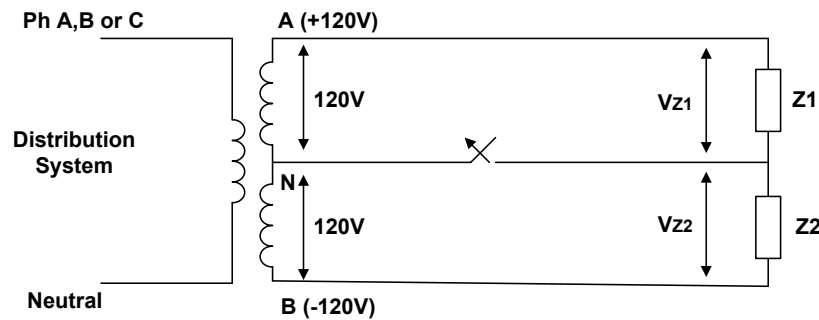


Figure A.1: Unequal loads are connected with an open neutral.

After extensive review of the existing ideas for open neutral detection, it is found that the existing methods can be categorized into two different types: passive and active schemes. The passive schemes use the passive elements, like capacitor, inductor or resistor to measure the related current and voltage to determine if there is an open neutral, while the active schemes have a signal generator to inject an appropriate signal into the circuit and measure the corresponding current and voltages. The existing methods are listed in Figure A.2.

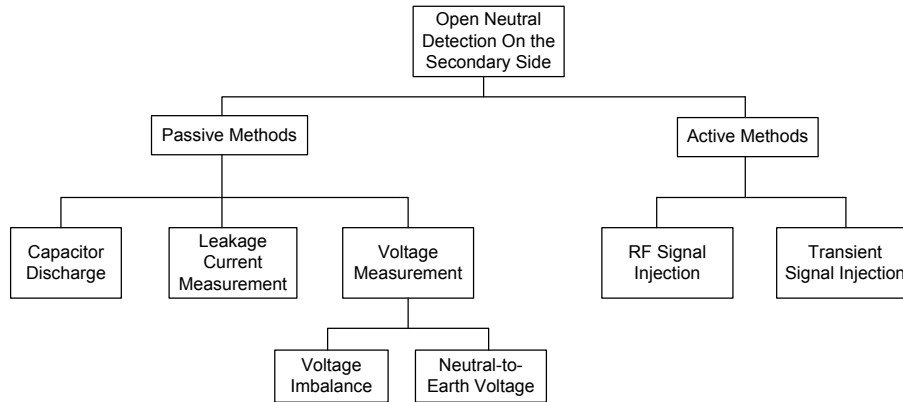


Figure A.2: Reviews of the existing open neutral detection methods.

## Passive Schemes

### Capacitor Discharge

As shown in Figure A.3, a loss of neutral protection circuit is disclosed in [94]. It contains a hot line lead 2, a neutral lead 3 and a ground lead 4. A bridge rectifier comprising diodes D1 to D4 is connected across the line lead 2 and the neutral lead 3 for DC output at a positive terminal 5 and a negative terminal 6. A load connected across these output terminals is represented in the drawing by Req.

In operation, the capacitor C2 charges through R1 in the negative half cycle of the AC supply when the line lead is at a negative potential with respect to the neutral lead. During the subsequent positive half cycle however, the diode D6 is forward biased and C2 discharges through D6 to the neutral lead 3. The circuit breaker for opening the power line controlled by solenoid 10 through SCR Q1 will not be activated as the maximum voltage across C2 never exceeds the tripping level for the SCR Q1.

However, if the neutral lead 3 is opened, the discharging path through D6 is not available to the capacitor C2 and it continues to charge until the breakdown voltage of ZD1 is exceeded. This forms a voltage energizing signal as the SCR Q1 is triggered. And then the solenoid 10 is energized to open the line lead 2 with the current flowing through D8, 10, Q1, D5 and ZD2 to earth.

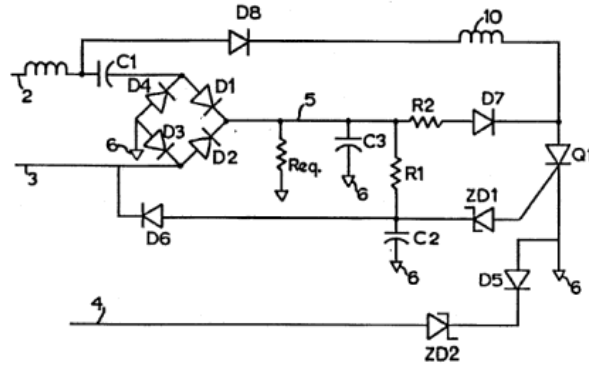


Figure A.3: A loss of neutral detector using capacitor discharge.

### Leakage Current Measurement

In [95], a ground fault circuit interrupter (GFCI) detect the imbalance of the hot wire and neutral current. If the imbalance current is significant enough, it will activate the interrupter through the winding 37 as shown in A.4. On the other side, a supplemental secondary winding 71 is located on core 31 of the differential transformer 29. When the neutral lead 13 and the ground lead 15 are properly connected, the supplemental secondary winding 71 is shorted out of the circuit and no appreciable current flows therein.

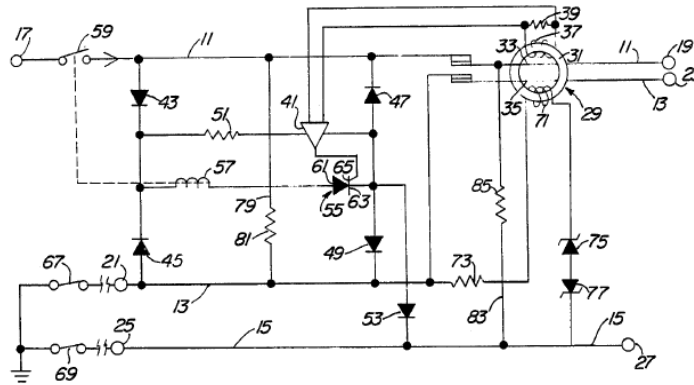


Figure A.4: A GFCI with open neutral protection using leakage current.

However, if the neutral line is open (represented by an opening of schematic

switch 67), the supplemental secondary winding 71 circuit provides the only current path for current in conductor 79. Thus, the supplemental secondary winding 71 would have a current flow produced therein that would generate a trip signal to initiate opening of line switch 59.

### Voltage Imbalance Detection

When the neutral is broken, the voltages of V1 and V2 are imbalance if the load impedances are not the same. An open neutral detector using the imbalance voltages is proposed in [96]. As shown in A.5, a voltage divider comprises an electrical series circuit of two equivalent impedances 25 and 26 and the voltage at the potential of the junction 28 therefore is always equal to zero ( $V_{n28} = 0$ ).

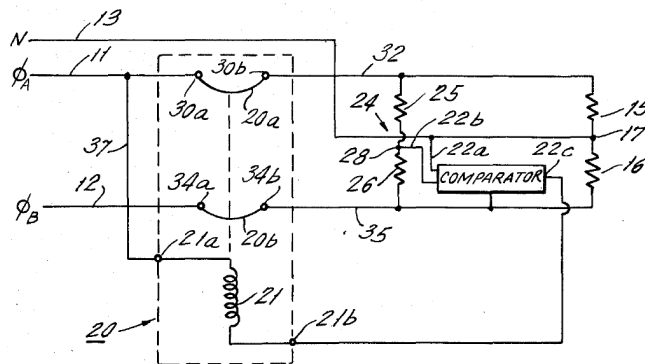


Figure A.5: A comparator with measuring the voltage between an artificial neutral and the neutral.

An open-neutral comparator measure the voltage between the junction 28 (an artificial neutral) and the neutral line. In the normal condition, this voltage is close to zero as the neutral line is essentially zero. But, if there is an open-circuit condition has been formed in neutral line, the neutral line voltage  $V_n$  is deviated from zero volts. The potential difference ( $V_n - V_{n28}$ ) measured by the comparator is greater than a preset value and then it energizes the circuit breaker to protect the circuit.

## Neutral-to-Earth Voltage Measurement

Conventional GFCI is powered by line-to-neutral voltage. When the neutral connection is broken, this kind of GFCI no longer has the energy to function. In [97], it provides a solution with utilizing the Neutral-to-Earth (NTE) voltage for open neutral protection. As shown in Figure A.6, a voltage sensitive device is installed between the neutral conductor and ground conductor.

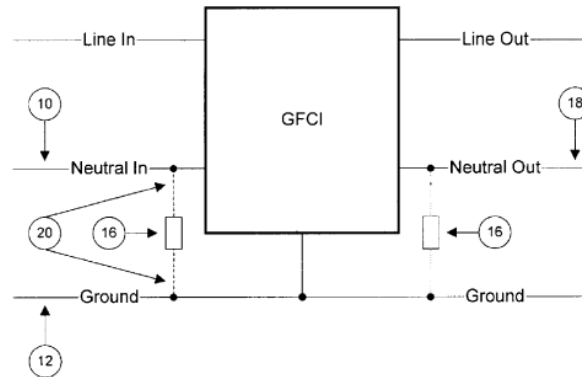


Figure A.6: A GFCI with a voltage sensitive device.

When the neutral line is disconnected, it is no longer capable of sinking any current, so if a load were connected, it would match the hot line potential. Based on this, a voltage sensitive device could be placed between neutral and earth ground such that if the potential should exceed a set point, the device would start to conduct current, thus pulling the open neutral's potential closer to the potential of earth ground. By pulling the open neutral-to-earth ground, the GFCI have adequate current to properly function.

## Active Schemes

### RF Signal Injection and Detection

In [98], a transmitter and a receiver were invented for the high frequency communication. The transmitter includes at least two tuning elements. One is connected between a hot wire and a neutral and the other is connected between the neutral wire and a ground. The tuning elements comprise one-port networks, which may include passive capacitors, inductor, and/or resistor

to provide the desired tuning function.

The input signal can be any communication data and the type of modulation may be amplitude modulation, frequency modulation or any other known method. Especially, for the detection of the broken neutral, the input signal can be very simple since the concern here is only the existence of the signal (Figure A.7). The receiver has a similar structure as the transmitter. It demodulates the carrier signal to produce an output signal at the power outlet where the receiver is installed. The transmitter and the receiver can be located on any outlets, or even be located on different phases of AC power, as long as they share a common service panel. Thus, with this neutral line communication based method, the condition of neutral conductors sharing a common service panel can be investigated.

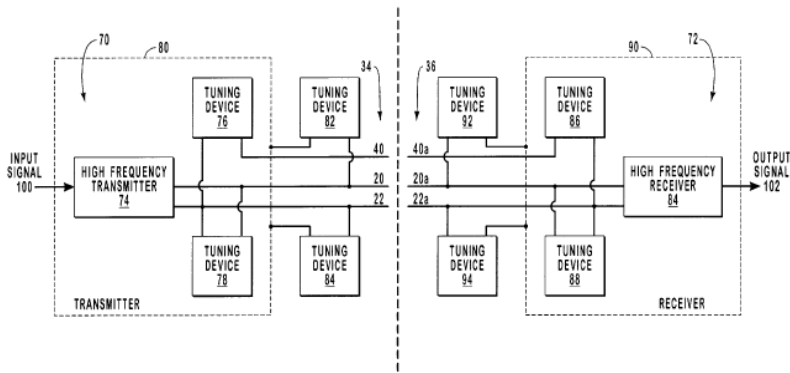


Figure A.7: The transmitter and receiver of the RF signal based scheme.

## Transient Signal Injection and Detection

A block diagram of a continuous grounding-neutral conductor monitoring system, which is disclosed in [99], is shown in Figure A.8. Three leads are connected to the hot wire (H), the neutral (N) and the ground (G) respectively. A resonant circuit, such as a series circuit, is coupled to the grounding G and neutral N. A regulated charging circuit 4 coupled to the hot wire and the resonant circuit 2 through the neutral N to supply an electrical charge to the resonant circuit by controlled by the timing means 7. Closing switch 3 allows the charge to decay through the grounding and neutral circuit to produce a damped sinusoidal waveform responsive to the impedance of the grounding to neutral circuit. The decay waveform is sampled to compare with a pre-determined value to see if unacceptably high neutral-to-ground impedance



exists. This method can indicate the connection of neutral and ground, but cannot distinguish the high resistance existing in the neutral conductor or ground conductor.

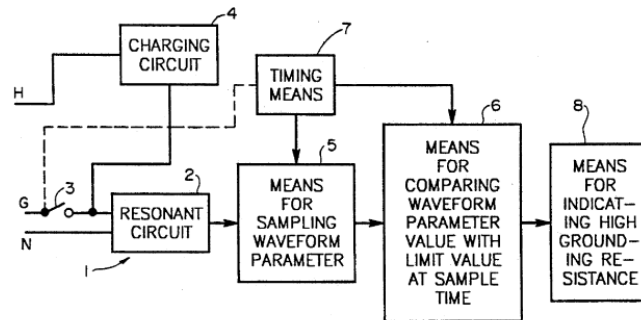


Figure A.8: A continuous grounding-neutral conductor monitoring system.

However, It is difficult to apply these methods to primary neutral. Firstly, the detectors designed in [94]-[97] are not practical for overhead lines. Secondly, some of the devices utilizing the voltages or currents imbalance are not applicable for three-phase system. Thirdly, primary neutral is not the only return path for unbalanced current when there are multiple grounding connections. Thus, the active method in [98] is not applicable.